SESSION 8

REACTOR ACCIDENTS

Tuesday: August 25, 1992
Co-Chairmen: W. H. Miller, Jr.
J. G. Wilhelm

OPENING COMMENTS OF SESSION CO-CHAIRMAN

REVISION OF REACTOR ACCIDENT SOURCE TERMS AND IMPLICATIONS FOR NUCLEAR AIR CLEANING REQUIREMENTS
L. Soffer

POST-ACCIDENT AIR LEAKAGE ANALYSIS IN A NUCLEAR FACILITY VIA T-METHOD AIRFLOW SIMULATION
T. Farajian, G. Grewal, R.J. Tsal

THE EXPERIENCE WITH THE EFFECTIVENESS OF FILTERING SYSTEMS FOR THE RADIOACTIVE FALL-OUT FROM THE CHERNOBYL ACCIDENT IN GERMANY
H. Braun

AEROSOL PENETRATION THROUGH A SEISMICALLY LOADED SHEAR WALL
C.R. Farrar, S.P. Girrens

BETA EXPERIMENTS ON AEROSOL RELEASE DURING MELT-CONCRETE INTERACTION AND FILTERING OF THE OFF-GAS
H.G. Dillmann, H. Pasler, H. Alsmeyer

ACTIVATED CHARCOAL BEDS FOR PASSIVE MITIGATION OF THE RADIOACTIVITY RELEASE FROM SEVERE ACCIDENTS HEAT TRANSPORT AND DYNAMIC NOBLE-GAS WATER-VAPOUR COADSORPTION
F. Castellani, G. Curzio, F. d'Errico, S. Lanza, A. Mori, G. Rossi, G. Sgalambro

DESIGN OF A PREFILTER TO IMPROVE RADIATION PROTECTION AND FILTERING EFFICIENCY OF THE CONTAINMENT VENTING SYSTEM
M. Kaercher

EXPERIMENTAL STUDY ON AEROSOL REMOVAL EFFECT BY POOL SCRUBBING
I. Kaneko, M.Fukasawa, M. Naito, K. Miyata, M. Matsumoto

THE PHEBUS FP INTEGRAL SOURCE TERM EXPERIMENTAL PROJECT WITH EMPHASIS ON IODINE SELECTIVE FILTERING
R. Zeyen, J.G. Wilhelm, M. Lucas

CLOSING COMMENTS OF SESSION CO-CHAIRMEN WILHELM AND MILLER

OPENING COMMENTS OF SESSION CO-CHAIRMAN MILLER

In this session we will hear presentations by nine speakers, many of whom have traveled great distances to share the results of their work. Their work is characterizing the challenges of reactor accidents to nuclear air treatment systems.

REVISION OF REACTOR ACCIDENT SOURCE TERMS AND IMPLICATIONS FOR NUCLEAR AIR CLEANING REQUIREMENTS

Leonard Soffer
Office of Nuclear Regulatory Research
US Nuclear Regulatory Commission
Washington, DC 20555

Abstract

Current NRC reactor accident source terms used for licensing are contained in Regulatory Guides 1.3 and 1.4 and specify that 100% of the core inventory of noble gases and 25% of the iodine fission products are assumed to be instantaneously available for release from the containment. The chemical form of the iodine fission products is also assumed to be predominantly elemental (I_2) iodine. These assumptions have strongly affected present nuclear air cleaning requirements by emphasizing rapid actuation of spray systems and filtration systems optimized to retain elemental iodine.

Severe accident research results have confirmed that although the current source term is very substantial and has resulted in a very high level of plant capability, the present source term is no longer compatible with a realistic understanding of severe accidents.

The NRC has issued a proposed revision of the reactor accident source terms as part of several regulatory activities to incorporate severe accident insights for future plants. A revision to 10 CFR 100 is also being proposed to specify site criteria directly and to eliminate source terms and doses for site evaluation. Reactor source terms will continue to be important in evaluating plant designs. Although intended primarily for future plants, existing and evolutionary power plants may voluntarily apply revised accident source term insights as well in licensing.

The proposed revised accident source terms are presented in terms of fission product composition, magnitude, timing and iodine chemical form. Some implications for nuclear air cleaning requirements are discussed.

I. Introduction and Background

Radionuclide releases, that is, the type, quantity, timing and energy characteristics of the release of radioactive material from reactor accidents ("source terms") are deeply embedded in the regulatory policy and practices of the U.S. Nuclear Regulatory Commission (NRC). The NRC's reactor site criteria[1] require for licensing purposes that an accidental fission product release from the core into the containment be postulated to occur and that its radiological consequences be evaluated assuming that the containment remains intact but leaks at its maximum allowable leak rate.

The characteristics of the "source term" into the containment, which must be distinguished from a release to the environment, is contained in Regulatory Guides 1.3 and 1.4[2,3], but is derived from the 1962 report TID-14844[4], and consists of 100% of the core inventory of

noble gases and 50% of the iodines (half of which are assumed to deposit on interior surfaces very rapidly).

Iodine fission products and the chemical form of iodine have played a key role. Regulatory Guides 1.3 and 1.4 specify that the iodine is assumed to be instantaneously available for release, and also specify that the iodine chemical form is assumed to be predominantly (91 percent) in elemental (I_2) form, with 5 percent assumed to be particulate iodine and 4 percent assumed to be in organic form. These assumptions have significantly affected the design of engineered safety features, which have largely been optimized to remove elemental iodine.

Use of the TID-14844 release has not been confined to an evaluation of plant mitigation features such as sprays and filtration systems and site suitability alone. The regulatory applications of this release cover a wide range, including the basis for (1) the post-accident radiation environment for which safety-related equipment should be qualified, (2) post-accident habitability requirements for the control room, and (3) post-accident sampling systems and accessibility.

Severe accident research insights[5] have confirmed that although the TID-14844 release is very substantial and has resulted in a very high level of plant capability, nonetheless, based upon the large amount of information obtained on severe accidents since the publication of TID-14844 about thirty years ago, the present recipe is no longer compatible with a realistic understanding of severe accidents. It has both conservative and non-conservative aspects. The assumption of an instantaneous appearance of a large fraction of the core inventory of noble gas and iodine isotopes within containment has long been recognized as highly conservative. It has also become clear that neglect of other important nuclides released into containment, such as cesium, may be non-conservative. Use of the TID-14844 prescription in its present form may force plant designers to include design features that may not enhance safety and that focus, instead, upon certain aspects of the prescription (e.g., very rapid closure of certain containment isolation valves and filter designs emphasizing removal of elemental iodine). Similarly, use of the present prescription may cause designers not to focus on other important aspects of plant accidents (e.g., release of cesium and potential containment failure under severe accident conditions).

The NRC is currently in the process of reviewing designs for future nuclear power plants and the NRC staff is applying these important research insights towards resolution of key issues associated with the licensing of these designs. Although these insights are intended to be applied toward licensing of future light water reactors, they are also expected to be made available for voluntary use by existing reactor licensees.

A revision of the NRC's reactor site criteria (10 CFR 100) has also been proposed[6]. The sizes of the exclusion area and low population zone (LPZ) are presently determined by the assumed source term and the dose criteria in Part 100 and regulated indirectly by the credit given for fission product cleanup systems such as sprays and filter systems as well as the allowable containment leak rate. Hence,

siting dose calculations actually have affected plant design, particularly fission product cleanup systems related to iodine, more than siting.

Because siting dose calculations are not strongly influencing reactor siting, and because improved source term insights are important in understanding how future plants should be designed to cope with potential severe accidents, source term and dose calculations will be eliminated for siting and relocated, on an interim basis, to Part 50, where they will continue to be used for plant design purposes. Exclusion area size and population density criteria are to be stated directly in Part 100. These proposed rule changes are expected to be issued for comment by late summer 1992.

A final revision of 10 CFR 50 to incorporate updated source term and severe accident insights will also be undertaken, with an Advance Notice of Proposed Rulemaking (ANPR) for comment presently expected to be issued in about autumn 1992.

This paper presents the NRC proposed revised accident source terms and discusses some possible implications of these for nuclear air cleaning requirements.

II. Revised Accident Source Terms

Overview of Severe Accident Progression

A major NRC research effort began about 1981 and has been under way since then to obtain a better understanding of fission product transport and release mechanisms in light water reactors (LWR) under severe accident conditions. This improved methodology on severe accident source terms has been reflected in NUREG-1150[7] which provides an updated risk assessment for five US nuclear power plants. An assessment of the chemical form of iodine found within containment as a result of a severe accident has also been carried out[8].

Despite differences in plant design and accident sequences, analyses of severe LWR accident sequences indicate that they can be generally categorized in terms of phenomenological phases associated with the degree of fuel melting and relocation, reactor pressure vessel integrity, and, as applicable, attack upon concrete below the reactor cavity by molten core materials.

Initially there is a release of coolant activity associated with a break or leak in the reactor coolant system (RCS). Assuming that the coolant loss cannot be accommodated by the reactor coolant makeup systems or the emergency core cooling systems, fuel cladding failure would occur with a release of the activity located in the gap between the fuel pellet and the fuel cladding.

As the accident progresses, fuel degradation begins, resulting in a loss of fuel geometry accompanied by gradual melting and slumping of core materials to the bottom of the reactor pressure vessel. During this period, the early in-vessel release phase, virtually all the noble gases and significant fractions of the volatile nuclides such as iodine, cesium, and tellurium are released into containment. The

amounts of volatile nuclides released into containment during this phase are strongly influenced by the residence time of the radioactive material within the RCS during core degradation. High pressure sequences result in long residence times and significant retention and plateout of volatile nuclides within the RCS, while low pressure sequences result in relatively short residence times and little retention within the RCS and consequently higher releases into containment.

If failure of the bottom head of the reactor pressure vessel occurs, two additional release phases may occur. Molten core debris released from the reactor pressure vessel into containment will interact with concrete structural materials of the cavity below the reactor (ex-vessel release phase). As a result, quantities of the less volatile nuclides may be released into containment. Ex-vessel releases are influenced somewhat by the type of concrete in the reactor cavity. Limestone concrete decomposes to produce greater quantities of CO and CO_2 gases than basaltic concrete. These gases may, in turn, sparge some of the less volatile nuclides, such as barium and strontium, and small fractions of the lanthanides into the containment atmosphere. Large quantities of non-radioactive aerosols may also be released as a result of core-concrete interactions. The presence of water in the reactor cavity overlying any core debris can significantly reduce ex-vessel releases (both radioactive and non-radioactive) into containment, either by cooling the core debris, or at least by scrubbing the releases and retaining a large fraction in the water. The degree of scrubbing will depend upon the depth and temperature of any water overlying the core debris. Simultaneously, and with a longer duration, late in-vessel releases of some of the volatile nuclides, previously deposited in the reactor coolant system during the in-vessel phase, will also occur.

A summary of the release phases and their estimated durations for pressurized water reactors (PWR) and boiling water reactors (BWR) is shown in Table 1.

Table 1 Release Phase Durations.

RELEASE PHASE	DURATION, PWRs (HOURS)	DURATION, BWRs (HOURS)
Coolant Activity	10 to 30 seconds*	30 seconds*
Gap Activity	0.5	1.0
Early In-Vessel	1.3	1.5
Ex-Vessel	2	3
Late In-Vessel	10	10

* Without approval for leak-before-break. Coolant activity phase duration is assumed to be 10 minutes with leak-before-break approval.

Accident Selection

The NRC has issued a draft report for comment[9] proposing revised LWR reactor accident source terms. A key choice to be made in defining an accident source term is the severity of the accident or group of accidents selected. Since reactor pressure vessel failure is estimated to be a possible result of a core damage accident, but is highly uncertain, it was considerd appropriate to select an accident source term based upon a complete core-melt, that is, reactor pressure vessel failure and subsequent core-concrete interactions. The basis for the revised accident source terms is an accident source term that is representative of the mean or average release fractions associated with a complete core-melt accident occurring at low pressure. Low pressure sequences were chosen because (1) a large fraction of the risk significant sequences analyzed in NUREG-1150 were low pressure sequences, (2) future plants are expected to have the capability to rapidly depressurize the reactor coolant system, and (3) the fission product release into containment from low pressure sequences is typically somewhat greater than that for high pressure sequences. It must also be emphasized that the characteristics of the revised source terms do not accurately represent any single accident sequence, but instead combine aspects of a number of core-melt sequences occurring at low pressure.

Fission Product Composition and Magnitude

The proposed accident source terms, including their composition, magnitude, timing and duration, are shown in Tables 2 and 3 for BWRs and PWRs, respectively.

Table 2 BWR Releases Into Containment*

	Gap Release	Early In-Vessel	Ex-Vessel	Late In-Vessel
Duration (Hours)	1.0	1.5	3.0	10.0
Noble Gases	0.05	0.95	0	0
Iodine	0.05	0.22	0.37	0.07
Cesium	0.05	0.15	0.45	0.03
Tellurium	0	0.11	0.38	0.01
Strontium	0	0.03	0.24	0
Barium	0	0.03	0.21	0
Ruthenium	0	0.007	0.004	0
Cerium	0	0.009	0.01	0
Lanthanum	0	0.002	0.01	0

* Values shown are fractions of core inventory.

The rate of release of fission products into the containment is assumed to be constant during the duration time of each phase. The releases shown for the ex-vessel phase are assumed to be for a dry reactor cavity having no water overlying any core debris. Where water is covering the core debris, aerosol scrubbing will take place and reduce the quantity of aerosols entering the containment atmosphere.

Chemical Form

Results from Reference 8 indicates that iodine entering the containment is at least 95% CsI with the remaining 5% as I plus HI, with not less than 1% of each as I and HI. Once the iodine enters containment, however, additional reactions are likely to occur. In an aqueous environment, as expected for LWRs, iodine is expected to dissolve in water pools or plate out on wet surfaces in ionic form as I^-. Subsequently, iodine behavior within containment depends on the time and pH of the water solutions. Because of the presence of other dissolved fission products, radiolysis is expected to occur and lower the pH of the water pools. Without any pH control, the results indicate that large fractions of the dissolved iodine will be converted to elemental iodine and be released to the containment atmosphere. Organic iodine will then be produced slowly over time from the elemental iodine available. However, if the pH is maintained at a value of 7 or greater, very little (less than 1%) of the dissolved iodine will be converted to elemental iodine.

All other fission products, except for the noble gases and iodine, discussed above, are expected to be in particulate form.

Table 3 PWR Releases Into Containment*

	Gap Release	Early In-Vessel	Ex-Vessel	Late In-Vessel
Duration (Hours)	0.5	1.3	2.0	10.0
Noble Gases	0.05	0.95	0	0
Iodine	0.05	0.35	0.29	0.07
Cesium	0.05	0.25	0.39	0.06
Tellurium	0	0.15	0.29	0.025
Strontium	0	0.03	0.12	0
Barium	0	0.04	0.10	0
Ruthenium	0	0.008	0.004	0
Cerium	0	0.01	0.02	0
Lanthanum	0	0.002	0.015	0

* Values shown are fractions of core inventory.

Nonradioactive Aerosols

In addition to the fission products, large quantities of nonradioactive or relatively low activity aerosols will also be released into containment. These aerosols arise from core structural and control rod materials released during the in-vessel phase and from concrete decomposition products during the ex-vessel phase. The quantities released into containment for one PWR (Sequoyah) sequence and for one BWR (Peach Bottom) sequence, were evaluated[10], and are shown in Table 4. The aerosol masses shown may have an effect upon pH level as well as on plant equipment such as filter loadings.

Table 4 Non-Fission Product Aerosol Releases into Containment*

BWR	BWR	PWR	PWR
In-Vessel	Ex-Vessel	In-Vessel	Ex-Vessel
780	5600	350	3800

* Values shown are in kilograms.

III. Implications for Air Cleaning Requirements

General

Fission products released into the containment atmosphere as a result of a severe accident can also be removed, both as a result of engineered features designed to accomplish this and/or by natural processes. Engineered Safety Features (ESF) include systems such as containment atmosphere sprays, BWR suppression pools, and ESF filtration systems. Natural removal includes processes such as aerosol deposition.

Possible implications for nuclear air cleaning requirements as a result of revised accident source terms fall into 4 areas. These arise from (1) revised insights on iodine chemical form, (2) the presence of other nuclides, in addition to iodine and the noble gases, released into containment, (3) revised timing and duration of fission product releases, and (4) the presence of quantities of non-radioactive aerosols. These are discussed below in connection with commonly utilized removal features.

Containment Sprays

Containment sprays are used in many PWR designs to provide post-accident containment cooling as well as to remove radioactive aerosols. Sprays are effective in reducing the airborne concentration of elemental and particulate iodines as well as other particulates, such as cesium, but are not effective in removing noble gases or organic forms of iodine. Typical PWR containment

spray systems are capable of rapidly reducing the concentration of airborne activity. Nourbakhsh[11] has examined the effectiveness of containment sprays, as evaluated in NUREG-1150 in decontaminating both in-vessel and ex-vessel releases. The overall effectiveness of spray systems, given in terms of a decontamination factor (DF), and assuming no containment failure, ranged from about 30 to 40 for PWRs and 10 to 20 for BWRs. Once the bulk of the activity has been removed, however, the spray becomes significantly less effective in reducing remaining fission products.

The NRC's Standard Review Plan (SRP), Section 6.5.2[12] currently indicates that the pH level of the containment sump solution should be maintained at values at or above 7, commencing with spray recirculation, to minimize revolatilization of iodine in the sump water. Current guidance states that containment spray systems be initiated automatically, because of the instantaneous appearance of the source term within containment, and that the spray duration not be less than 2 hours.

Revised source term insights suggest that spray systems are highly effective in the removal of particulate aerosols, both radioactive and non-radioactive. Revised insights on timing imply, however, that spray system actuation might be somewhat delayed for radiological purposes, but that the spray system should operate over a longer period of up to about 10 or more hours.

BWR Suppression Pools

BWRs use pressure suppression pools to condense steam resulting from a loss-of-coolant accident. Prior to the release to the reactor building, these pools also scrub radioactive fission products that accompany the steam. Regulatory Guide 1.3 does not allow credit for fission product scrubbing by BWR suppression pools, but SRP Section 6.5.5[13] has been revised to allow such credit. The pool water will retain soluble, gaseous, and solid fission products such as iodines and cesium but provides no attenuation of the noble gases. Calculations for a BWR with a Mark I containment[14] used in NUREG-1150 indicate that DFs ranged from 1.2 to about 4000 with a median value of about 80. The variation in DFs for different release phases has also been examined[11]. Median DFs during the in-vessel release phase ranged from 50 to 80, whereas for the ex-vessel phase these were markedly lower and ranged from about 7 to 10. Hence, the suppression pool has been shown to be effective in scrubbing some of the most important radionuclides such as iodine, cesium, and tellurium, as these are released in the early in-vessel phase.

Suppression pool bypass is an important aspect that places an upper limit on the overall performance of the suppression pool in scrubbing fission products. For example, if as little as 1 % of the fission products bypass the suppression pool, the effective DF, taking bypass into account, will be less than 100, regardless of the pool's ability to scrub fission products.

Although decontamination factors for the suppression pool are significant, both for radioactive as well as non-radioactive aerosols, a key question is the potential for iodine re-evolution. Re-evolution of iodine was judged to be important in WASH-1400 for accident sequences where the containment had failed and the suppression pool was boiling. There is presently no requirement for pH control in BWR suppression pools. Hence, it is possible that suppression pools would scrub substantial amounts of iodine in the early phases of an accident, only to re-evolve it later as elemental iodine. Therefore, if credit were to be given for long-term retention of iodine in the suppression pool, maintenance of the pH at or above a level of 7 would need to be shown. The effect on the pH level of additional materials likely to be in the suppression pool as a result of a severe accident, such as cesium borate or cesium hydroxide and core-concrete decomposition products, may be important in this regard and is presently being investigated for the NRC by ORNL. It is important to note, however, that this is not a matter of concern for present plants since all BWRs employ safety-related filtration systems designed to cope with large quantities of elemental iodine. Hence, even if the suppression pool were to re-evolve significant amounts of elemental iodine, it would be retained by the existing downstream filtration system.

Filtration Systems

ESF filtration systems are optimized to remove and retain radioactive iodine released during postulated accident conditions. Regulatory Guide 1.52[15] provides NRC guidance in the design and evaluation of these systems.

Charcoal adsorbers can be provided, as indicated in Regulatory Guide 1.52, to remove from 90 to 99 % of the elemental iodine and from 30 to 99 % of the organic iodide, depending upon the specific filter train design. Because of the presence of HEPA filters and demisters, it is clear that particulate aerosols will also be effectively removed.

Revised accident source terms may have several implications for ESF filtration systems. Present ESF filtration systems, while effective in removal of particulates, are not sized to handle the mass loadings of non-radioactive aerosols that might be released as a result of the ex-vessel release phase. However, ESF filtration systems are often employed in BWRs in conjunction with suppression pools. Under these conditions, or if significant quantities of water are overlaying molten core debris, large quantities of nonradioactive (as well as radioactive) aerosols will be scrubbed and retained by these water sources, thereby reducing the aerosol mass loads upon the filter system.

A second implication of revised source term insights for ESF filtration systems is the impact of revised understanding of the chemical form of iodine within containment. Present ESF filtration systems presume that the chemical form of iodine is primarily elemental iodine, and these systems include charcoal adsorber beds to trap and retain elemental iodine. Assuming that pH control is

maintained within the containment, a key question is whether charcoal beds are necessary. Two questions appear to have a bearing on this issue and must be addressed, even assuming pH control. These are (1) to what degree will CsI retained on particulate filters decompose to evolve elemental iodine? and (2) what effect would hydrogen burns have on the chemical form of the iodine within containment? Based on preliminary information, CsI retained on particulate filters as an aerosol appears to be chemically stable provided that it is not exposed to moisture. Exposure to moisture, however, would lead to CsI decomposition and production of iodine in ionic form (I^-), which in turn would lead to re-evolution of elemental iodine. Although ESF filtration systems are equipped with demisters and heaters to remove significant moisture before it reaches the charcoal adsorber bed, an additional concern is that the demisters themselves may trap some CsI aerosol. At the present time the question of whether charcoal adsorbers could be eliminated from ESF filtration systems, assuming pH control, remains unresolved.

Water Overlying Core Debris

Significant depths of water overlying any molten core debris after reactor pressure vessel failure are likely to scrub and retain particulate fission products. The question of coolability of the molten debris as a result of water overlying it is still under investigation. At the present time, the degree of scrubbing as a function of water depth is under investigation by the NRC and its contractors.

Existing data[16] indicate that both subcooled as well as boiling water layers having a depth of about 3 meters had measured DFs of about 10. Hence, significant depths of water overlying any core debris, in conjunction with other systems, such as filters, are seen as providing a highly effective means of coping with large masses of released aerosols.

Aerosol Deposition

Aerosol deposition depends upon several natural processes that remove aerosols from the containment atmosphere over a period of time. Of these, gravitational settling is generally considered to be the most important, and is influenced by the degree of aerosol agglomeration.

Containment atmosphere aerosol removal rates were also evaluated[11] for the NUREG-1150 plants plus LaSalle. Typical removal rates, or lambdas, for natural aerosol deposition ranged from about 0.2 to 0.4 per hour. The major factor to be noted in natural aerosol deposition is its relatively slow rate compared to engineered features, such as sprays. Spray systems are capable of reducing the containment atmospheric concentration by about an order of magnitude in about 15 to 20 minutes, but natural aerosol deposition processes will require 4 to 10 hours, depending on the plant and sequence, for the same reduction factor.

V. Conclusions

Revised reactor accident source terms based upon a complete core-melt accident, and making use of improved insights with regard to fission product timing, composition and iodine chemical form have been issued by the NRC for public comment.

Preliminary implications for nuclear air cleaning requirements suggest that existing air cleaning systems, together with sources of water such as BWR suppression pools and other water sources provided to cool core debris can provide a high degree of mitigation for such releases. Hence, reactor designers should recognize that nuclear air cleaning requirements may be accomplished both by conventional, existing systems as well as by combining these with other plant features. Additional aspects regarding timimg and the need to retain the capability to remove elemental iodine, however, remain to be determined.

V. References

1. *U.S. Nuclear Regulatory Commission: "Reactor Site Criteria", Title 10, Code of Federal Regulations (CFR), Part 100, Washington, DC (1962).*

2. *U.S. Nuclear Regulatory Commission: "Assumptions Used for Evaluating the Potential Radiological Consequences of a Loss of Coolant Accident for Boiling Water Reactors", Regulatory Guide 1.3, Rev. 2, Washington, DC (1974).*

3. *U.S. Nuclear Regulatory Commission: "Assumptions Used for Evaluating the Potential Radiological Consequences of a Loss of Coolant Accident for Pressurized Water Reactors", Regulatory Guide 1.4, Rev.2, Washington, DC (1974).*

4. *DiNunno, J.J., et. al.,: "Calculation of Distance Factors for Power and Test Reactor Sites", Technical Information Document (TID)-14844, U.S. Atomic Energy Commission, Washington, DC (1962).*

5. *U.S. Nuclear Regulatory Commission: "Reactor Safety Study-An Assessment of Accident Risks in U.S. Commercial Nuclear Power Plants", WASH-1400, Washington, DC (1975).*

6. *U.S. Nuclear Regulatory Commission: "Revision of 10 CFR Part 100, Revisions to 10 CFR Part 50, New Appendix B to 10 CFR Part 100 and New Appendix S to 10 CFR Part 50", Commission Paper SECY-92-215, Washington, DC (1992).*

7. *U.S. Nuclear Regulatory Commission: "Severe Accident Risks: An Assessment for Five U.S. Nuclear Power Plants", NUREG-1150, Final Summary Report, Washington, DC (1990).*

8. *Beahm, E.C., Weber, C.F., and Kress, T.S. : "Iodine Chemical Forms in LWR Severe Accidents", NUREG/CR-5372, Oak Ridge National Laboratory, Oak Ridge, Tennessee (1992).*

9. *Soffer, L. et. al.,: "Accident Source Terms for Light-Water Nuclear Power Plants", NUREG-1465 (Draft Report for Comment), U.S. Nuclear Regulatory Commission Washington, DC (1992).*

10. *Silberberg, M., et. al.,: "Reassessment of the Technical Bases for Estimating Source Terms", NUREG-0956, Final Report, U.S. Nuclear Regulatory Commission, Washington, DC, (1986).*

11. *H.P. Nourbakhsh and S.E. Perez: "Assessment of In-Containment Aerosol Removal Mechanisms",Draft NUREG/CR Report, Brookhaven National Laboratory, Upton, New York, (1992).*

12. *U.S. Nuclear Regulatory Commission, "Containment Spray as a Fission Product Cleanup System", Standard Review Plan, Section 6.5.2, Rev. 2, NUREG-0800, Washington, DC, (1988).*

13. *U.S. Nuclear Regulatory Commission: "Pressure Suppression Pool as a Fission Product Cleanup System", Standard Review Plan, Section 6.5.5, Rev. 0, NUREG-0800, Washington, DC, (1988).*

14. *Denning, R.S., et. al.,: "Radionuclide Release Calculations for Selected Severe Accident Scenarios: BWR Mark I Design", NUREG/CR-4624, Vol. 1, Batelle Columbus Laboratories, Columbus, Ohio, (1986).*

15. *U.S. Nuclear Regulatory Commission, "Design, Testing, and Maintenance Criteria for Engineered-Safety-Feature Atmosphere Cleanup system Air Filtration and Adsorption Units of Light-Water-Cooled Nuclear Power Plants", Regulatory Guide 1.52, Revision 2, (1978).*

16. *Hakii, J. et. al.,:"Experimental Study on Aerosol Removal Efficiency for Pool Scrubbing Under High Temperature Steam Atmosphere," Proceedings of the 21st DOE/NRC Nuclear Air Cleaning Conference, August 1990.*

POST-ACCIDENT AIR LEAKAGE ANALYSIS IN A NUCLEAR FACILITY VIA T-METHOD AIRFLOW SIMULATION

Tony Farajian, Gurinder Grewal, and Robert J. Tsal
Fluor Daniel Inc.
Irvine, CA

Abstract

This paper explains application of the T-Method for calculating air leakages and pressure differentials in a nuclear facility following a Design Basis Accident (DBA).

The nuclear facility ventilation systems are designed to maintain confinement of airborne radioactive material during normal operation and after a DBA. The confinement is achieved by maintaining the negative pressure below the outside atmospheric pressure. The ventilation exhaust capacity, required to maintain negative pressures in the facility during normal operation, is estimated using building components leakage data. However, following a DBA, the ventilation system equipment, ductwork, shielding windows, doors, etc. may be damaged and create new leakage paths. The system designer needs to know the exhaust airflow capacity required to maintain radioactive material confinement in the facility following a DBA.

The T-Method is a new computational tool for hydraulic networks optimization and simulation. Simple numerical computation in conjunction with airflows, pressures, and fan characteristics simulation for a complicated tree-network makes this method an efficient tool for studying air leakage flows and pressure in a facility following a DBA.

I. Nomenclature

C = local loss coefficient, dimensionless
D = duct diameter, m [in]
D_f = equivalent-by-friction diameter of rectangular duct, m [in]
D_v = equivalent-by-velocity diameter of rectangular duct, m [in]
H = duct height, m [in]
Ks = Sectional flow conductivity coefficients, dimensionless
Kt = Flow conductivity coefficients for a subtree, dimensionless
Kt_{sys} = System flow conductivity coefficients, dimensionless
L = duct length, m [in]
P = pressure, Pa [in.H_2O]
Pdn = pressure at downstream node, Pa [in.H_2O]
P_{fan} = fan total pressure, Pa [in.H_2O]
P_{sys} = System total pressure, Pa [in.H_2O]
Pup = pressure at upper node, Pa [in.H_2O]
Q = duct airflow, m^3/s [cfm]

Pup = pressure at upper node, Pa [in.H_2O]
Q = duct airflow, m^3/s [cfm]
Q_{fan} = fan airflow rate, m^3/s [cfm]
Q_{sys} = system airflow, m^3/s [cfm]
Re = Reynolds number, dimensionless
V = mean air velocity, m/s [fpm]
W = duct width, m [in]
DP = total pressure loss, Pa [in.H_2O]
DPex = excessive pressure in a path, Pa [in.H_2O]
DPs = system pressure loss, Pa [in.H_2O]
DP_{sys} = System pressure loss, Pa [in.H_2O]
DPp = path pressure loss, which is the sum of pressure losses for all sections in a path, Pa [in.H_2O]
f = friction factor, dimensionless
g_c = dimensional constant, 1.0 (kg-m)/(N-s^2) [32.2 (lb_m-ft)/(lb_f-s^2)]
y = degree of node
e = absolute roughness factor, m [ft]
q = air density, kg/m^3 [lbm/ft^3]
m = kinematic viscosity, m^2/s [ft^2/s]

Subscripts: r = Return part of the system
s = Supply part of the system

I. Introduction

The protection of the public and the environment from radioactivity is of paramount importance in the design of nuclear facilities. The ventilation systems of the nuclear facilities provide confinement of radioactive material by maintaining negative pressure differentials in the facility during normal operation and after a Design Basis Accident (DBA). The negative pressure differentials in the facility assure that the air leakage is always from the outside into the facility and, within the facility, from clean areas towards areas with increasing potential of contamination. The exhaust air is filtered through multiple stages of HEPA filters for protection of the public and the environment. The facility exhaust fans of larger capacity than the supply fans will compensate for leakage into the facility. The facility inleakage is calculated using leakage data from available sources in the literature.[1] The calculated leakage rate is increased by an appropriate safety factor to size the facility exhaust fans. The outleakage from the facility after a DBA is prevented by stopping the supply fans and operating one exhaust fan. The damage to the ventilation system equipment, ductwork, shielding windows, doors, etc. may create new leakage paths in the facility following a DBA. These leakage paths can only be postulated, because it is impossible to predict accurately the extent of damage to the facility. If the operating exhaust fan capacity is significantly larger than actual leakage into the building, then the building pressure becomes excessively negative and hinders safe exit of the operating personnel. Conversely, if the exhaust capacity of the operating exhaust fan is not sufficient to maintain significant negative pressure in the building or minimum

velocity across confinement openings, then confinement of radioactive material within the building can not be assured.

The T-Method simulation technique is used for studying airflow leakage distribution and pressure differentials in a facility and for optimum sizing of the exhaust fans for post DBA operation.

II. T-Method Theory

T-Method was initially developed for fan-duct system optimization using life cycle cost as the objective function and was further developed to simulate steady state performance of an existing fan-duct system. The theory, calculation procedures, and simulation techniques are fully published.[2,3]

The pressure losses at nodes of an airflow network will always balance in accordance with the Kirchoff's Law. If the network design does not provide this balancing, the flow rates will balance themselves and the total flow and pressure loss will match the fan performance curve. The purpose of the T-Method simulation is to find actual flow and pressure losses in a network.

The T-method is based on the same tee-staging concepts as Dynamic Programming[4,5,6] and incorporates the following major procedures:

1. **System condensing.** Condense the branched tree system into a single imaginary duct section with identical hydraulic characteristics and the same owning cost as the entire system.

2. **Selection of an operating point.** Determine the system flow and pressure by locating the intersection of fan and system curves.

3. **System expansion.** Expand the condensed imaginary duct section into the original system with the distribution of actual pressure losses.

A. Definition of Parameters

The Darcy-Weisbach equation for round and rectangular airflow path is

Round:
$$\Delta P = \left(\frac{f\,L}{D} + \Sigma C \right) \frac{V^2 \rho}{2\, g_c} \qquad (1a)$$

Rectangular:
$$\Delta P = \left(\frac{f\,L}{D_f} + \Sigma C \right) \frac{V^2 \rho}{2\, g_c} \qquad (1b)$$

where the equivalent-by-friction diameter is

$$D_f = 2 \frac{H W}{H + W} \quad (2)$$

Introducing the equivalent-by-velocity diameter for a rectangular path

$$D_v = 1.128 (H W)^{0.5} \quad (3)$$

and the coefficient μ

Round: $$\mu = f L + \Sigma C D \quad (4a)$$

Rectangular: $$\mu = \left(\frac{f L}{D_f} + \Sigma C \right) D_v \quad (4b)$$

Then substitute μ into the Darcy-Weisbach equation (1a and 1b) to obtain the following equation for a single duct pressure loss

Round: $$\Delta P = 0.811 g_c^{-1} \mu \rho^2 D^{-5} \quad (5a)$$

Rectangular: $$\Delta P = 0.811 g_c^{-1} \mu \rho^2 D_v^{-5} \quad (5b)$$

Since D and D_v are the same for round and equivalent round rectangular paths it is possible to identify flow in terms of a diameter and a pressure loss by using coefficient μ. Thus

$$Q = 1.1107 \left(\frac{g_c}{\mu \rho}\right)^{0.5} D^{2.5} (\Delta P)^{0.5} \quad (6)$$

By introducing the variable Ks

$$Ks = 1.1107 \left(\frac{g_c}{\mu \rho}\right)^{0.5} D^{2.5} \quad (7)$$

the pressure loss at duct section becomes

$$\Delta P = \left(\frac{Q}{Ks}\right)^2 \quad (8)$$

and flow is

$$Q = Ks \Delta P^{0.5} \quad (9)$$

Physically, the sectional coefficient Ks is path conductivity.

B. Condensing two duct sections connected in series.

The system in Figure 1 contains two paths connected in series. Let us introduce an imaginary duct section (1-2) called condensed. This section must satisfy the following conditions:

- flow of the condensed section (1-2) must be the same as the flow of the original sections; namely

$$Q_{1-2} = Q_1 = Q_2 \qquad (10)$$

- pressure loss of the condensed section (1-2) must be equal to the sum of the pressure losses for the original sections as named below

$$\Delta P_{1-2} = \Delta P_1 + \Delta P_2 \qquad (11)$$

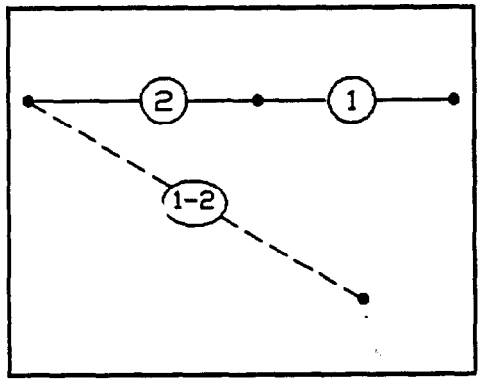

Figure 1. Two Sections Connected in Series

From Equations 8, 10, and 11 following relationship is derived

$$Ks_{1-2} = (Ks_1^{-2} + Ks_2^{-2})^{-0.5} \qquad (12)$$

C. Condensing duct sections connected in parallel.

When condensing two sections, 1 and 2, in parallel into an imaginary section (1-2) (Figure 2), the condensed section must satisfy the following conditions.

Flow:
$$Q_{1-2} = Q_1 + Q_2 \qquad (13)$$

Pressure:
$$\Delta P_{1-2} = \Delta P_1 = \Delta P_2 \qquad (14)$$

After substituting Equation 9 into Equation 13, the relationship between the characteristics of a condensed duct section and the original ducts is

$$Ks_{1-2} = Ks_1 + Ks_2 \qquad (15)$$

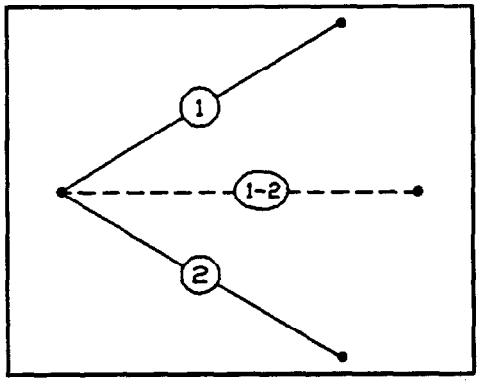

Figure 2. Two Sections Connected in Parallel

D. Condensing a tee

Let us condense the tee shown in Figure 3 containing one node, two children (sections 1 and 2) in parallel, and one parent (section 3) in series (see Terminology Section VII for definitions). First, condense the parallel sections 1 and 2 using Equation 15. Thus

$$Ks_{1-2} = Ks_1 + Ks_2 \qquad (16)$$

Then using Equation 12 condense sections (1-2) and 3 in series to obtain Equation 17.

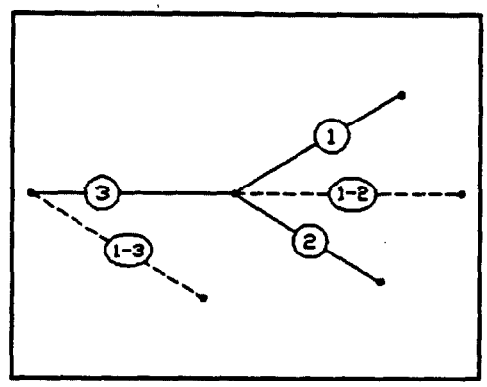

Figure 3. Condensing a Tee

$$Kt_{1-3} = [(Ks_1 + Ks_2)^{-2} + Ks_3^{-2}]^{-0.5} \qquad (17)$$

E. Condensing a subsystem

The purpose of condensing a subsystem is to decrease the tree depth from the maximum to 1 by a series of repetitive calculations using Equation 17 for all tees. The starting tee must be any infant tee. For the 5-section system illustrated by Figure 4, the starting tee is 1-2-3. This tee must be condensed into the imaginary section (1-3) by using Equation 17. Then the tee (1-3)-4-5 condensed into the imaginary root section (1-5). Therefore, the entire subsystem is condensed into one section only. The number of operations is equal to the number of internal nodes minus one.

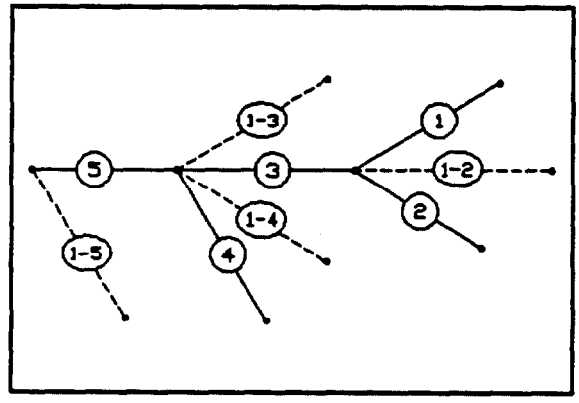

Figure 4. Condensing a Tree

A practical condensing procedure rule is that the next section can be selected only when its children sections have already been used in previous calculations.

F. Operating Point Selection

The T-method is based on condensing the entire system into one single root section. The cumulative coefficient of conductivity for the system, Kt_{sys}, is the last step for the condensed root section. Therefore, from Equation 9 we obtain Equation 18, where Ks is replaced by Kt_{sys} for the condensed system.

$$Q_{sys} = Kt_{sys} \Delta P_{sys}^{0.5} \tag{18}$$

Since $Q_{sys} = Q_{fan}$ and $\Delta P_{sys} = P_{sys} = P_{fan}$ the actual operating point is where the system curve, represented by Equation 18, and the fan performance curve intersect.

G. Expansion

The expansion procedure distributes the available fan pressure throughout the system sections. Unlike the condensing procedure, the expansion procedure starts at the root section and continues in the direction of the terminals. Substitute Q_{1-2} and Q_2 from Equation 9 into Equation 13, and rearrange with respect to Q_1. Thus,

$$Q_1 = Ks_{1-2} \Delta P_{1-2}^{0.5} - Ks_2 \Delta P_2^{0.5} \tag{19}$$

Apply Equation 15 for two duct sections in parallel and substitute $\Delta P_{1-2}^{0.5}$ by Q_{1-2} / K_{1-2} to yield the following equation.

Section 1:
$$Q_1 = Q_{1-2} \; T_1 \tag{20}$$

where

$$T_1 = \frac{Ks_1}{Ks_1 + Ks_2} \tag{21}$$

Section 2:
$$Q_2 = Q_{1-2} \; T_2 \tag{22}$$

where

$$T_2 = \frac{Ks_2}{Ks_1 + Ks_2} \tag{23}$$

Analogous equations can be derived for each duct section excluding the root section. Coefficients T_r and T_s for the root sections are always equal to 1, as well as any other section with no brothers (degree of node is 1).

H. Iterations

The T-Method is iterative like most other existing analytical and numerical flow distribution methods, except Dynamic Programming.[6] Many parameters, such as the C-coefficients for junctions and transitions, depend on airflows and are not known at the beginning. The operating point on the fan curve performance is selected after the cumulative system coefficient Kt_{sys} is known.

In order to calculate pressure loss and duct size in each section, equal air velocity is assigned to all duct sections, except for the presized sections. This step in the simulation process is known as data initiation. The T-method converges very efficiently, and usually three iterations are sufficient to obtain solution with a high degree of accuracy.

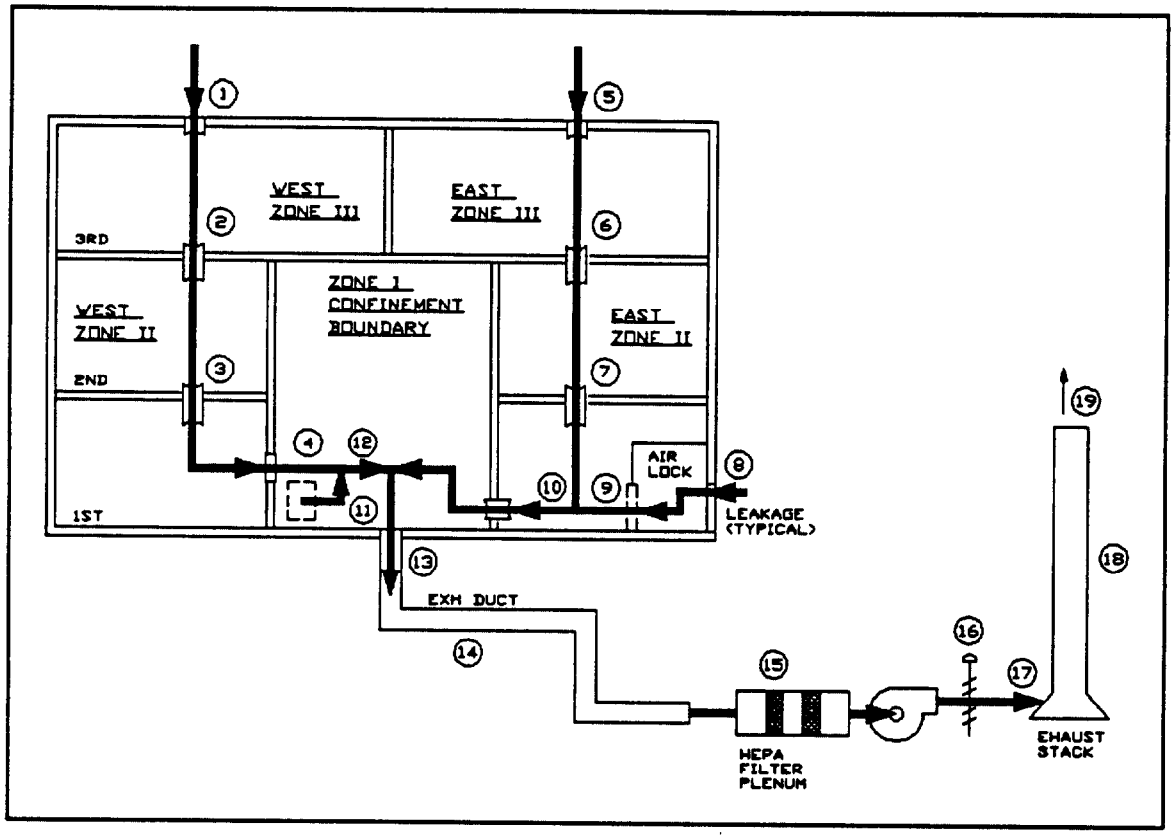

Figure 5. Schematic Airflow

III. T-Method Application

A. System Description

A typical application for a nuclear facility is illustrated in Figure 5. The building is divided into three confinement Zones. The interior cells are designed for handling highly radioactive material and are designated as

Zone I. The cell operating areas surrounding the Zone I are classified as Zone II. The equipment room has minimum potential for radioactive contamination and is classified as Zone III. Zones II and III are divided into east and west areas. The Zone I exhaust system contains the airborne radioactive material within the hot cell following a DBA. The confinement is achieved by maintaining airflow into the hot cell. The hot cell pressure is to be maintained between -25 and -45 Pa (-0.1 and -0.18 in.WG) following a DBA. The T-Method simulation is applied for calculating negative pressure in the cell and air leakage into the cell under different scenarios of facility damage.

The exhaust system consists of an exhaust fan and a 2-stage HEPA filtration unit. The exhaust air from the Zone I is filtered and exhausted through the stack.

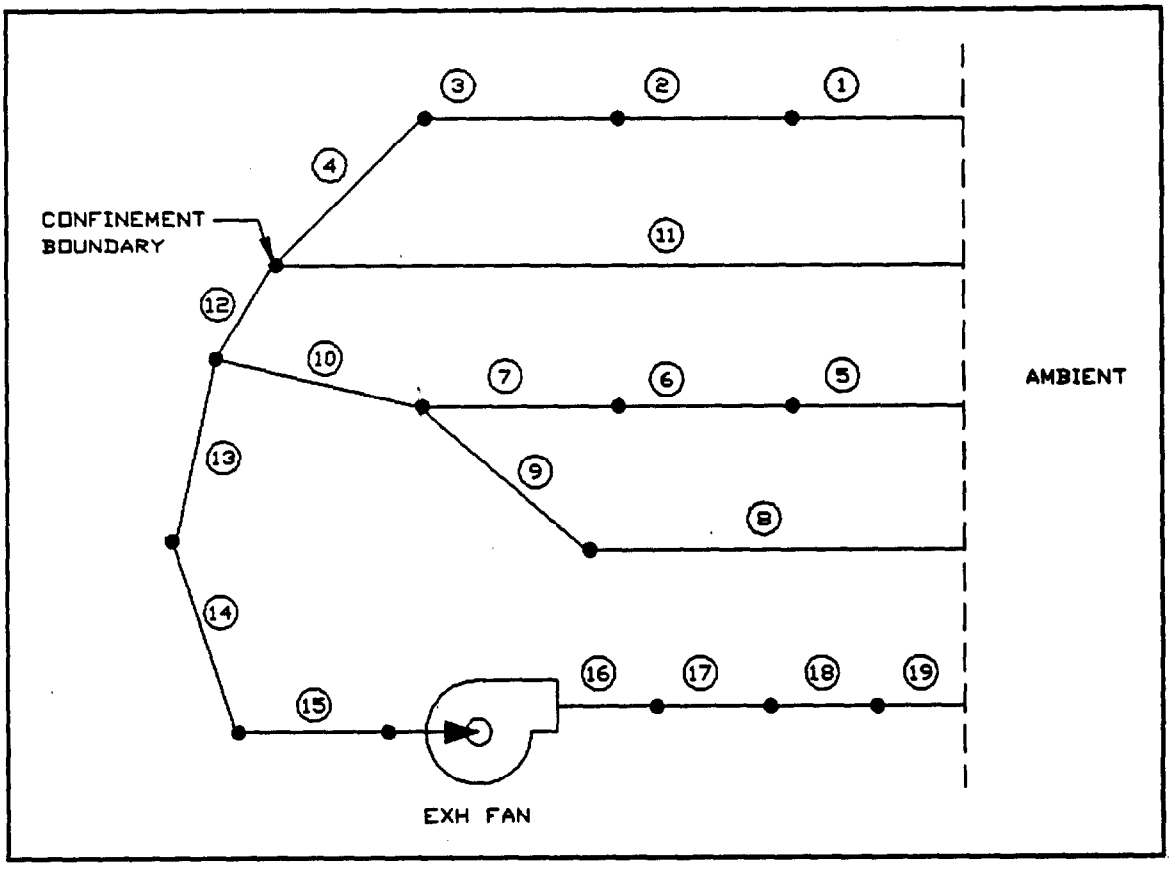

Figure 6. Network Model

B. Network Model

The exhaust system is sized based on the maximum credible breach in the confinement boundary. All credible failures of the facility boundary following a DBA and associate airflow paths are identified. A network model representing the airflow paths is developed (Figure 6).

Following are the postulated failure scenarios in the building after a DBA:

-- Outside air intake ductwork in the equipment room is broken creating open flow paths to the ambient,

-- Supply and exhaust ducts in the operating areas are broken creating open flow paths between the Zone II area and the equipment room,

-- Shielded viewing window between the operating areas and the Zone I confinement boundary is broken, causing open flow path between the two areas,

-- The piping to the Zone I confinement boundary is broken creating leakage flow path between the Zone II areas and the Zone I cell.

Network Description

1) Flow path into the equipment room from outside ambient through damaged outside intake ductwork ..... Sections 1, 5
2) Flow path between floors through damaged ducts .... Sections 2, 3, 6, 7
3) Flow paths into the cell through broken shielding windows ..... Section 4
4) Flow paths from the ambient through air lock doors. The interior airlock doors are considered open in the analysis ..... Sections 8, 9
5) Flow path into the cell through broken pipes ..... Section 10
6) Air leakage into Zone I through emergency exit door ..... Section 11
7) A dummy section to link Sections 11 and 4 for the purpose of network modeling by the T-Method. (No air resistances is considered across this section) ..... Section 12
8) Hot cell connection to the exhaust duct system ..... Section 13
9) Exhaust duct ..... Section 14
10) HEPA Filter Plenum ..... Section 15
11) Isolation damper ..... Section 16
12) Exhaust Stack entrance ..... Section 17
13) Exhaust Stack ..... Section 18
14) Exhaust Stack Exit ..... Section 19

Input Data

The master input data in the T-Method includes air temperature, duct roughness, kinematic viscosity, air density, fan motor efficiency, etc. The fan curve is represented by a number of fan flow-pressure points. These points are confirmed by the program output as the fan curve intersects with the system curve. Computer program indicates if intersection between the fan and system curves is obtained.

Local resistance C-coefficients and size of each section are part of the input data. Obtaining C-coefficients is one of the critical parts of analysis by the T-Method simulation. The ASHRAE Handbook of Fundamentals is recommended as one of the main sources to obtain C-coefficients for various fittings and flow paths. C-coefficients used in this calculation are shown in Table 1.

Table 1. Local Resistance Coefficients

Sec.No.	Fitting	C	Source
1	Entry	0.5	ASHRAE[7], p.32.27, 1-1
2	Entry, Exit	1.0+1.0	ASHRAE[7], p.32.27, 1-1, p.32.28, 1-2
3	Entry, Exit	1.0+1.0	ASHRAE[7], p.32.27, 1-1, p.32.28,
4	Orifice	0.9	Idelchik[8], p.171
5	Entry	0.5	ASHRAE[7], p.32.27, 1-1
6	Entry, Exit	1.0+1.0	ASHRAE[7], p.32.27, 1-1, p.32.28, 1-2
7	Entry, Exit	1.0+1.0	ASHRAE[7], p.32.27, 1-1, p.32.28, 1-2
8	Exit door	Variable	ASHRAE[7], p.23.15, Fig.11., $Q=250(\Delta P/0.3)^{0.55}$, $\Delta P=C(Q/A)^2\rho/2$, $C=5260\ A^2\Delta P^{-0.1}$
9	Orifice	2.3	Idelchik[8], p.171
10	Entry, Exit	2.0	ASHRAE[7], p.32.27, 1-1, p.32.28, 1-2
11	Exit door	Variable	ASHRAE[7], p.23.15, Fig.11., $Q=250(\Delta P/0.3)^{0.55}$, $\Delta P=C(Q/A)^2\rho/2$, $C=5260\ A^2\Delta P^{-0.1}$
12	Dummy	0	
13	Entry	0.5	ASHRAE[7], p.32.27, 1-1
14	3 Elbows, Transition	3.6 + 0.58	ASHRAE[7], p.32.32, 3-6, and p.32.36, 4-4
15	Filter	Variable	ASHRAE[7], p.32.9, $\Delta P=C(V)^2\rho/2$, C=1780
16	Damper	0.52	ASHRAE[7], p.32.47, 6-5
17	Entry	1.0	ASHRAE[7], p.32.27, 1-1
18	None	0	
19	Exit	1.0	ASHRAE[7], p.32.28, 2-1

C. T-Method Computer Calculation

Case 1

Case 1 considers all credible leakage paths shown in Figure 6. The T-Method computer run for a preselected fan and an alternate fan are shown in Table 2 and 3 respectively.

Case 2

The network model for this case is similar to Case 1 except the flow path through section 10 (pipe) is considered closed. The results of the Case 2 computer run are presented in Table 4.

Case 3

The network model for this case is similar to Case 1 except the flow path through section 4 (shielding window) is considered closed. The results of the Case 3 computer run are presented in Table 5.

Input Data Considerations

A large flow coefficient (100,000) is purposely assumed for the closed flow paths to simulate no flow conditions for cases 2 and 3. The total airflow through the system and pressure loss in the filters (section 15) are substantially reduced in this case. C-coefficients that are flow dependent are calculated by using equations presented in Table 1.

E. Analysis of the Results

Case 1 is simulated by the T-Method for a preselected exhaust fan. If the cell pressure is higher (less negative) than the limits, a larger fan is needed to achieve desired pressure in the cell. If the cell pressure is lower (more negative) than the limits, a smaller fan should be selected. This procedure is repeated until a satisfactory fan is selected.

The T-Method output results for Case 1 are presented in Table 2. The results indicate that an exhaust fan with a capacity of 6.62 m^3/s at 1612 Pa will maintain a negative pressure of -65.2 Pa in the hot cell (section 12). Since this pressure is much lower than the desired range of -25 to -45 Pa, a smaller fan is needed. The results with a new fan of 4.88 m^3/s at 1236 Pa capacity indicate a negative pressure of -34.9 Pa in the hot cell (Table 3). This pressure is within the desired limits. The selected exhaust fan is then evaluated for Cases 2, and 3.

TABLE 2. CASE 1 WITH PRESELECTED FAN

FAN–SYSTEM CHARACTERISTIC

Flow, m3/s =	0.8	3.0	5.0	7.0	8.5
Fan dP, Pa =	3600	3200	2300	1450	400
Fan Et, % =	0.60	0.70	0.80	0.70	0.60
System dP, Pa =	23	329	913	1790	2640

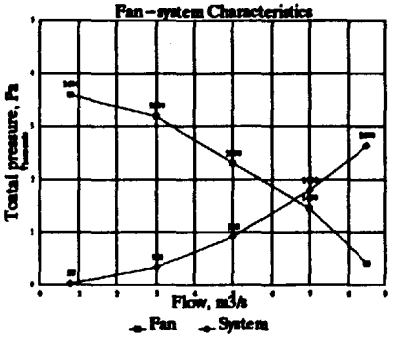

GENERAL DATA

Motor Efficiency	=	0.8	Air Density	=	1.17 kg/m3
Absolute Roughness	=	0.002 m	Kinematic Viscosity	=	1.5E–05 m2/s
Air Temperature	=	45 C	Fan : Airflow	=	6.63 m3/s
Initial velocity	=	0 m	Operating : Pressure	=	1607 Pa
Flow condition	=	0.019 kg/kg	Point : Brake Power	=	18.54 kW
Fan discharge area	=	1 m2			

INPUT DATA							Equiv. Diameter		Velocity–Flow–Pressure				CONDENSING				EXPANSION			
Section No.	Duct Length m	Abeolute Roughness m	Duct Size Height m	Width m	Dia. m	C–Coeff.	by Friction m	by Velocity m	Flow m3/s	Air Vel. m/s	Friction Factor	Actual Press. Loss Pa	Sectional Coefficients		Tee Coefficients		Estimated Flow m3/s	Pressure at Nodes Upper Pa	Pressure at Nodes Lower Pa	Exceed. Pressure Loss in Path Pa
No.	L	R	H	W	D	C	Df	Dv	Q	V	f	ΔP	M	Ks	Kt	T	Qs	Pup	Pdn	ΔPp
1	1.00	0.002	2.000	2.000		0.50	2.000	2.256	5.03	1.26	0.0213	0.5	1.152	7.305	7.305	1.000	5.034	–1.4	–1.9	1.9
2	1.00	0.002	1.000	1.000		2.00	1.000	1.128	5.03	5.04	0.02383	30.2	2.283	0.917	0.910	1.000	5.034	28.8	–1.4	
3	1.00	0.002	1.000	1.000		2.00	1.000	1.128	5.03	5.04	0.02383	30.2	2.283	0.917	0.646	1.000	5.034	58.9	28.8	
4	1.00	0.002	1.200	1.200		1	1.200	1.354	5.03	3.50	0.023	6.6	1	1.960	0.614	0.965	5.034	65.5	58.9	
5	1.00	0.002	2.000	2.000		0.50	2.000	2.256	1.37	0.34	0.02458	0.0	1.156	7.293	7.293	1.000	1.376	–1.8	–1.9	1.9
6	1.00	0.002	1.000	1.000		2.00	1.000	1.128	1.37	1.37	0.02518	2.2	2.284	0.917	0.910	1.000	1.376	0.4	–1.8	
7	1.00	0.002	1.000	1.000		2.00	1.000	1.128	1.37	1.37	0.02518	2.2	2.284	0.917	0.646	0.971	1.376	2.8	0.4	
8	0.10	0.010	0.150	0.150		2.35	0.150	0.169	0.05	2.09	0.05657	6.1	0.404	0.019	0.019	1.000	0.040	2.8	–3.5	3.5
9	0.10	0.010	2.100	0.910		2.30	1.270	1.559	0.05	0.02	0.04942	0.0	3.593	1.643	0.019	0.029	0.040	2.8	2.8	
10	1.00	0.002			0.500	2	0.500	0.500	1.42	7.22	0.02814	62.9	1.0	0.179	0.173	0.214	1.417	65.5	2.8	
11	0.10	0.002	0.150	0.150		1.74	0.150	0.169	0.18	7.99	0.03796	66.3	0.299	0.022	0.022	0.035	0.181	65.5	–0.8	0.8
12	0.10	0.010	10.000	10.000		4.18	10.000	11.280	5.21	0.05	0.02567	0.0	47.153	63.8	0.636	0.786	5.215	65.5	65.5	
13	0.10	0.010	2.000	1.500		0.50	1.714	1.954	6.63	2.21	0.03075	1.4	0.980	5.527	0.800	1.000	6.632	67.0	65.5	
14	20.00	0.010	2.000	1.500			1.714	1.954	6.63	2.21	0.03075	1.0	0.701	6.537	0.794	1.000	6.632	68.0	67.0	
15	4.00	0.002	2.500	2.200		1780	2.340	2.645	6.63	1.21	0.02055	1521.1	4709	0.170	0.166	1.000	6.632	1589.1	68.0	
16	0.10	0.002	1.500	1.000		0.52	1.200	1.382	6.63	4.43	0.02284	6.0	0.721	2.710	0.166	1.000	6.632	1595.1	1589.1	
17	0.10	0.002	2.000	1.500		1.00	1.714	1.954	6.63	2.21	0.02142	2.9	1.956	3.913	0.166	1.000	6.632	1596.0	1595.1	
18	40.00	0.002			2.500		2.500	2.500	6.63	1.35	0.02005	0.3	0.802	11.319	0.166	1.000	6.632	1598.3	1596.0	
19	0.10	0.002			1.500	1.00	1.500	1.500	6.63	3.75	0.0217	8.3	1.502	2.306	0.165	1.000	6.632	1606.6	1598.3	
FAN	1.00						Fan	Fan	6.63	Fan		Fan	Fan	Fan	0.165	1.000	6.632	1606.6	1606.6	

TABLE 3. CASE 1 WITH ALTERNAVE FAN

FAN-SYSTEM CHARACTERISTIC

Flow, m3/s=	3.0	4.0	5.0	6.0	7.0
Fan dP, Pa=	1600	1500	1200	800	400
Fan Ef, %=	0.60	0.70	0.80	0.70	0.60
System dP,Pa=	467	831	1299	1870	2545

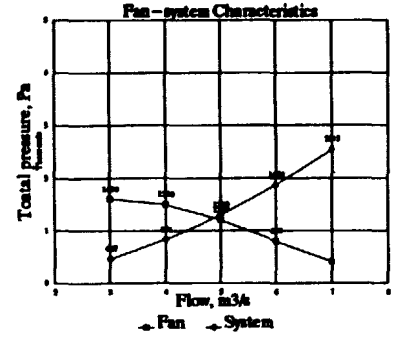

GENERAL DATA

Motor Efficiency	=	0.8	Air Density	=	1.17 kg/m3
Absolute Roughness	=	0.002 m	Kinematic Viscosity	=	1.5E-05 m2/s
Air Temperature	=	45 C	Fan : Airflow	=	4.88 m3/s
Initial velocity	=	0 m	Operating : Pressure	=	1236 Pa
Flow condition	=	0.019 kg/kg	Point : Brake Power	=	9.57 kW
Fan discharge area	=	1 m2			

INPUT DATA							Equiv. Diameter by		Velocity-Flow-Pressure				CONDENSING				EXPANSION			
Section No.	Duct Length m	Absolute Roughness m	Duct Size Height m	Width m	Dia. m	C-Coeff.	Friction m	Velocity m	Flow m3/s	Air Vel. m/s	Friction Factor	Actual Press. Loss Pa	Sectional Coefficients		Tee Coefficients		Estimated Flow m3/s	Pressure at Nodes Upper Pa	Pressure at Nodes Lower Pa	Exceed. Pressure Loss in Path Pa
No.	L	R	H	W	D	C	Df	Dv	Q	V	f	ΔP	M	Ks	Kt	T	Qs	Pup	Pdn	ΔPp
1	1.00	0.002	2.000	2.000		0.50	2.000	2.256	3.70	0.93	0.02184	0.3	1.153	7.303	7.303	1.000	3.697	-1.2	-1.4	1.4
2	1.00	0.002	1.000	1.000		2.00	1.000	1.128	3.70	3.70	0.02403	16.3	2.283	0.917	0.910	1.000	3.697	15.1	-1.2	
3	1.00	0.002	1.000	1.000		2.00	1.000	1.128	3.70	3.70	0.02403	16.3	2.283	0.917	0.646	1.000	3.697	31.4	15.1	
4	1.00	0.002	1.200	1.200		1	1.200	1.354	3.70	2.57	0.02326	3.6	1	1.960	0.614	0.963	3.697	34.9	31.4	
5	1.00	0.002	2.000	2.000		0.50	2.000	2.256	1.01	0.25	0.02581	0.0	1.157	7.289	7.289	1.000	1.006	-1.4	-1.4	1.4
6	1.00	0.002	1.000	1.000		2.00	1.000	1.128	1.01	1.01	0.02578	1.2	2.285	0.917	0.910	1.000	1.006	-0.2	-1.4	
7	1.00	0.002	1.000	1.000		2.00	1.000	1.128	1.01	1.01	0.02578	1.2	2.285	0.917	0.646	0.969	1.006	1.0	-0.2	
8	0.10	0.010	0.150	0.150		1.95	0.150	0.169	0.03	1.45	0.05686	2.4	0.336	0.021	0.021	1.000	0.033	1.0	-1.4	1.4
9	0.10	0.010	2.100	0.910		2.30	1.270	1.559	0.03	0.02	0.05334	0.0	3.593	1.643	0.021	0.031	0.033	1.0	1.0	
10	1.00	0.002			0.500	2.00	0.500	0.500	1.04	5.30	0.02831	33.9	1.0	0.179	0.173	0.213	1.041	34.9	1.0	
11	0.10	0.002	0.150	0.150		1.55	0.150	0.169	0.14	6.27	0.03812	36.3	0.266	0.023	0.023	0.037	0.141	34.9	-1.4	1.4
12	0.10	0.010	10.000	10.000		4.18	10.000	11.280	3.84	0.04	0.02707	0.0	0.003	7931.9	0.637	0.787	3.838	34.9	34.9	
13	0.10	0.010	2.000	1.500		0.50	1.714	1.954	4.88	1.63	0.03087	0.8	0.980	5.527	0.801	1.000	4.879	35.7	34.9	
14	20.00	0.010	2.000	1.500		4.18	1.714	1.954	4.88	1.63	0.03087	7.1	8.870	1.837	0.734	1.000	4.879	42.8	35.7	
15	4.00	0.002	2.500	2.200		2560	2.340	2.645	4.88	0.89	0.02106	1184.1	6772	0.142	0.139	1.000	4.879	1226.9	42.8	
16	0.10	0.002	1.500	1.000		0.52	1.200	1.382	4.88	3.26	0.02305	3.2	0.721	2.710	0.139	1.000	4.879	1230.1	1226.9	
17	0.10	0.002	2.000	1.500		1.00	1.714	1.954	4.88	1.63	0.02177	1.6	1.956	3.913	0.139	1.000	4.879	1231.7	1230.1	
18	40.00	0.002			2.500		2.500	2.500	4.88	0.99	0.02053	0.2	0.821	11.186	0.139	1.000	4.879	1231.9	1231.7	
19	0.10	0.002			1.500	1.00	1.500	1.500	4.88	2.76	0.02193	4.5	1.502	2.306	0.139	1.000	4.879	1236.3	1231.9	
FAN	1.00						Fan	Fan	4.88	Fan		Fan	Fan	Fan	0.139	1.000	4.879	1236.3	1236.3	

The exhaust fan throttling is necessary for Cases 2 and 3 to prevent excessive negative pressures in the hot cell.

Table 6. Summary of Results.

Case No.	Fan flow, m^3/s Fan pressure, Pa	Fan break horse-power, kW	Confinement pressure, Pa
Case 1: all paths are opened	4.88 m^3/s 1236 Pa	9.57 kW	34.9 Pa
Case 2: Section 10 is closed	4.30 m^3/s 1411 Pa	10.39 kW	480.2 Pa
Case 3: Section 4 is closed	4.30 m^3/s 1411 Pa	10.39 kW	478.7 Pa

VI. Conclusion

The T-Method provides a technique for simulating effects of exhaust fan operation on pressure differential and leakage airflow in a facility following a DBA. This simulation can be used to perform "what if" type analyses by changing exhaust fans, and number and size of the leakage paths. The results are used to optimize selection of the exhaust fans, safety classification of components, and pressure controls.

VII. Terminology

The following terminology is adapted from Horowitz and Sahni[9]. Refer to Figure 4 for example.

Ancestors of a node - All sections connected to the given node on the parent's side. The ancestor of the node 1-2-3 is section 5.

Brother - Child section linked to the same node as the current section.

Children and parent - Duct sections connected at the same node. The parent section is the one which collects or distributes the total flow. The rest are children sections. Children sections 1 and 2 have parent section 3.

Degree of a node - The number of children of the node. The degree of node 1-2 is 1.

Degree of a tree - The maximum degree of any node in a tree. The degree of tree for the system in Figure 4 is 2 (no crosses or pentagons).

Descendants of a node - All sections connected to a given node on the children's side.

Down node - The node where the section is linked to its children.

Infant section - Terminal section which has either terminal brothers or no brothers at all. Sections 1 and 2 are infant sections.

Infant tee - A tee which consists of parent and infant sections. Tee 1-2-3 is an infant.

Internal sections (nodes) - Duct section or node which is not a terminal: Sections 3 and 5.

Node level - The maximum number of nodes (including terminals) in any path within a tree or subtree.

Parent and children - Duct sections connected at the same node. The parent section is the one which collects or distributes the total flow. The rest are children sections. Terminal sections have no children and root sections have no parents.

Path - A set of descendants connected in series, for example 1-3-5.

Root - The oldest parent section in a subsystem, mostly the duct section connected to the fan or to the outside air. Section 5 is the root.

Subtree - Same as **descendants of a node.**

Tee - Sections linked at the same node. The tee 1-2-3 consists of Sections 1, 2, and 3.

Terminal sections (nodes) - Sections connected to the terminals: Sections 1, 2, and 4.

Tree - A system of duct sections connected at nodes (junctions) with no circuits. Only unique path can be determined for any section in a tree connected to the root.

Tree depth - The maximum node level for the whole subtree.

Upper node - The node where the section is linked to its parent. For Section 1 the upper node is the intersection of the Sections 1, 2, and 3.

VII. References

1. Koontz, R.L. et.el "Conventional Buildings for Reactor Confinment", Atomic International, A Division of North American Aviation, P.O. Box 309, Canoga Park, California

2. Tsal, R.J.; Behls, H.F. and Mangel,R. "T-Method Duct Design. Part I: Optimization Theory" and "Part II: Calculation Procedure and Economic Analysis." ASHRAE Transactions, Vol. 92, Part 1A, pp. 347-361, 1988.

3. Tsal, R.J.; Behls, H.F. and Mangel, R. "Duct Design. Part III: T-Method Duct Simulation." ASHRAE Transactions, Vol. 96, Part 2, 1990.

4. Bellman, R.E. Dynamic programming. New York: Prinston University Press, 1957.

5. Tsal, R.J. and N.Z. Shor "The use of the steepest descent method for calculating flow distribution in a duct system." Economical cybernetics and operation research, No.2. Kiev: Institute of Cybernetics Publication, 1967.

6. Tsal, R.J. and Chechik, E.I. The use of computers in HVAC systems design. Kiev: Budivelnick Publishing House. Available from the Library of Congress, Washington D.C. ,Service Number TD153.T77, 1968.

7. ASHRAE Handbook - 1989 Fundamentals. Chapter 32, Duct Design. Atlanta: American Society of Heating, Refrigerating and Air-Conditioning Engineers, Inc.

8. Idelchik, Handbook of Hydraulic Resistance, Second edition, Hemisphere Publishing House, New York, 1986

9. Horowitz, E.; and Sahni, S. Fundamentals of Data Structures. New York: Computer Science Press, 1976.

DISCUSSION

PARKER, C. W.: For the simulation method discussed, would it be possible to assume an atmospheric pressure transient - such as that described in Regulatory Guide 1.76 for a design basis tornado - and determine building wall differential pressures during the event?

TSAL: T-method calculates only steady-state flow for different regimes.

THE EXPERIENCE WITH THE EFFECTIVENESS OF FILTERING SYSTEMS FOR THE RADIOACTIVE FALL-OUT FROM THE CHERNOBYL ACCIDENT IN GERMANY

Dr. H. Braun
Federal Ministry for Environment, Nature Conservation and Reactor Safety
Husarenstr.. 30
5300 Bonn
GERMANY

Abstract

The reactor accident in Chernobyl on April 26, 1986 lead to the release of approximately $2 \cdot 10^{12}$ MBq of aerosol bound activity. The aerosols were transported by the air around the world. In Germany the survalence monitors at nuclear power plants registered an increase in the air born activity due to the accident. More than 80% of the aerosol bound activity was removed by the inlet filters at the nuclear power plants. The ^{131}I activity was mostly in gas form, approx. 70% to 80%, and was therefore not retained in the filter systems.

1. Introduction

On April 26, 1986 in Block 4 of the Chernobyl nuclear power plant a series of events lead to the most serious accident in the history of the civil nuclear power industry. The accident did not occur during normal operation but rather as a result of an extraordinary situation in which a poorly planned experiment ignored normal safety precautions. Reconstruction of the situation that lead to the accident indicates that the reactor went through two uncontrolled power excursions. The first excursion lead to reactor pressure tube damage causing the coolant to boil. This caused a rapid increase in the pressure which burst the reactor tubes blowing the 1000 t shield covering the reactor into the roof of the reactor building. The hole in the roof allowed the radioactive gases, aerosols and larger particles from the core to escape into the environment. The second excursion lead to a chemically cause explosion, due to a zirconium water reaction creating hydrogen. The explosions and the thermally driven plume above the core melt down drove large amounts of radionuclides into the atmosphere, from where they were transported around the world. It is estimated that a total activity of $2 \cdot 10^{12}$ MBq in condensible fission products plus again as much activity in nobel gases, ^{85}Kr and ^{133}Xe, was released over the 10 days after the accident[1].

2. Nuclide Spectrum and Release History

After the reactor accident at Chernobyl the Russian officials made measurements of the particle bound radionuclides in the air above the reactor at various times after the accident, table 1[1]. The values are listed in percent of the total activity measured. The nuclide spectrum is missing the noble gasses since they are not particle bound. For example missing in the nuclide spectrum are ^{133}Xe and ^{85}Kr which made up a large portion of the released activity but were not captured in the sampling device's filter since they were not bound to air carried particles. Likewise the portion of ^{131}I which was in gas form is not accounted for in this table.

Characteristic of this accident was the release of large amounts of radionuclides over a time span of about 10 days. Only 25% of the activity was released on the first day, about $74 - 81 \cdot 10^{10}$ MBq[1]. The majority of this was released within the first few minutes coupled to the initial reactor core melt down and the two explosions. The nuclide spectrum for this phase was nearly identical to the melted fuel enriched with noble gases and highly volatile compounds, especially tellurium. During the next 4 days after the explosions the release rate died down exponentially until on April

29 it was approximately 10^{11} MBq/d. The release rate continued to decrease until May 2 when the release was measured to be about $7.4 \cdot 10^{10}$ MBq/d. The radionuclides from this second phase were carried into the atmosphere by the heat driven plume caused by the melted down reactor core. The nuclide spectrum was similar to the nuclide spectrum release by the explosions. In the period from 28 April to 2 May 40 t of B_4C, 800 t of granit, 1800 t of sand and 2400 t of lead were dumped onto the reactor by helicopter.

TABLE 1: **Activity bound to aerosols, measured above the Reactor after the accident in 1986 in % of the total emission of aerosols**

Isotope*	Date after the Accident					
	April		May			
	26	29	2	3	4	5
^{95}Zr	4.4	6.3	9.3	0.6	7.0	20
^{95}Nb	0.6	0.8	9.0	1.3	8.2	18
^{99}Mo	3.7	2.6	2.0	4.4	2.8	3.7
^{103}Ru	2.1	3.0	4.1	7.2	6.9	14
^{106}Ru	0.8	1.2	1.1	3.1	1.3	9.6
^{131}I	5.6	6.4	5.7	25	8.2	19
^{132}Te + ^{132}I	40	31	17	45	15	8.6
^{134}Cs	0.4	0.6	0.6	1.6	0.6	
^{136}Cs	0.3	0.4	0.5	0.9		
^{137}Cs			1.4	3.7	1.3	2.2
^{140}Ba	3.2	4.1	8.0	3.3	13	12
^{140}La	11	4.7	15	2.3	19	17
^{141}Ce	1.4	1.9	7.6	0.9	6.4	15
^{144}Ce	1.6	2.4	6.1		5.1	11
^{147}Nd	1.4	1.7	2.5		2.1	5.4
^{239}Np	23	3.0	11	0.6	2.8	6.8

In bold type face the nuclides which dominated the fall out in Germany.
* Radioactive nuclides in the gas form are missing, e.g. ^{85}Kr, ^{133}Xe and iodine.

On May 3 a third phase began with a rapid increase in the quantity of radionuclides being released. Volatile fission products such as iodine and cesium, were proportionally over-represented, compared to the initial spectrum, while the non-volatile oxides such as oxidized cerium, barium and zircronium, were under-represented. Nine to ten days after the actual accident the radionuclide release reached 40% of the original release rate. The cause of this increase in the release rate can be explained by the heating of the badly damaged core, which was now insulated from the environment. The increased temperature caused fission products to migrate out of the core matrix and caused chemical changes in the core material, which lead to the increased amount of fission products escaping into the atmosphere in the form of aerosols[1].

The release was stopped by special actions from the Russian officials, which included injecting liquid air into the damaged reactor building to reduce the temperature. As a result of the liquid air injection the reactor core began to cool and air shafts were created so that further cooling due to

natural convection occured. The cooling lead to a rapid decrease in the activity release. By May 9 the release rate had been reduced to $4 \cdot 10^8$ MBq/d and by May 20 to about $7 \cdot 10^{11}$ Bq/d[1].

3. Nuclide Transport to Germany

Radioactivity in the air is continuously monitored from ground based sensors in Germany including the surveillance monitors at nuclear power plants. The first air carried radionuclides from Chernobyl to arrive in Germany were registered in Berlin, Munich and Regensburg on the night of April 29 through April 30. On May 1 radioactivity was registered in Freiburg, Offenbach a.M. and Saarbrücken. Finally on May 2 activity in the air was measured in the extreme west of Germany in Aachen, Essen and Norderney. In the northern areas of Germany, Hannover and Schleswig, only a minimal increase over the normal background was registered. The contamination in southern Germany was the highest. The highest daily averages for the total activity concentration in the air for selected cities are listed below[2],

Southern Germany
Regensburg 31 Bq/m^3 on April 30
Munich 54 Bq/m^3 on May 1

Northern Germany
Hannover 1.7 Bq/m^3 on May 4
Schleswig 0.7 Bq/m^3 on May 6.

By May 10 the activity concentration in the air at all the German monitoring stations was below 1 Bq/m^3[2]. The German annual average activity in the air is normally below 1.1 mBq/m^3. In 1986 due to the Chernobyl accident the annual average was 116 mBq/m^3, where Munich had the highest with 434 mBq/m^3 and Schleswig the lowest with 7.6 mBq/m^3[2]. The nuclide spectrum was dominated by short lived nuclides with a small fraction of long lived volatile fission products. The dominate nuclides registered in Germany were, ^{103}Ru, ^{131}I, ^{132}Te/^{132}I, ^{137}Cs, ^{134}Cs and ^{140}Ba/^{140}La. Strontium isotopes were also registered in small amounts. The ^{89}Sr concentration was 7.5% of the ^{137}Cs concentration and ^{90}Sr 1.2%. An increase in the alpha activity in the air was not registered. This was confirmed by many laboratory nuclide specific measurements which found no increase in the actinides[2].

In Fig. 1 the average monthly air born radioactivity from all the monitoring stations is plotted against the month. The peak values from Chernobyl are significantly higher compared to the air born activity from the nuclear tests, in the year 1971.

4. Filter Class and Retention Capability

The ability of a filtering system to remove dust and aerosols from the air depends on the filter type. The most important classification parameter for a filter is its retention grade, which depends on the particle size. Filters are divided into various classes, A for coarse grade filters, B for fine dust and C for aerosol filters. Most filter systems are multi-stage with a coarse filter followed by fine filters.

Table 2 shows the filter classes and their percent retention as a function of particle size[3]. The filter classifications in table 2 column 2, are the European EUROVENT standards[4] and in column 3 the older German DIN 24185 standards[4]. The columns 4 to 8 in table 2 give the percent of the particles having that diameter which are retained by the filter class. For example an EU 6 filter will retain 30% of the particles with diameter between 0.5 an 1.0 μm. The retention percentages in table 2 are average values. The actual value for a particular filter can vary greatly depending on the filter material and construction.

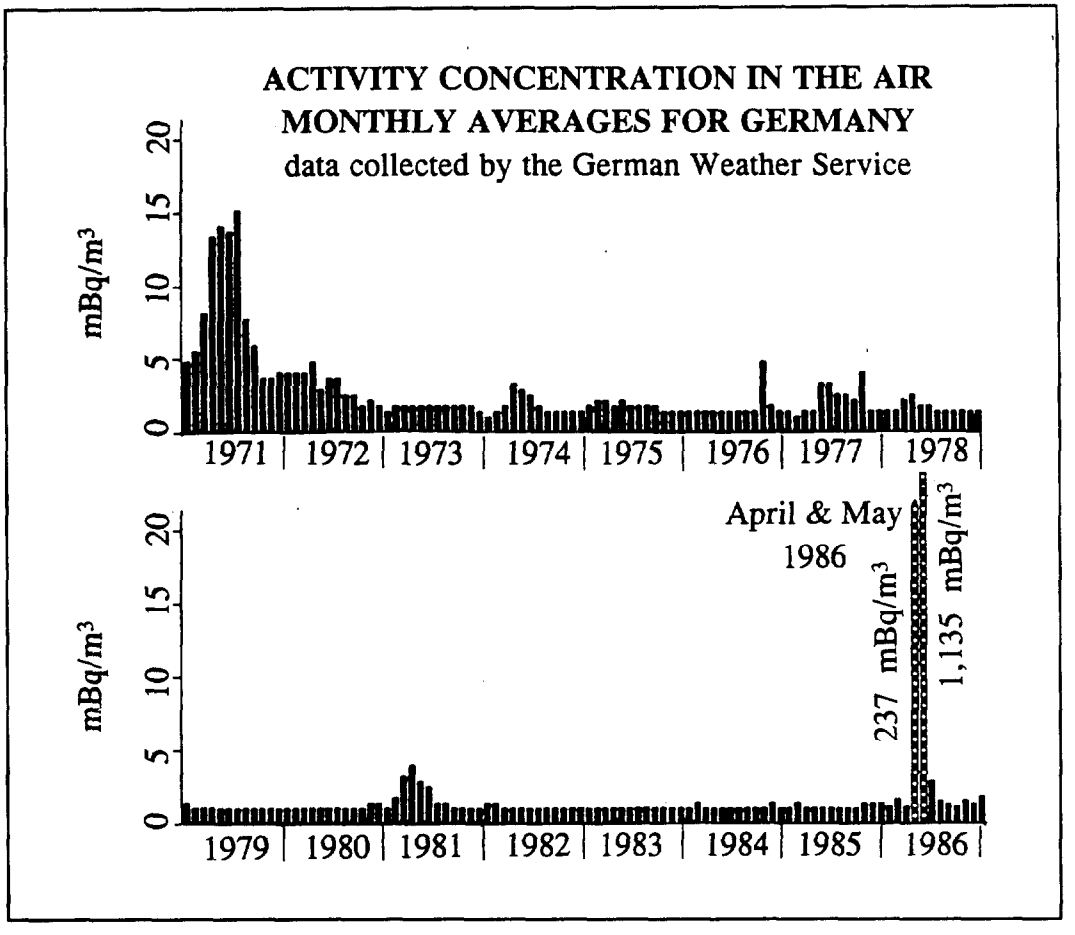

Figure 1 shows the total air born activity averaged over Germany from 1971 to 1986.

To calculate the expected reduction in the concentration of radioactivity in the air after filtering, information about the activity distribution as a function of particle size is needed. The percent activity distribution with respect to the particle size is shown in table 3[3]. The first row is the ^{131}I activity, note that 80% is in the gas form according to these measurements. The second row is the total activity bound to aerosols, excluding ^{131}I, as a function of particle size and the following 3 rows are the activity distribution of the 3 leading radionuclides. The measured activity distribution is expected to be representative for middle Europe.

5. Filter System in Nuclear Power Plants

Licensing procedures in Germany require that nuclear power plants monitor their surroundings to control the release of radionuclides. The power plants monitor the outside air before bringing it into the reactor building. The incoming air is filtered through a multi-stage filter system. The exhaust air is also filtered through a multi-stage filter system before being released. At all stages the air is monitored for the presence of radioactive aerosols. The multi-stage filters are composed of a coarse filter to retain the large dust particles, followed by fine and aerosol filters. After the Chernobyl accident the monitors at German nuclear power plants registered an increase in the radioactivity in the air. The aerosol activity was partially removed by the filtering system so that the air leaving the nuclear power plant had less activity than the air entering the plant. In the following sections data from the nuclear power plants at Philipsburg and Grafenrheinfeld are given which demonstrate the efficiency of the filtering systems at eliminating radioactivity from the air.

TABLE 2: **Filter retention as a function of filter type and particle size**

Filter-group	Filter Class		Average retention for different particle diameters in %				
	(a) EUROVENT	(b) DIN	< 0.3 μm	0.3-0.5 μm	0.5-1.0 μm	1.0-5 μm	> 5 μm
Coarse	EU 1	A	~ 0	~ 0	~ 0	~ 0	70
	EU 2	B_1	~ 0	~ 0	~ 0	~ 10	80
	EU 3	B_2	~ 0	~ 0	~ 0	~ 20	90
	EU 4		~ 0	~ 5	~ 10	~ 35	95
Fine	EU 5	C_1	~ 10	20	30	65	98
	EU 6		~ 15	30	50	80	99
	EU 7	C_2	~ 25	50	70	90	~ 100
	EU 8	C_3	~ 35	70	90	95	~ 100

(a) European standard
(b) Older German standard

5.1 Nuclear Power Plant at Grafenrheinfeld

The radioactivity arrived at the nuclear power plant at Grafenrheinfeld (KKG) in the night of April 30 and reached its maximum value between 14:20 and 21:30 on May 1. The incoming air was monitored with a set of temporary monitors from April 30 to May 11. The nuclides ^{131}I and ^{137}Cs dominated the nuclide spectrum with significant amounts of $^{132}Te/^{132}I$ and ^{134}Cs being present. Niobium and Ruthinium were detected in trace amounts[5].

In table 4 the activity concentration in the air is given before and after filtering the incoming air. The air was passed through a multistage filter (class A, B2 and C) and the activity concentration monitored by the normal instrumentation in the power plant. The temporary monitoring devices located outside the reactor building probably under-measured the ^{137}Cs concentration since measurements of the ^{137}Cs in the filters indicated a 10 times higher activity concentration outside than was expected from the calculations using the filter retention specifications and the air flow volume. This would mean that the retention of activity in the filters is better than the data in table 4 indicates. The low retention of ^{131}I can be explained by the large percentage of iodine in the gas form which was not retained by the filtering system, and due to the filter material, glass-wool. Using charcoal filters, as are implemented in the exhaust air filtering systems, a larger percentage of the iodine could be retained.

TABLE 3: **Activity distribution as a function of particle size**

Isotope	Activity per particle size in %					
	gasform	< 0.3 μm	0.3-0.5 μm	0.5-1.0 μm	1.0-5.0 μm	> 5 μm
^{131}I	80	7	7	4	2	0
Aerosol*	-----	7	26	43	23	1
^{137}Cs	-----	9	25	43	23	0
^{103}Ru	-----	9	26	40	20	5
^{132}Te	-----	6	26	44	24	0

* Does not include ^{131}I.

TABLE 4: **Activity concentrations before and after the Inlet filter at KKG**

Time Period	Outside Bq/m³ $^{131}I^*$ / ^{137}Cs	Inside Bq/m³ $^{131}I^*$ / ^{137}Cs	Removed activity $^{131}I^*$ / ^{137}Cs
April 28, 10:00 to May 5, 10:00	5.1 / 0.31	3.3 / 0.052	35% / 83%
May 5, 10:00 to May 12, 10:00	1.06 / 0.073	0.62 / 0.0051	41.5% / 93%

* total iodine activity, gas plus aerosol bound.

5.2 Nuclear Power Plant at Philipsburg

The radioactivity arrived at the nuclear power plant at Philipsburg (KKP) in the night of April 30. The incoming air was filtered through a multi-stage filter consisting of a coarse filter followed by a fine dust filter and an aerosol filter stage, filter class B2 and C respectively[6]. The radioactivity in the filters was analysed once a week. The results of the analysis are given in table 5. The ^{131}I values include the elementary (gas form), organic bound iodine and the aerosol bound iodine. The ratio of organic to elementary ^{131}I was 1:4 in agreement with the measurements presented in table 3 of section 4. The values listed under "Aerosol" are the sum of the aerosol bound activity from the nuclides, ^{103}Ru, ^{106}Ru, ^{132}Te, ^{134}Cs, ^{137}Cs, ^{140}Ba and ^{140}La. At the beginning the activity was dominated by ^{132}Te, while later ^{137}Cs and ^{103}Ru dominated the nuclide spectrum[6]. The data shows that the filters were not very effective in reducing the ^{131}I concentration. This can be attributed to the large percentage of ^{131}I that was not bound to aerosols and therefore was not retained by the filters. Furthermore the data shows that after the initial contamination by ^{131}I the building and filter system desorbed iodine over the following weeks so that the concentration inside the reactor building was higher than outside.

TABLE 5: Activity concentrations before and after the Inlet filter at KKP

Time Period	Outside Bq/m³ $^{131}I^*$ / Aerosols	Inside Bq/m³ $^{131}I^*$ / Aerosols	Removed activity $^{131}I^*$ / Aerosols
April 28 to May 4	12/ 11	9/ 1.3	25%/ 88%
May 5 to May 11	0.3/ 0.07	0.5/ 0.005	-- / 93%
May 12 to May 18	0.04/ 0.02	0.07/ 0.0003	-- / 98%

* total iodine activity, gas plus aerosol bound.

6. Discussion and Conclusions

Using the data from sections 4 and 5 a comparison can be made between the expected removal of activity from the air due to filtering and the actual measured reduction. This is accomplished for each filter type by multiplying the percent retention for the particle size from table 2 by the percent of the activity found on this particle size. This results in the percent of the activity retained in the filter dependent on the particle size. The sum of these retained percentages gives the percent of the total activity which the filter removed. For multi-stage filters the percent of the activity passing through the previous filter stage is used as the input for the next stage and the sum of the retained activity percentages is summed after passing through all the stages. In table 6 a summary of the results from calculating the expected retention for multi-stage filters typically used to filter the incoming air in a nuclear power plant is compared to the measurements presented in tables 4 and 5.

TABLE 6: Expected and measured retention values for filtering systems

	theoretical EU4 & EU7 / EU4 & EU8	measured week 1 / week 2
^{137}Cs	68.5% / 82.5%	83% / 93% (KKG)
Aerosols	68.9% / 82.9%	88% / 93% (KKP)
^{131}I total	10.2% / 13.0%	35% / 41.5% (KKG), 25% / -- (KKP)
^{131}I bound	51.1% / 65.2%	no data

The calculated 83% retention of activity in the filters for aerosol bound activity, which includes ^{137}Cs, compares very well with the 83% and 88% retention measured in the first week after arrival of the activity. The data shows that the retention percentage is better when the filters are exposed to less activity, as was the case in the second week. For aerosol bound activity where it can be assumed that the particle size is the determining factor, the retention can be estimated fairly well.

The retention for ^{131}I does not compare well with the expected retention from the calculations. There are a number of factors which can possibly explain this. Firstly the retention depends strongly on the amount of ^{131}I which is in gas form which could vary from region to region. Secondly the determination of the total ^{131}I depends on how well the ^{131}I gas can be determined, which will depend on the sampling techniques used at the different power plants. Another critical factor is the chemical reactivity of iodine gas. Iodine is more chemically reactive in gas form than when it is bound to aerosols and can therefore react more strongly with the filter material than when

it is bound up on aerosols. This means the retention of iodine can't be calculated simply by using particle size but has to consider the surface chemistry of the filter-iodine interaction in order to accurately estimate its retention.

7. Bibliography

(1) W. KRÖGER, S. CHAKRABORTY

Tschernobyl und weltweite Konsequenzen. Köln 1989.

(2) DER BUNDESMINISTER FÜR UMWELT, NATURSCHUTZ UND REAKTOR-SICHERHEIT (HRSG.)

Umweltpolitik. Umweltradioaktivität und Strahlenbelastung. Jahresbericht 1986. Bonn 1986.

(3) R. WEPFER

Moderne Filtertechnik bei extremen Außenluft-Zuständen. In: CCI. Karlsruhe 11/1986. S.10-11.

(4) RECKNAGEL, SPRENGER, HÖNMANN

Taschenbuch für Heinzung und Klimatechnik einschl. Brauchwassererwärmung und Kältetechnik. 63. Auflage 1986/87. (Hrsg. von W. Hönmann und E. Sprenger). München, Wien 1985.

(5) H. SCHUB

Persönliche Mitteilung an Herrn Dr. Braun, Bundesministerium für Umwelt, Naturschutz und Reaktorsicherheit. Anfrage über Zu- und Fortluftwerte KKG während des Unfalls in Tschernobyl. Juni 1992.

(6) BLASER

Persönliche Mitteilung an Herrn Dr. Braun, Bundesministerium für Umwelt, Naturschutz und Reaktorsicherheit. Kernkraftwerk Philippsburg GmbH. Juni 1992

(7) BAYERISCHES LANDESAMT FÜR UMWELTSCHUTZ (HRSG.)

13. Symposium über branchenspezifische Emissionen - Auswirkungen des Reaktorunfalls in Tschernobyl. Vorträge.

(Schriftenreihe Bayerisches Landesamt für Umweltschutz. Heft 71.) München 1986.

DISCUSSION

MILLER: I take it from what you are saying, then, that in the period after the Chernobyl accident there probably was a considerable loading of normal air conditioning filters in businesses, etc. with cesium particles and that when servicemen changed the filters, they got a significant dose. Is that true?

BRAUN: That is true.

KOVACH: Current U.S. source term research expects Cs and iodine to be present as CsI. Your paper indicates that even after long transport from Chernobyl there is a separation of cesium activity from iodine activity. Do you think this is significant for current source term studies?

BRAUN: We think this is very important with regard to the source term evaluation. Measurements of iodine performed by helicopter sampling directly above the Chernobyl reactor showed high amounts of iodine in the gaseous form. Up to May 1986 it was 30%. From May 8 until the May 19, 1986, 90% of iodine was present in the gaseous form.

KOVACH: I intended to ask a question on the first paper. I doubt that there will be much elemental iodine. A serious accident, by the heat of the melt, will generate enormous amounts of organic material. When there is no oxygen, it can get worse because large molecules will be in the air and irradiation will produce enormous amounts of radicals that will react. Therefore, I don't think the figures we have to date are the right ones because most of the experiments have been conducted under clean conditions whereas in a reactor accident, we have nothing but extreme conditions. We have to remember that we have tons of organics, e.g., insulation, oil, grease, and the like, in the reactor building and heating up all that stuff will generate enormous amounts of organic reactants.

MILLER: So, the German Nuclear Power Plants were actually acting to clean up the air after the accident.

BRAUN: That is right. We always tested the carbon filters with radioiodine, I-131. The grass from my lawn was one of the strongest samples I ever tested.

MILLER: Because of the cesium, you are not going to be eating mushrooms for years, perhaps thirty?

BRAUN: I like to eat them, but certain mushrooms just concentrate cesium: twenty thousand bq/kilogram is the mushroom radiation concentration.

AEROSOL PENETRATION THROUGH A SEISMICALLY LOADED SHEAR WALL

Charles R. Farrar and Steven P. Girrens
Los Alamos National Laboratory
Advanced Engineering Technology, MEE-13/MS J576
Los Alamos, New Mexico 87545 USA

Abstract

An experimental study was performed to measure the aerosol penetration through a reinforced concrete shear wall after simulated seismic damage. Static load-cycle testing, to stress levels sufficient to induce visible shear cracking, was used to simulate the earthquake loading. Air permeability tests were performed both before and after the simulated seismic loading damaged the structure. Aerosol penetration measurements were conducted on the cracked shear wall structure using 0.10 mm monodisperse particles. The measured aerosol number penetration through the cracked shear wall was 0.5%.

Introduction

Under normal operating conditions, the ventilation system in reinforced concrete facilities that handle hazardous materials provides a negative pressure differential that prevents unfiltered leakage from the building. A loss of the ventilation system would allow the air pressure inside the building to equilibrate with the external ambient air pressure. Normal or extreme wind loading on the building will result in regions where the external stagnation pressure is up to 7 kPa less than the internal pressure. This condition creates a driving potential for air leakage from the facility. A design basis earthquake (DBE) event could cause structural damage and ventilation system failure, thereby reducing the building's resistance to unfiltered exhaust. Fires that typically occur after an earthquake can also generate the pressure differential necessary to cause exhaust from the facility.

Estimating the leakage rate from a facility after a DBE event requires that the air permeability of the concrete walls, which have been loaded to their seismic-design limit, be quantified. If the leakage can be shown to be small, the requirements for using backup power systems to maintain the negative air

pressure can be relaxed. The term "small" is not quantified because its definition will depend on the toxicity of the material being confined. If the leakage is large, information concerning the airflow rates through damaged walls can be used in the design of the ventilation system to prevent the exhaust of toxic material from the facility.

The objective of this study was to measure the aerosol penetration through a reinforced concrete shear wall after the wall was loaded to stress levels that induce shear cracking. An experiment designed to satisfy this objective was developed by constructing a single-prototype shear wall test structure, simulating seismic loading by static load cycling the structure, measuring the airflow before and after damaging the wall, and performing aerosol penetration tests on the cracked structure. The test structure construction, simulated seismic testing, and air permeability measurements are described in detail by Girrens and Farrar[1] and are briefly outlined in this paper. Because air permeability is a function of crack parameters, only the data published on gas permeabilities in undamaged concrete[2-6] could be used to verify the experimental results. These data were used to verify the air permeability measurements made on the undamaged test structure.

Test Structure

A shear wall structure was selected for the initial study because this structural element forms a significant portion of the confining barrier and provides the dominant lateral load-carrying capability in reinforced concrete facilities that confine hazardous materials. The test structure fabricated contained a 150-mm-thick shear wall, as shown schematically in Figure 1. Two layers of reinforcement (ASTM A615 Grade 60, No. 3 rebar, 10 mm-diam) were placed throughout the model. Vertical layers were spaced at 75-mm centers, providing a 1.15% wall reinforcement ratio by area. Horizontal layers were spaced at 150-mm centers, providing a 0.41% wall reinforcement ratio by area. A minimum 25-mm cover was provided for all reinforcement. The concrete used to place the model was purchased from a commercial source. The structure was left in its form for a 28-day curing period, and exposed surfaces were kept moist and covered with a tarpaulin. Table 1 summarizes the mix portions, and Table 2 lists the measured concrete properties. Mix portion, wall geometry, and reinforcement were based on the design of a typical facility that handles hazardous materials.

Table 1 Concrete mix constituent portions.

Constituent	Weight (N)
Sand	13 500
Coarse aggregate	15 200
Cement	5 480
Water	1 930

Table 2 Measured concrete properties.

	Ultimate Compressive Strength (MPa)	Tensile Strength (MPa)	Modulus of Elasticity (MPa)
Average	42.0	3.6	3.19×10^4
Minimum	39.4	3.0	2.83×10^4
Maximum	46.0	4.1	3.36×10^4

Simulated Seismic Testing

The model was constructed in place on the load frame base used in the cyclic testing. A hydraulic actuator was used to load the structure. Force input was monitored with a load cell located between the actuator and the test structure. A steel load frame was assembled adjacent to the test structure on which to mount the actuator and load cell as shown in Figure 2. Displacement transducers were placed against the outside of the model to measure overall structural deformation.

The structure was loaded for 3 cycles, each to nominal base shear stress (NBSS) levels of $\pm$0.41 MPa, $\pm$0.90 MPa, and $\pm$1.31 MPa. In this context, NBSS is defined as the applied force divided by the cross-sectional area of the shear wall (0.19 m^2). Complete load reversals were applied to represent the forces induced in a structure during seismic excitation. These quasi-static load cycles simulate an earthquake by applying the positive and negative shear forces associated with a DBE to the structure. The magnitude of the maximum shear stress corresponded to the actual design limit for the facility under study.

The structure showed linear response through all of the load cycles. The linear response indicated that the structure experienced no internal damage when loaded up to the maximum nominal-design shear stress of 1.31 MPa. The structure was then subjected to one 1.97-MPa NBSS load cycle. The

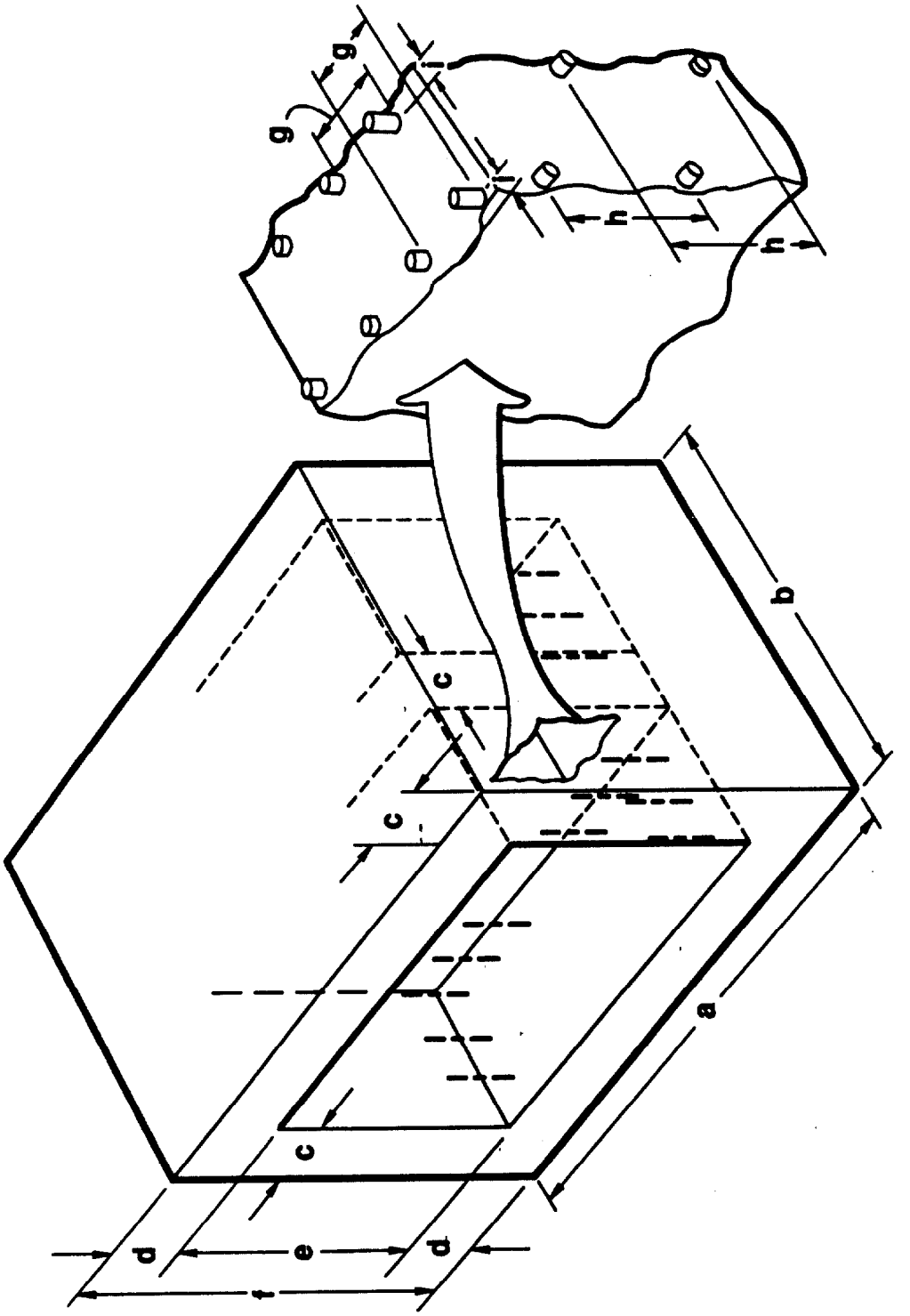

STRUCTURE	DIMENSIONS (mm) a	b	c	d	e	f	g	h	i	REBAR diam	MAX AGGREGATE SIZE
MODEL 1	1220	910	150	150	610	910	75	150	25	10	19

Figure 1 Shear wall test structure detail.

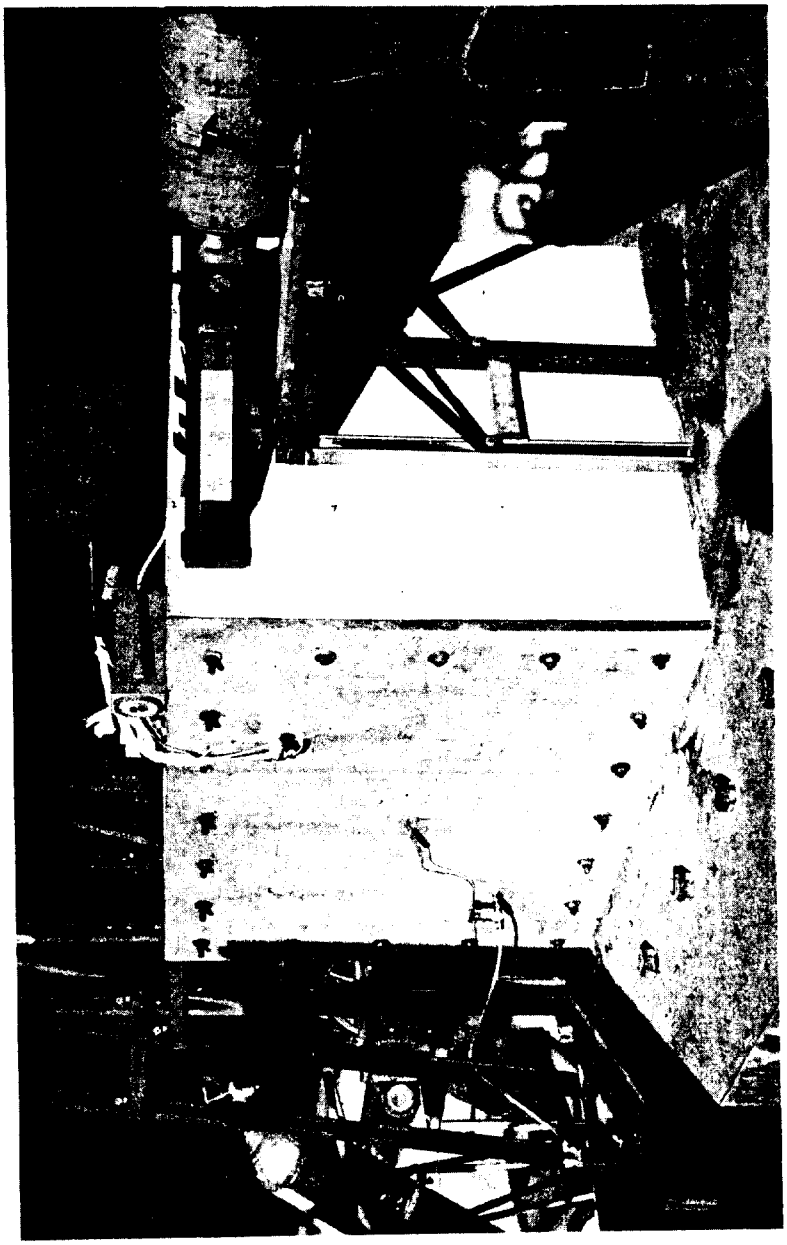

Figure 2 Air permeability test setup.

structure cracked on the first load increment above the 1.31-MPa NBSS level. The actual shear wall crack pattern is shown in Figure 3. Most of the shear cracks identified appear to have penetrated completely through the wall.

Air Permeability Tests and Results

Air permeability measurements were made on the shear wall before and after subjecting the test structure to static load cycling. The air permeability was determined by pressurizing one side of the test structure slightly above atmospheric levels and recording the transient-pressure decay associated with the air leakage through the shear wall.

An aluminum cover plate was attached to the structure to accommodate structure pressurization (see Figure 2.). The cover plate provided resistance and sealing support for internal pressurization. Square (7.0-mm) Buna-N O-ring cord stock and flooring contact cement were used to form an airtight seal between the concrete face and the cover plate. Helium leak tests were performed to ensure that the aluminum cover plate seal and fittings were not leaking. The interior surfaces of the side walls, and the top and bottom slabs on the side of the shear wall to be pressurized were spray painted with three coats of epoxy paint to ensure impermeability. Internal pressurization of the test structure did not exceed 4.8 kPa gage. The pressurized volume, 0.21 m^3, was filled with dry bottled air and purged with a vacuum pump three times before filling the volume for testing. Pressure levels were monitored with a digiquartz pressure transducer having a range of 0 to 0.2 MPa and a resolution of 0.0007 kPa. After pressurization, transient internal pressure, atmospheric pressure, and internal temperature were monitored with a data scanner.

Air permeability testing was initiated 11 weeks after removing the model forms. During those 11 weeks, the relative humidity was 20 to 30%. Transient pressure and temperature data were recorded over a period of several days. The volume (or block) was initially pressurized to approximately 82.7 kPa and allowed to decay over a period of 3 days. After the 3-day period of data collection, the volume was again repressurized. The actual data used to compute the permeability were the specific values recorded at midnight each day. This sampling provided an average of the daily variation in temperature, which was necessary because the experiment was located outside. The average permeability measured before loading the structure was 7.9×10^{-17} m^2.

The transient pressure and temperature data measured after load cycling the structure up to a shear stress of 1.31 MPa produced similar air-permeability results. No internal damage occurred to the structure during the load cycling, and, thus, the concrete air permeability was not affected. The average air permeability, 7.4×10^{-17} m^2, computed after the 1.31 MPa load cycling is in agreement with the preload data.

Airflow measurements were also made after the test structure was damaged. The shear cracking had a significant effect on the air leakage through the shear wall. Helium leak-testing equipment verified that significant leakage was occurring through the shear cracks in the wall. Both transient and steady-state airflow data were taken. The average value of pseudo air permeability, corresponding to the transient airflow data taken with the cracked wall, was 3.5×10^{-15} m^2.

A flowmeter was attached to the air-charging orifice on the aluminum cover plate. While maintaining an approximately constant pressure in the block, the airflow through the shear wall was monitored for 168 hours. The steady airflow through the shear wall was 3.1 cm^3/s. The pseudo air permeability corresponding to the steady flow rate, and an average pressure gradient of 4.8 kPa, was 3.0×10^{-15} m^2. Thus, air permeability in the shear wall increased by a factor of 40 after the wall experienced shear cracking.

Aerosol Test Method

Aerosol penetration tests were also conducted by pressurizing the upstream side of the cracked shear wall above ambient conditions to drive a steady airflow through the wall. A second cover plate was installed to enclose the downstream ambient pressure side of the test structure, permitting the measurement of the accumulation of nontest particles for a background particle distribution. Figure 4 is a schematic drawing of the aerosol penetration test setup. Throughout the penetration tests, the ambient pressure measured inside the downstream volume remained constant at 77.9 kPa. The steady airflow through the wall stabilized at 1.5 cm^3/s, for an average pressure gradient of 2.8 kPa. The 2.8 kPa pressure gradient was selected for the penetration test because this value corresponds to the negative pressure gradient calculated for the worst case wind-loading condition on the hazardous materials building under consideration.

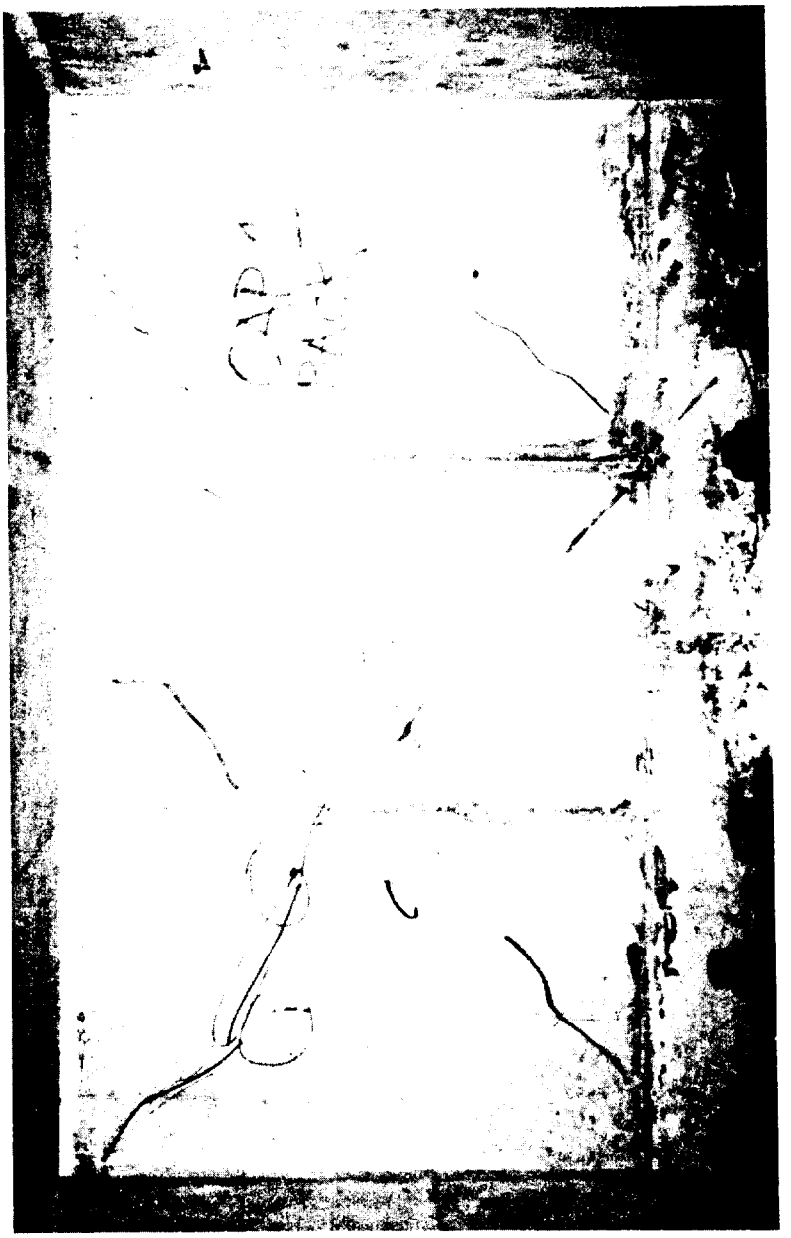

Figure 3 Shear wall crack pattern.

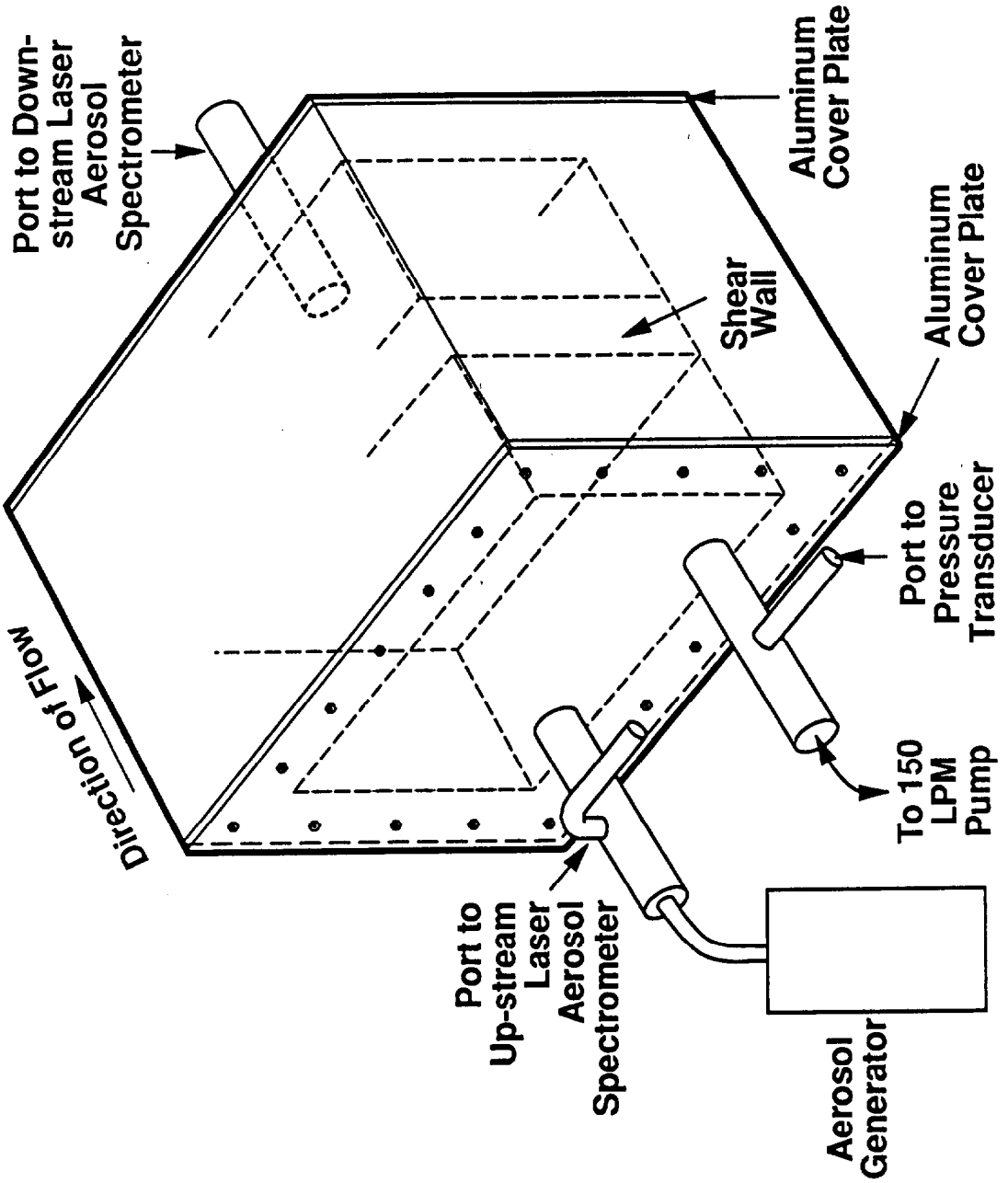

Figure 4 Aerosol penetration test setup.

When a steady airflow was achieved, a mondisperse aerosol of spherical polystyrene latex (PSL) particles was injected on the upstream side of the wall and allowed to come into equilibrium in the pressurized volume before sampling. Samples were extracted through a penetration in the cover plate, then run through a laser aerosol spectrometer (LAS) to measure the aerosol challenge to the shear wall. Samples were also extracted from the downstream side of the wall, then analyzed with the LAS to measure the penetrating particle distribution.

Aerosol Penetration Results

The spherical particle diameter selected for the monodisperse PSL aerosol was 0.1 mm. The degree of dispersity of an aerosol is characterized by a, the relative standard deviation, or the ratio of the standard deviation of the particle sizes to the mean particle size. A criterion for monodispersity can be expressed by a < 0.2. An 0.23 a value was calculated for the aerosol challenge to the wall. Table 3 is a summary of the measured aerosol challenge distribution and the penetration distribution; these distributions are shown graphically in Figure 5. The total aerosol penetration through the cracked wall was 0.5%.

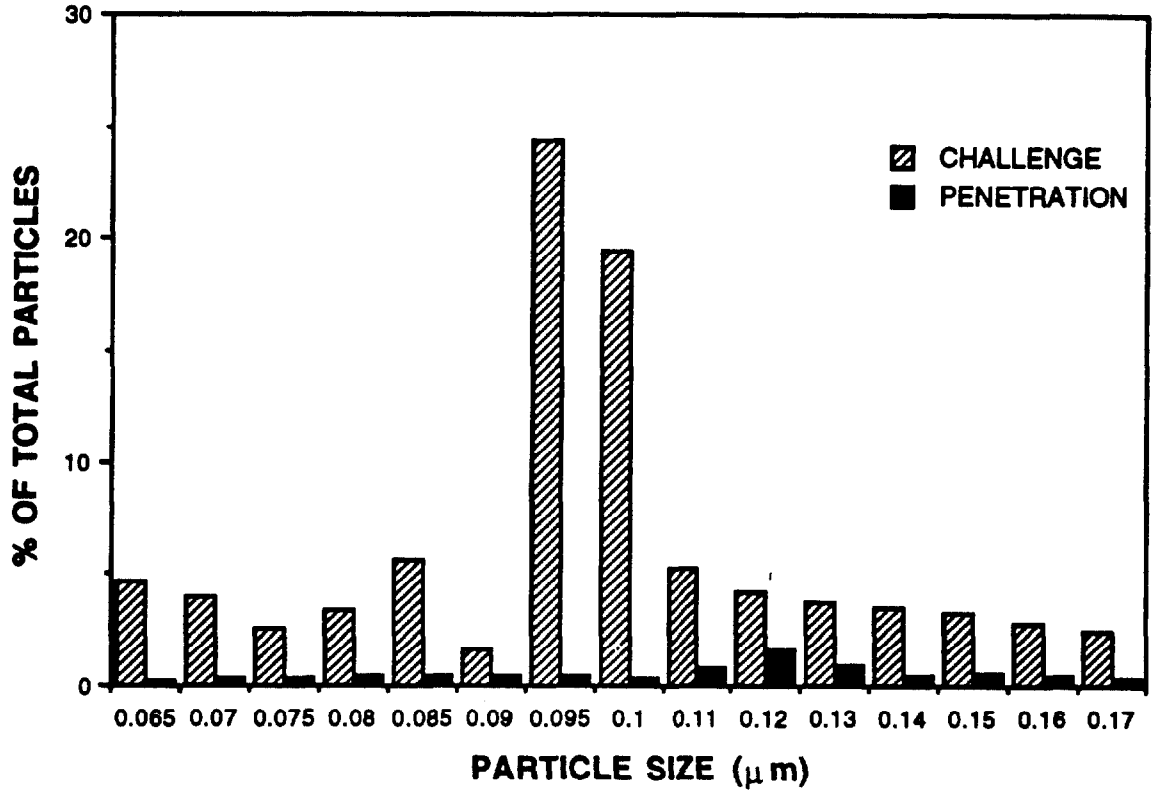

Figure 5 Distributions of aerosol particle challenge and penetration.

Table 3 Aerosol particle distributions.

Particle Size (μm)	Challenge (counts/min)	Penetration (counts/min)	Penetration (%)
0.065	146	0.4	0.27
0.07	126	0.4	0.32
0.075	80	0.3	0.38
0.08	106	0.5	0.47
0.085	176	0.8	0.45
0.09	332	1.4	0.42
0.095	760	3.2	0.42
0.10	606	2.3	0.38
0.11	164	1.3	0.79
0.12	132	2.2	1.67
0.13	114	1.1	0.96
0.14	108	0.5	0.46
0.15	102	0.6	0.59
0.16	88	0.4	0.45
0.17	78	0.3	0.38

The most penetrating particle sizes were 0.11 to 0.13 mm. The explanation of why the predominant penetrating particles are slightly larger than the predominant challenge particles is uncertain. Limitations on aerosol penetration through cracked concrete would likely include high pressure gradients that would induce inertial impaction, and physical crack dimensions that would limit particle size. Particle penetration associated with low pressure gradients and smaller particle size would be limited by the filter efficiency of the cracked concrete. The filter efficiency for the cracked shear wall panel tested is 99.5%. To put this value in perspective, the filter efficiency of graded sand (1.8 m, 50 mesh) under a 1.2-kPa pressure gradient, challenged by 1-mm dust particles, is also 99.5%.(7) Though shear cracks will, in general, extend completely through a shear wall, the cracks will have a tendency to close tightly when the load is removed. This tendency for shear crack closure is probably responsible for the high filter efficiency in the damaged wall.

Summary

The objective of this study was to measure the aerosol penetration through a reinforced concrete shear wall after simulated seismic damage. Accomplishing this objective required fabricating a 150-mm-thick shear wall test structure, representative of a wall in a typical facility that handles hazardous materials, with standard concrete mix and rebar materials.

Static load-cycle testing was used to simulate earthquake loading. The initial load-cycling levels did not damage the shear wall. However, a higher level load-cycle (shear stress above 1.31 MPa) resulted in damage (shear cracking) to the structure. Airflow measurements taken after the structural damage occurred, show that the cracking resulted in a factor of 40 increase in the air leakage through the shear wall. The steady airflow through the cracked shear wall, corresponding to a pressure gradient of 4.8 kPa, was measured to be 3.1 cm^3/s.

Aerosol penetration measurements were conducted on the cracked shear wall structure. The sample collection airflow was maintained at 1.5 cm^3/s, with an average pressure gradient of 2.8 kPa. An 0.10-μm monodisperse PSL aerosol was injected into the steady airflow. The aerosol penetration through the cracked shear wall was 0.5%. The corresponding filter efficiency was 99.5%.

An accurate estimate of the total aerosol leakage from a facility after a damaging seismic event would include the additional leakage that can occur around penetrations. Because cracking is a function of the concrete's material properties, reinforcement, and loading, discretion must be used when applying the results presented in this study to studies of other facilities.

References

1. Girrens S. P. and Farrar, C. R., "Experimental assessment of air permeability in a concrete shear wall subjected to simulated seismic loading, "Los Alamos National Laboratory report LA–12124–MS, (1991).
2. Fintel M., Ed., Handbook of Concrete Engineering,Van Nostrand Reinhold, New York, 1974.
3. Hansen A. J., et al., "Gas permeability of concrete *in situ*: theory and practice," *In* situ/Nondestructive Testing of Concrete, American Concrete Institute, Detroit, Michigan, SP-82, 543-556, (1984).

4. Nagataki S. and Ujike I., "Air permeability of concretes mixed with fly ash and condensed silica fume," Fly Ash, Silica Fume, Slag, and Natural Pozzolans in Concrete, American Concrete Institute, Detroit, Michigan, SP-91, 1049-1068, (1986).
5. Dhir R. K., et al., "Near surface characteristics of concrete: intrinsic permeability," Magazine of Concrete Research, 41(147), 87-97, (1989).
6. Huovinen P., "Air permeability of concrete," Nordic Concrete Research, No. 1, 1-33, (1982).
7. Dennis R., Ed., "Handbook on aerosols," US Energy Research and Development Administration report TID-26608, (1976).

BETA EXPERIMENTS ON AEROSOL RELEASE DURING MELT-CONCRETE INTERACTION AND FILTERING OF THE OFFGAS

H.G.-Dillmann*, H. Pasler*, H. Alsmeyer **

Kernforschungszentrum Karlsruhe GmbH
*Laboratorium für Aerosolphysik und Filtertechnik
**Institut für Angewandte Thermo- und Fluiddynamik
Postfach 3640, W-7500 Karlsruhe 1
Federal Republic of Germany

Abstract

The BETA facility is a test rig for core melt accident experiments. This rig is described. Up to now, 7 melt-concrete interaction experiments have been carried out. Results of sampling and analysis are given for the aerosol size distribution and the chemical components of the simulating fission products added in the offgas line. The size distribution ranges from 0.1 to 1 µm. High-volatile aerosols are found in the samplers. The erosion data in downward and radial directions are summed up. The initial melt used in the tests was produced by a thermite chemical reaction of 300 kg steel, 80 kg Zircaloy 4 and 50 kg oxides with Al_2O_3, SiO_2 and CaO. The starting temperature is typically 2250 K. In induction heating the net power inputs may differ between 200 kW and 1000 kW. A metal fiber filter is installed in the offgas line as a protection against the environment. The data of the filter will be presented. The amount of collected aerosols is in the range of 1.5 to 3.7 kg/per experiment. A video clip will be presented showing the melt and the optically visible difference in the offgas with and without filtering.

I. Layout of the BETA Facility

The Beta Facility was built to enable us to determine the behavior of molten metal interacting with concrete. It serves to simulate the behavior of a core melt in concrete with a view to determine the rates of penetration of melts into concrete and to obtain data on the resulting containment loadings. A further aspect has been to obtain information on the aerosol loading of the containment in terms of the behavior over the time of the particulate size distribution and aerosol masses released.

Figure 1 shows the schematic layout of the facility. Conditioned concrete crucibles equipped with thermocouples are filled with a thermite melt (Fig. 2). The melt front of the concrete can be traced by means of the thermocouples. The melt can be heated and kept in the liquid state by induction heating of up to 1000 kW at 27 MHz which simulates the decay heat. An offgas line is routed from the crucible to the outside via two 90° bends. It accommodates a number of analytical instruments for gas analysis and for collecting aerosol data. The offgas temperature in the experiments is about 250 °C.

One particular goal consists in the determination of the fission products released. They are thrown into the melt by means of lances at defined points in time and serve as inactive simulants. The respective amounts have been entered in Table 1.

Table 1: Main Parameters for the BETA Experiments

BETA Test	Initial Melt ~ 2200 K	Fission Product Mockups and Additives	Planned Heating Power
V 5.1	300 kg Fe+Cr+Ni 80 kg Zry-4 50 kg Al_2O_3 +SiO_2+CaO	none	400 kW
V 5.2	similar to V 5.1	1 kg Mo, 0.5 kg $ZrTe_2$, 1.5 kg CeO_2, 1 kg BaO, 0.5 kg La_2O_3, 0.5 kg SrO, 6 kg B_4C in steel containers	200 kW
V 5.3	similar to V.5.1	1 kg Mo, 1 kg CeO_2, 1 kg BaO, 0.5 kg La_2O_3, 0.5 kg SrO, 6 kg B_4C in steel containers	800 kW

As some of the fission product simulants are toxic, a stainless steel fiber filter module has been installed in the offgas line and designed for a volume flow rate of about 500 m^3/h [1].

The Laboratorium für Aerosolphysik und Filtertechnik (Laboratory for Aerosol Physics and Filter Technology) operated two sampling systems in the offgas line (350 mm inner dia., inclusive of insulation about 600 mm dia.), one installed at about 1.5 m distance from the crucible outlet and comprising 3 + 1 samplers, the second sampling system placed some 4 m more further distant in direction of blowdown and comprising 5 + 1 samplers. The layout has been represented in Fig. 3. For simplification of volume flow control the bypass sampler is always open from a defined point in time on, while the pump is running. The bypass is closed at defined times of measurement and, at the same time, a sampler is opened for a defined period of time.

Depending on the goal pursued in the respective experiment, different times of sampler opening are chosen. The duration of exposure chosen is about 30 s for determination of the particulate size distribution. Rather large amounts of aerosol are needed for wet chemical analyses to be performed. Therefore, 2 min. opening time were usually chosen in that case. The times of sampler opening correlated with the times at which the material lances dropped the fission product simulant. The rate of penetration into concrete was about 40 cm during 30 - 45 min., depending on the grade of concrete.

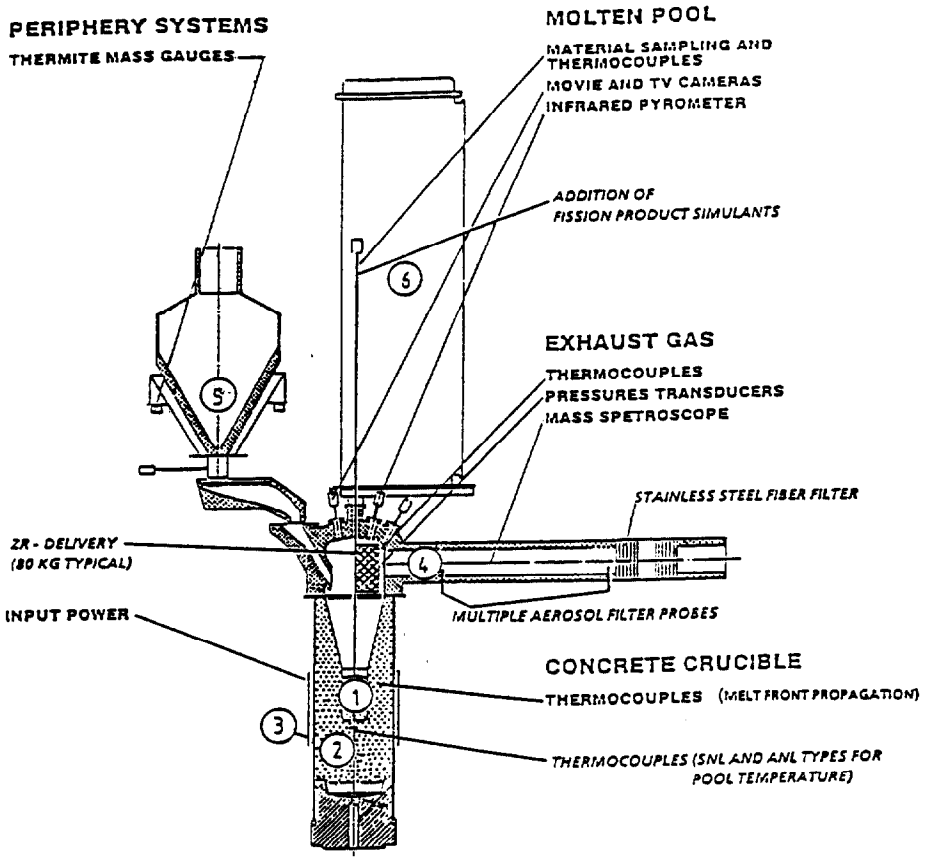

Figure 1: Schematic View of BETA Facility in Zr Related Tests

II. Layout of the Filter in the Offgas Duct

As both high temperatures occur in the melt-concrete reaction and H_2 is released and ignited at the outlet, a commercially available metal fiber filter is used similar to that described in (1, 3) and installed as venting filter for pressure relief in all German LWRs. A sufficient amount of operating experience with that filter is available as regards the loading, behavior in moist environment, removal behavior, and mechanical loadability. The filter consists of two stages, a high-loading pre-filter stage and a free space preceding the fine filter stage in order to prevent condensed water from penetrating (Fig. 4).

With this filter decontamination factors of 8500 were achieved in preliminary experiments in which uranin had been used. This corresponds to HEPA quality. As a rule, decontamination factors of ~ 10,000 were measured for aerosols with rather large particulate diameters (2, 1).

III. Results

The amounts of filter loading in each BETA experiment were determined by weighing of the fiber cores. Depending on the type of concrete used and on the way the experiment was conducted (duration, power input), 1.5 to 3.7 kg of aerosols were entrained from the melt and carried to the filter over a distance of about 10 m. The loaded gas stream consisted of argon as the cover gas, supplied at a rate of about 150 - 350 m^3/h, as well as H_2, H_2O, CO, CO_2 released in the melt-concrete interaction so that a maximum rate of 500 m^3/h had to be filtered.

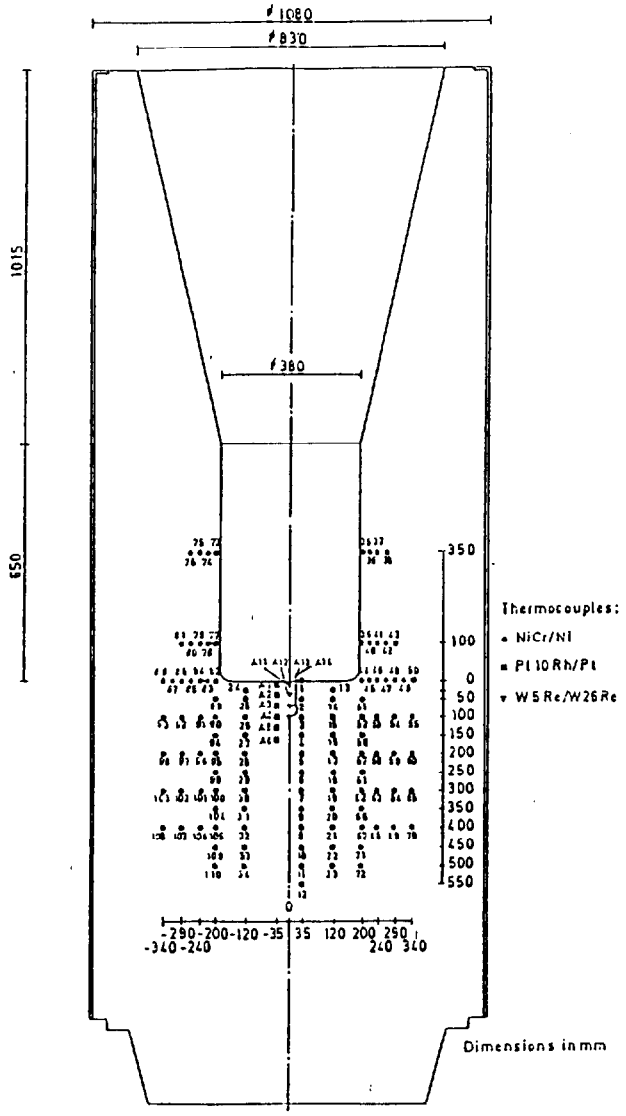

Figure 2
Crucibles Used in BETA Experiments V 5.1, V 5.2, V 5.3

Figures 5 - 12 show by way of example scanning electron micrographs (SEM). Micrographs 11 and 12 show excessive loadings which are typical of too long opening times of the valves at the samplers. Some of the micrographs show a distribution of particulate sizes as described by the computer codes for a primary aerosol with a high fraction of very small particulates from the melt-concrete reactions (Figs. 13 and 14). This distribution of particulate sizes must be expected for the relatively long period of melt-concrete reaction and must be taken into account in the design of the venting filters.

Particular phenomena are evident from Figs. 5 - 8. Reactions and condensation processes took place which had brought about bizzare shapes of aerosols. Similar aerosols were found also in subsequent experiments. They are probably attributable to the fission product simulants added by means of the material lances.

In Table 2 the loadings and aerosol rates have been entered which were determined by weighing.

Table 2: Aerosol Data From Filter Samples; V 5.1

Filter	Time (s)	Collected Mass (mg)	Mass Concentration		Aerosol Rate (mg/s)
			With Ar-Cover Gas (mg/m^3 STP)	Without Ar-Cover Gas (mg/m^3STP)	
MV1	73-317	15.8	583	1170	60.3
MV2	440-739	28.9	873	2423	53.5
MV3	1205-2046	7.4	79	246	4.5
MV4	73- 204	12.4	855	1520	111
MV5	204- 281	11.7	1370	4110	105
MV6	440- 739	17.7	534	1480	32.7
MV7	825-1205	7.7	182	525	10.8
MV8	1205-2046	21.0	118	367	6.7

Typical compositions of the aerosols as determined in wet chemical analyses are given in Table 3. The analyses were made by the Institut für Materialforschung (Institute for Material Research) of KfK. It appears that the highly volatile aerosols accumulate to a much higher extent in the offgas line than could be anticipated from the input.

IV. Some Remarks on the Video Clip

It is not intended to show by this film the phenomena of melt-concrete interactions but rather to demonstrate the function of the offgas filter.

The first scene shows the melt contained in the concrete cavern as well as a dropping lance with the simulant material.

The second scene shows the offgas line running in the open. About one minute after tapping of the melt, gas and aerosols are released. It can be concluded from the evolving smoke that no filter had been installed in the offgas line. The H_2 and CO is ignited outside and burns off.

In the third scene burning of the filtered gases can be seen and later condensing vapor fractions, but no release of smoke particulates.

Table 3: Chemical Composition of Aerosol Samples
Selected aerosol Samples from BETA V 5.3

Sampler	MV1	MV4	MV3	MV8	BP1	BP2
Time Interval [s]	40 - 70	40 - 70	405-480	810-930	0 - 1000	0 - 1000
Mass [mg]	10.04	77.91	0.41	0.66	43.39	78.21
Elements of Concrete [%]						
Si	5.09	5.41	< 9.0	14.40	8.81	7.90
Ca	0.38	0.20	< 1.5	< 1.0	0.18	0.28
Al	1.12	2.10	4.0	< 2.3	1.35	1.30
Mg	2.86	1.32	0.29	0.27	1.02	2.49
K	14.95	17.29	9.47	11.09	11.42	13.92
Na	8.32	3.43	4.38	2.98	3.72	5.38
Ti	< 0.1	0.005	< 0.5	1.05	0.011	0.021
Mn	0.25	0.51	< 1.5	< 1.0	0.51	0.47
Elements of Metal Melt [%]						
Fe	0.48	0.68	< 1.0	< 0.8	0.87	0.81
Cr	< 0.3	0.15	< 2.0	< 1.3	0.26	0.23
Ni	< 0.3	0.19	< 2.5	< 1.5	< 0.1	< 0.1
Zr	< 0.1	0.015	< 0.5	< 0.3	< 0.05	<0.01
Sn	< 0.5	0.66	<5.0	9.05	1.63	1.66
B	1.25	3.37	3.01	2.85	7.80	5.14
Simulated Fission Products [%]						
Mo	< 1.0	< 0.1	< 8.3	< 5.2	< 0.3	< 0.2
Ce	< 0.5	< 0.5	< 4.0	< 2.5	< 0.1	<0.1
Te	< 1.0	< 0.5	< 11.0	< 7.0	< 0.5	< 0.3
Ba	0.56	0.086	< 1.3	< 0.8	0.20	0.60
Sr	0.60	0.061	<0.5	< 0.3	0.34	0.72
La	< 0.5	< 0.1	< 4.0	< 2.5	< 0.1	< 0.1
Other ELements [%]						
Zn	0.57	0.27	0.69	1.64	0.45	0.68

(Numbers preceded by "<" indicate the chemical detection limit)

Te from $ZrTe_2$ in V 5.2 is released; typical concentration in the aerosol 20 to 60 %.

V. References

(1) Dillmann, H.-G; Wilhelm, J. G; "Investigations into the Design of a Filter System for PWR Containment Venting." CONF 900 813, Vol. 2, p. 898 (1990).

(2) Wall, Ian; Merilo, Mati; "Containment Filtration Systems Tests" Andvanced Containment Experiments (ACE) Project: Summary Report. EPRI TR-100346s

(3) Dillmann, H.-G; Pasler, H.; Wilhelm, J. G.; "Off-Gas Cleaning Devices for Containment Venting System." CONF 880 822, Vol. 1, p. 709 (1988).

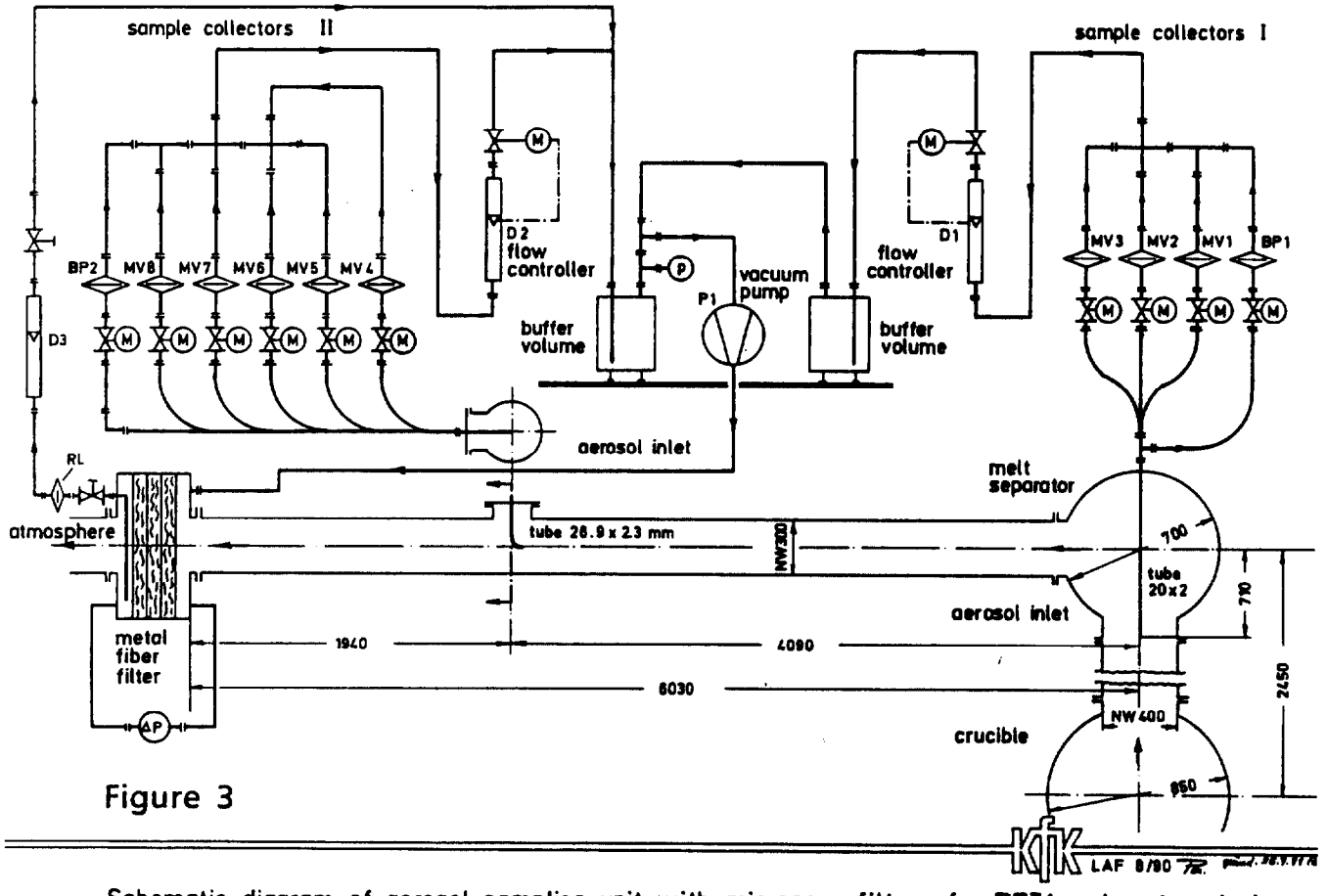

Figure 3

Schematic diagram of aerosol sampling unit with micropore filters for BETA exhaust analysis

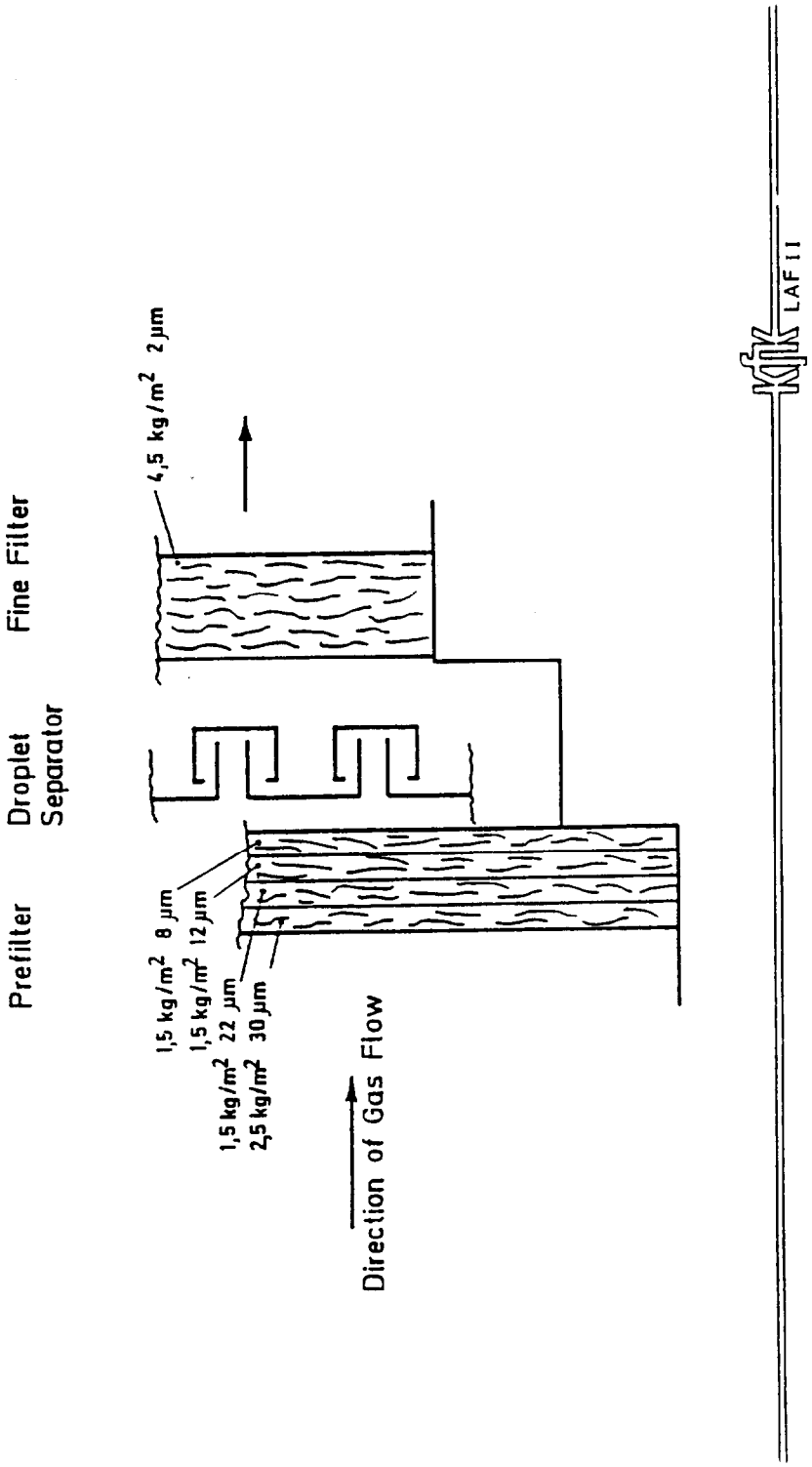

Figure 4 A Section of a Deep-Bed SS-Fiber Filter

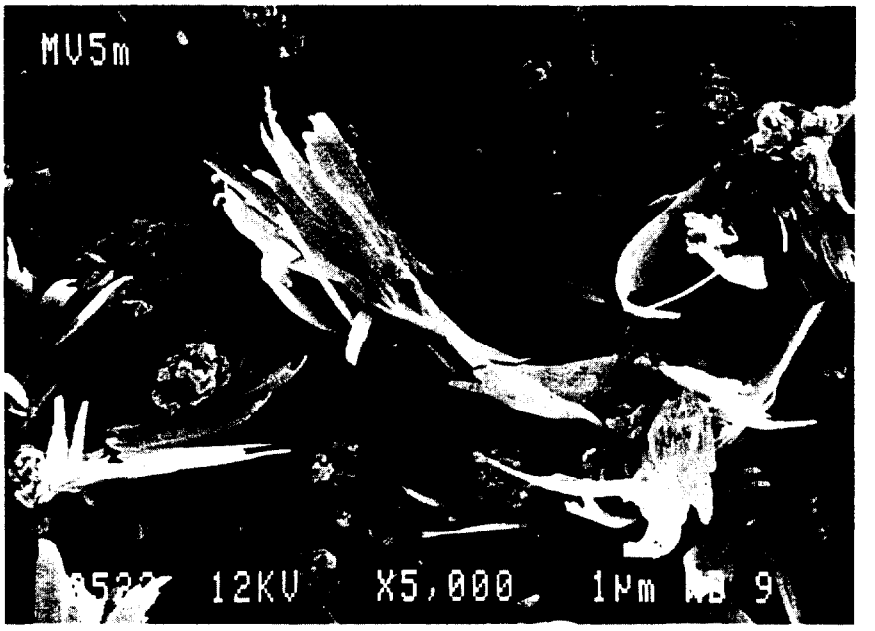

Figure 5

Figure 6

Figure 7

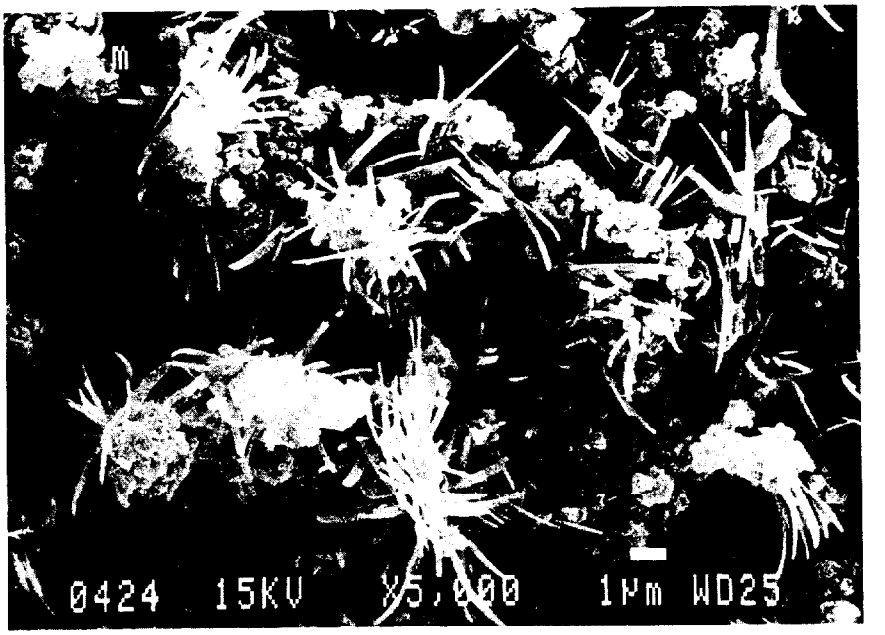

Figure 8

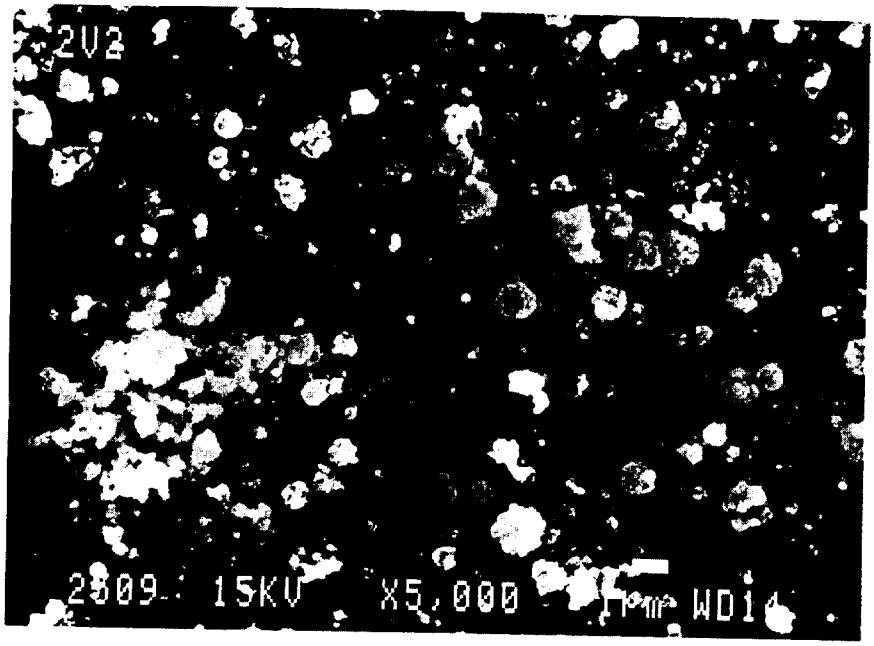

Figure 9

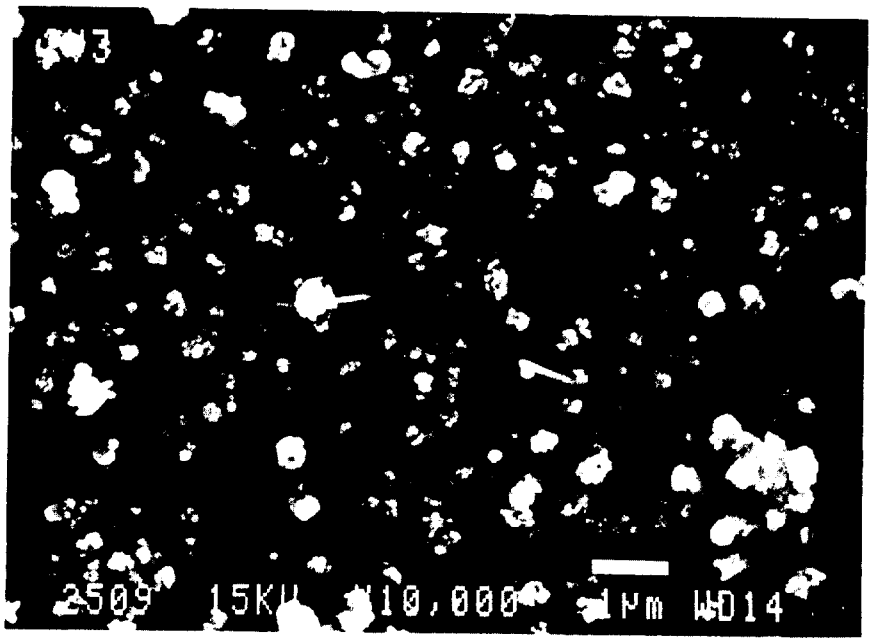

Figure 10

Figure 11

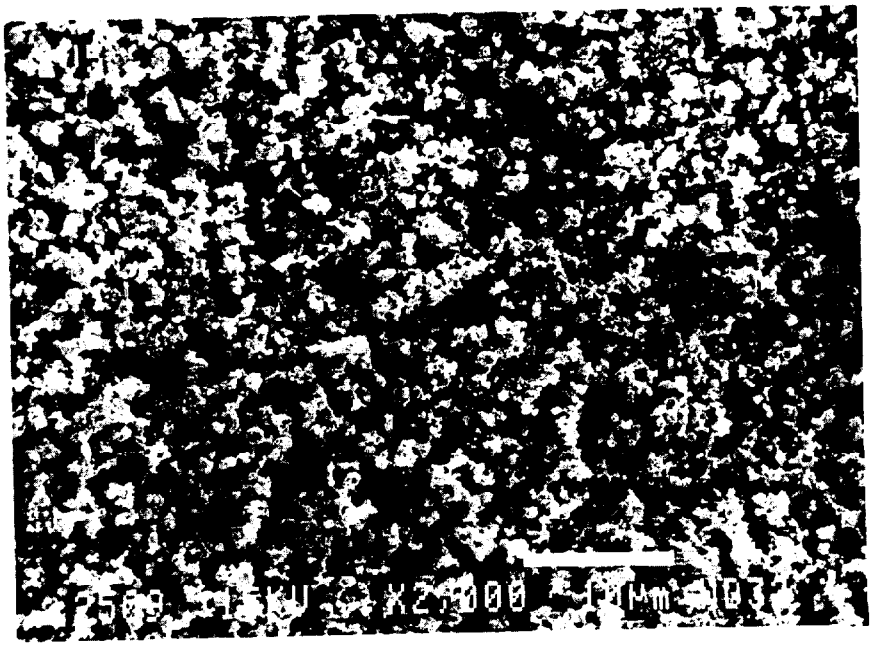

Figure 12

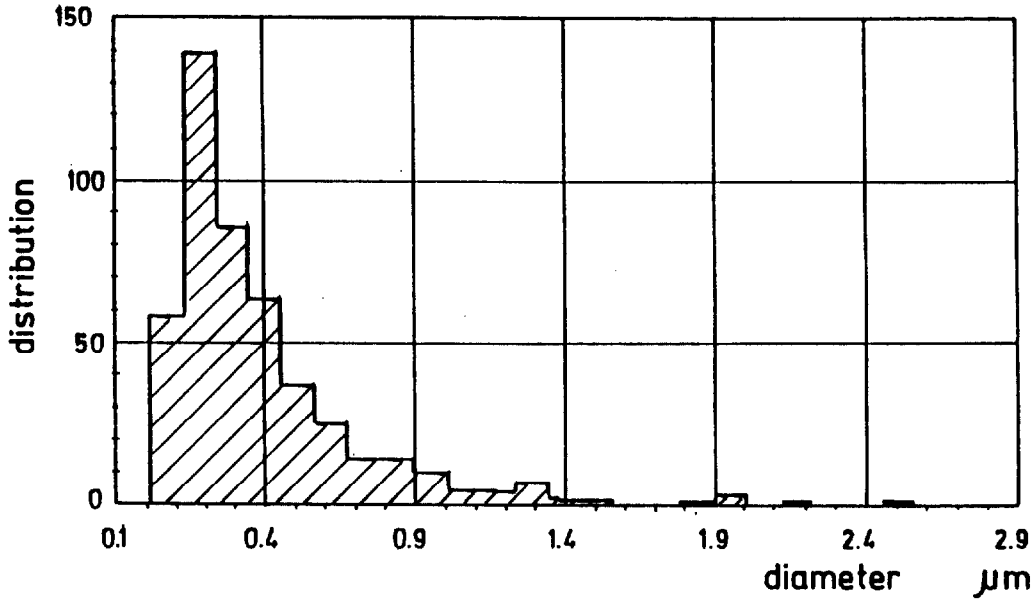

Fig. 13

Particle - distribution BETA 5.3

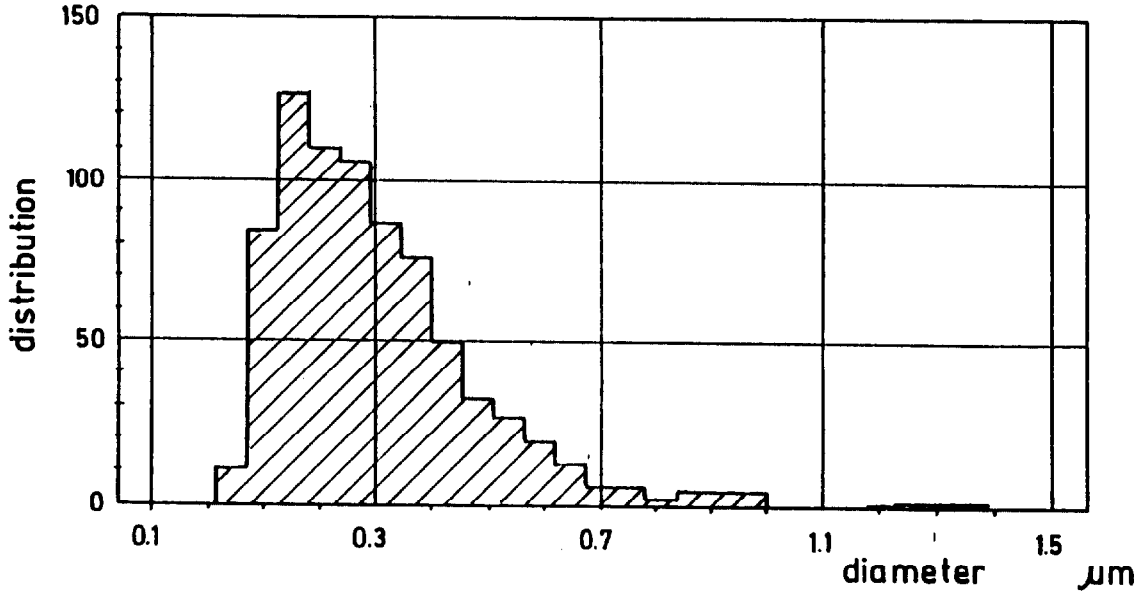

Fig. 14

Particle - distribution BETA 6.1

ACTIVATED CHARCOAL BEDS FOR PASSIVE MITIGATION OF THE RADIOACTIVITY RELEASE FROM SEVERE ACCIDENTS. HEAT TRANSPORT AND DYNAMIC NOBLE-GAS WATER-VAPOUR COADSORPTION.*

F. Castellani°, G. Curzio°, F. d'Errico°, S. Lanza°,
A. Mori°°, G. Rossi°, G. Sgalambro°°°

° DCMN, Università di Pisa, I-56126 Pisa
°° ENEA-AMB, I-56126 Pisa
°°° ENEA-DISP, I-00144 Roma

Abstract

A typical severe accident sequence involves the combined loss of large amounts of cooling water and radioactive fission products. A possible approach to the reduction of the radioactivity release is the design of activated charcoal beds capable of withstanding the maximum pressure and holding the gaseous products long enough to reduce their activity while effectively exchanging their decay heat. Two of the main problems arising are confronted here: the characterisation of a filter response to dynamic transients and the determination of its bulk thermal conductivity.

I. Introduction.

In view of the possible resumption of nuclear power production in Italy, ENEA-DISP, the Italian regulatory body for nuclear safety, recently entered a joint research project with DCMN, the Department of Nuclear Engineering of the University of Pisa. The objective of this collaboration is the analysis of the safety characteristics of new reactor designs.

* Work partially supported by ENEA-DISP.

According to the INSAG-3 Report,[1] "the principle of defence in depth is implemented primarily by means of a series of barriers," which provide "for the confinement of radioactive material at successive locations. The reliability of the physical barriers is enhanced protecting each of them by a series of measures."

Therefore, the protection of the containment, the ultimate barrier against the release of fission products, is of fundamental importance. Venting is one of the options investigated for the prevention of early failure of the containment. This may result in a large release of radioactive material into the environment, particularly noble gases which constitute the bulk of the activity transferred to the containment during the first stages of severe accident sequences.[2,3,4]

ENEA-DISP and the General Electric SBWR project team have analysed the possibility to employ the Off-Gas Treatment System (OGTS) for filtered containment venting, either through an extension of the normal duty or through the design of new dedicated systems.

Within this framework, DCMN-Pisa was assigned the task of analysing the noble gas retention properties of charcoal filters in the presence of massive amounts of water, and the thermal conductivity of wet charcoal. From these data we may derive the decontamination factor (DF) provided by charcoal filters during a severe accident, and their capability to exchange the heat released by steam condensation and fission product decay.

Upon successful completion of this study, the applicability of the system described in Figure 1 will be demonstrated.

This consists of:

- a condensing pool, containing at least 500 m^3 of water and an equivalent volume of air. Steam condenses here, water and entrained solids are then removed by a filter/demister.
- a set of charcoal columns. These are operated in parallel so that the pressure drop due to the high venting flow rates is minimised.

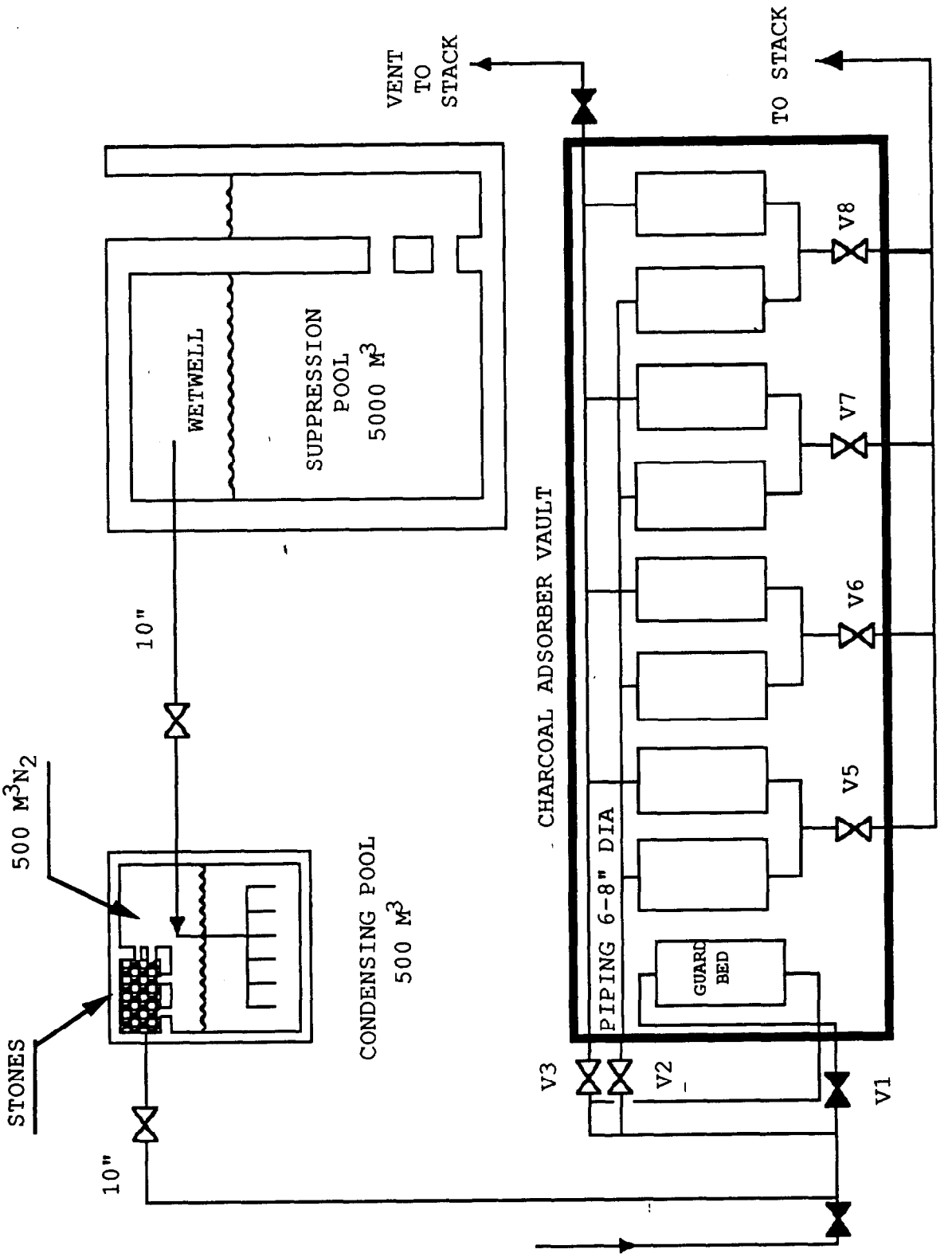

Figure 1. SBWR primary containment venting through off-gas charcoal following a severe accident.

In order to reduce the pressure values, minimum pipe line diameters are 8 to 10 inches, depending on the line length.

The present study will show whether a drier should be inserted before the OGTS.

Our estimates indicate that this system would effectively operate during accident sequences involving a containment failure after over ten hours.[5,6] Preliminary dose assessments also reveal that standard OGTS would keep the effective-dose release below values requiring site evacuation.[3]

II. Noble-Gas Water-Vapour Coadsorption.

Charcoal columns are usually employed in nuclear power plants as radioactivity-release delaying devices, and not as part of the containment system. Their role is to retain radioactive noble gas mixtures containing, in particular, Xenon isotopes until their radioactivity has fallen below assigned values. In order to achieve a DF equal to 1000, a typical design figure is a 30 day delay for Xenon under standard working conditions, i.e., with dried air and constant temperature.

Adsorption processes of Krypton and Xenon on charcoal are similar and may be correlated.[7] For the experimental investigations, however, Krypton is a better choice than Xenon since its adsorption coefficient is an order of magnitude lower, thus making retention tests proportionally quicker. Moreover, ^{85}Kr may be conveniently employed as a tracing isotope due to its long mean life.

The behaviour of charcoal beds must be analysed as a function of temperature and humidity of the air, and in terms of heat removal capability, in order to employ standard OGTS's, or other dedicated systems, for accident mitigation purposes.

Based on these observations, we planned the series of tests described in Table 1, aiming at the following objectives:

- determination of the dynamic adsorption properties of noble gases on activated charcoals;

- modelling and simulation of the co-adsorption of noble-gas and water-vapour;
- measurement of the thermal conductivity of charcoals, also in the presence of water.

Table 1. Summary of the experimental programme (K_{ads}: adsorption coefficient measurements, D_e: diffusivity measurements).

T °C / Relative Humidity	0	20	40	60	80
0	K_{ads}		K_{ads}		K_{ads}
40		K_{ads}	K_{ads}	K_{ads}	
60		K_{ads}	K_{ads}	K_{ads}	
80		K_{ads}		K_{ads}	

T °C / Water/ Charcoal*	40	60
0	D_e	D_e
5	D_e	D_e
10	D_e	D_e

* weight per cent

Reference working conditions were chosen in terms of surface velocity (10 ÷ 20 times the normal service values), temperature (equal to or greater than ambient values), and relative humidity (up to 80%).

Table 2. Typical analyses of NORIT 2030 charcoal.

Apparent bulk density (dry basis)	g/l	525
Pellet diameter	mm	2.9
Moisture, as packed	wt%	2
Total ash content	wt%	5
Abrasion resistance (ASTM)	%	99
Pore size distribution:		
Micropores (under 1 nm)	cm^3/g	0.26
Transition pores (1 - 100 nm)	cm^3/g	0.06
Macropores (above 100 nm)	cm^3/g	0.35
Total internal surface area from benzene adsorption according to B.E.T.	m^2/g	700
Ignition temperature (ASTM)	°C	above 450

All our tests were carried out employing Norit R2030 charcoal. This is a steam activated, extruded charcoal, particularly suitable for gas retention purposes thanks to the large internal surface of its fine micropores. The manufacturer-declared main characteristics of this charcoal are reported in Table 2.

The ability of Norit R2030 to adsorb noble gases has been tested extensively. Our experimental apparatus is shown in Figure 2. A ^{85}Kr-traced gas pulse is injected into the flow of dry air passing through a charcoal loaded container. This is a stainless steel cylinder, 58 mm in diameter and 600 mm in height. These dimensions were chosen in order to optimise the elution time in the case of DBA flow rates.

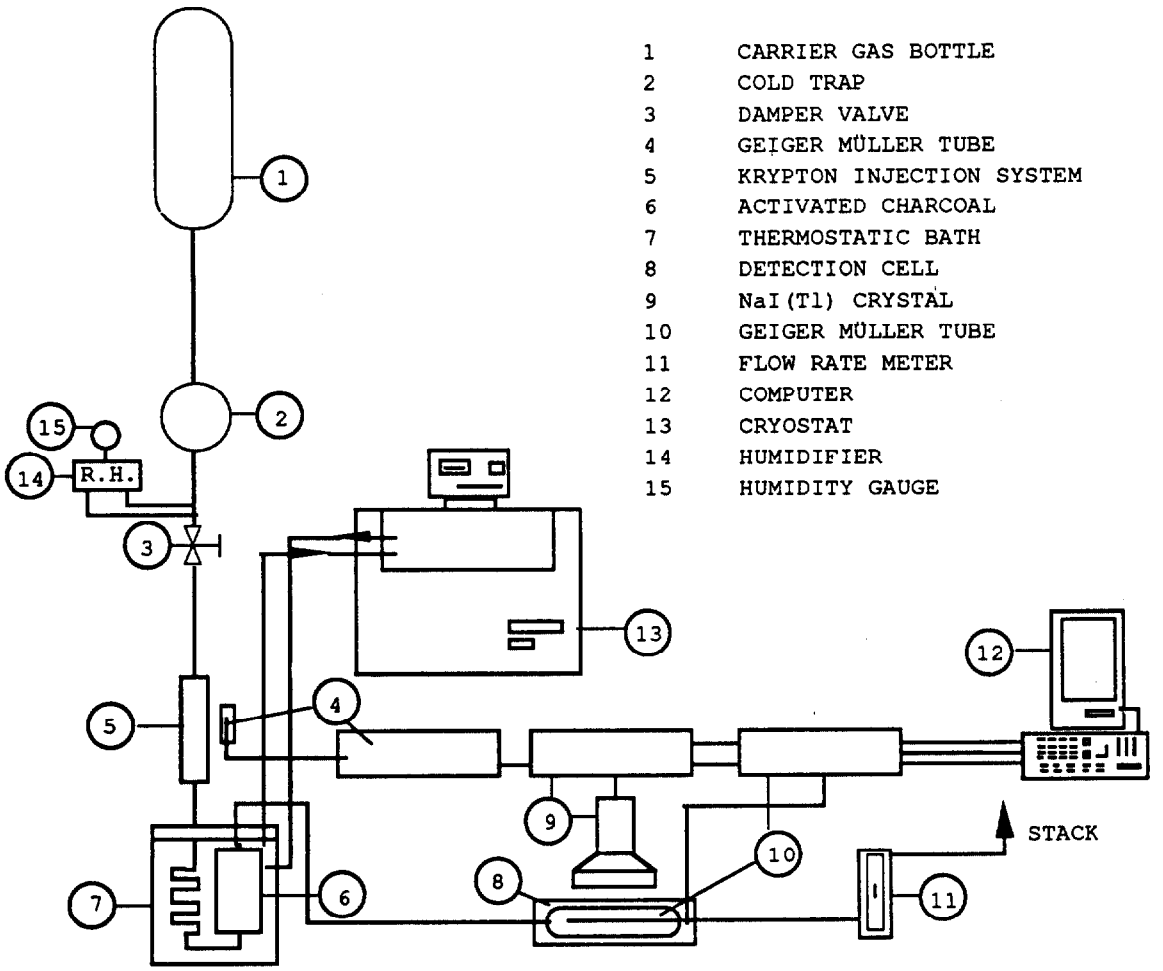

Figure 2. Adsorption measurement apparatus.

The charcoal is dried at 110 °C for 24 hours before filling the container. This is kept on a vibrating plate during the loading operations in order to prevent preferential path formation. The cylinder is then immersed in a thermostatic bath at temperatures ranging from 0 to 60 °C. The adsorption coefficient of Norit R2030 for ^{85}Kr may be determined from the analysis of the elution curves.[8] The typical shape of such curves is shown in Figure 3. A plot of the adsorption coefficient versus temperature for dry charcoal and dry air flows is reported in Figure 4. Our data are consistent with the results of similar studies.[9]

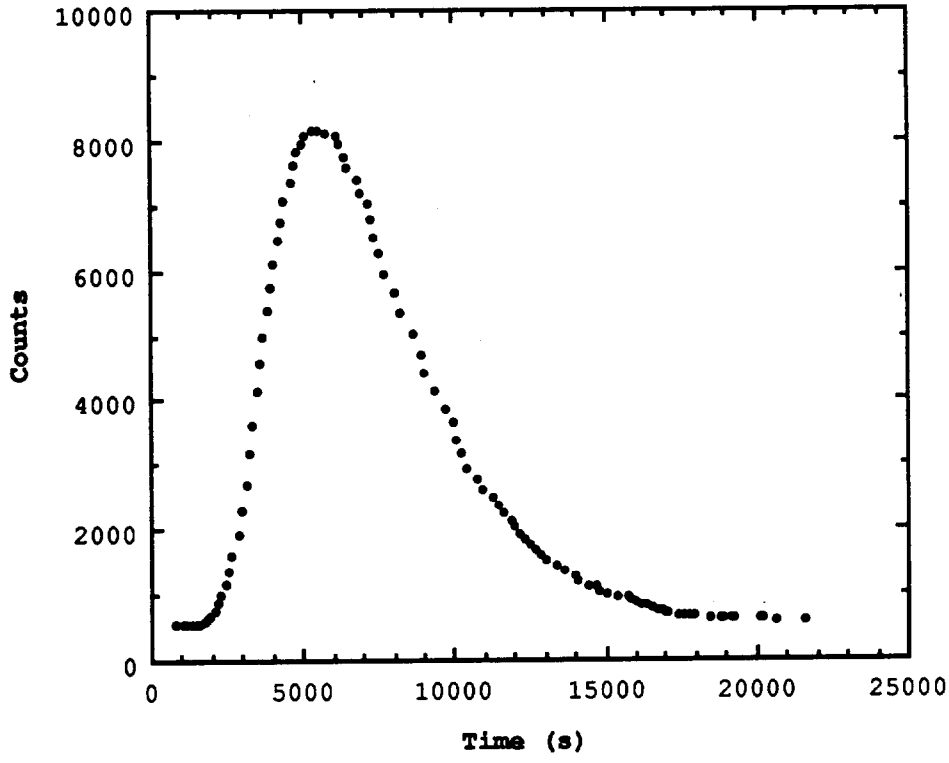

Figure 3. Typical Krypton-85 elution curve.

In order to analyse the behaviour of charcoal in the presence of vapour, a system for the generation of air with the desired RH values was inserted in the circuit of Figure 2. This is a cylinder which contains a constant amount of evaporating water and is connected to the dry air line. The evaporation is caused by the presence of a heater inside the container, while the water is

continuously supplied by a small volumetric pump. The level of water is kept constant by controlling both the heating power and the pump flow rate.

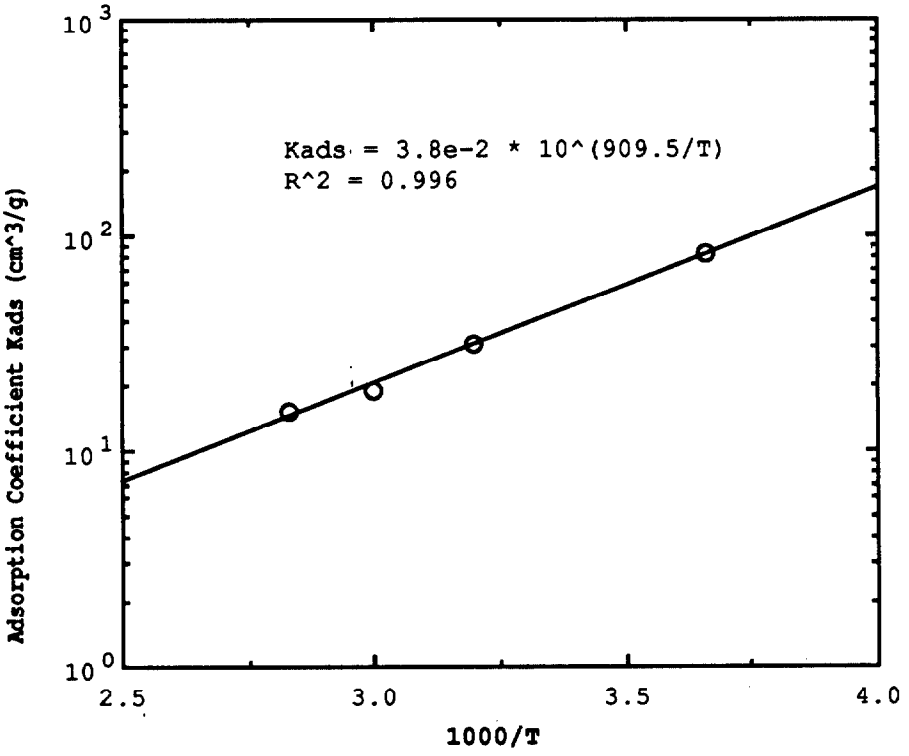

Figure 4. Adsorption coefficient as a function of temperature for Krypton on dry charcoal.

With this set-up, the previously described tests shall be repeated in order to determine the Krypton adsorption coefficient for charcoal in equilibrium with a humid air flow.

The same apparatus is also employed in the simulation of the impact of a severe accident on the radioactive-gas retention capability of an activated charcoal bed. In this case, the response of a charcoal column is analysed in terms of elution curves following the arrival of both a humid air front and a mixture of Krypton and humid air. Data are acquired by means of a mass spectrometer connected to the output of the charcoal column.

With this approach, both the contents of vapour and of several other gases in the air may be monitored accurately and simultaneously.

III. Thermal Conductivity of Charcoal Beds.

The thermal conductivity is necessary in order to derive the temperature profiles, and their time histories, inside the charcoal columns.

We realised an apparatus generating temperature transients in activated charcoal beds and inferred the thermal conductivity from the variation of the charcoal temperature. This coefficient, in turn, will be introduced into the theoretical model describing the heating of charcoal beds due to steam condensation and radioactive decay.

We chose to employ a cylindrical system for simple analytical modelling and easy experimental procedures. The apparatus consists of a waterproof stainless steel cylindrical vessel (58 mm diameter, 600 mm height) which is loaded on a vibrating plate with the charcoal to be tested. The container is immersed in a thermostatic bath until it reaches the equilibrium temperature T_0, then it is transferred into another thermostatic bath at temperature T_1.

A data acquisition system records the temperature reading of a sensor (a 0.5 mm type-K Chrom-Alumel thermocouple) placed in the centre of the cylinder. The correct positioning of the temperature sensor is guaranteed by keeping it inside a sheath which is gradually extracted while the cylinder is loaded.

Heat transfer along the axis is assumed to be negligible given the ratio between diameter and height of the cylinder. The thin thermocouple wire has no significant effect, either. Thermostatic bath and cylinder-wall temperatures are monitored as well.

We performed some preliminary tests with charcoal previously dried at 110 °C. We operated in the 23 ÷ 60 °C temperature range and both $T_0 > T_1$ and $T_0 < T_1$.

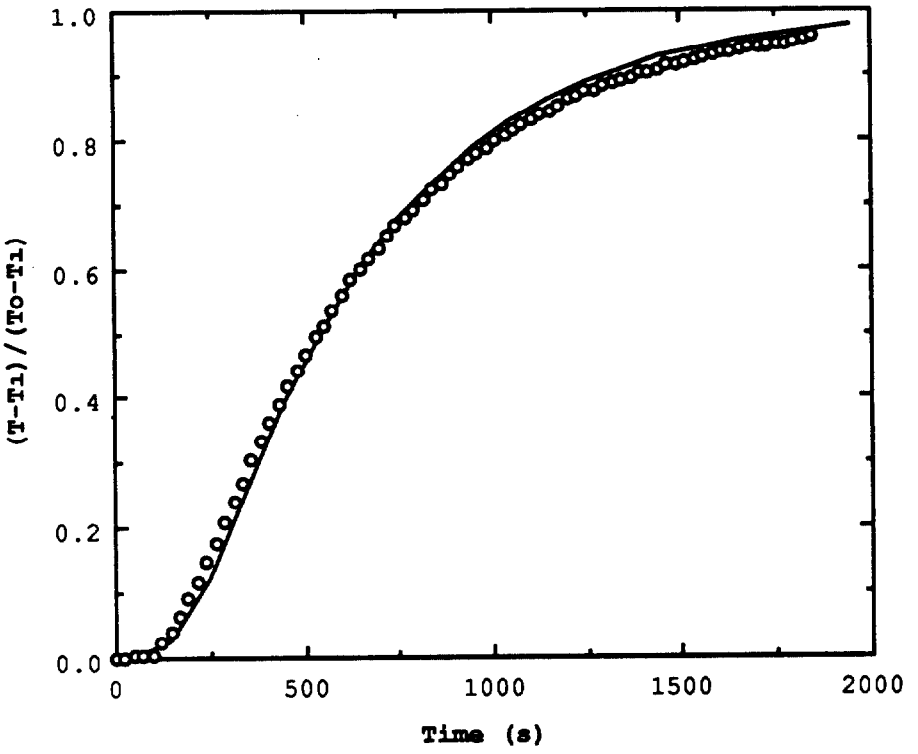

Figure 5. Mid-axis temperature as a function of time.

Figure 5 shows an experimental plot of temperature versus time, against the solution of the following differential equation:

$$\frac{\partial T}{\partial t} = D_e \frac{1}{r} \frac{\partial}{\partial r}\left(r \frac{\partial T}{\partial r}\right)$$

$$T = T_1, \quad 0 \leq r < a, \quad t = 0,$$

$$T = T_0, \quad r = a, \quad t \geq 0,$$

where T_0 and T_1 have been previously defined, and a is the radius of the cylinder.

This mathematical description of the physical phenomena does not treat separately the two processes of diffusion and adsorption, the term D_e is therefore to be intended as an effective diffusion coefficient. This approach is often successfully adopted when lattice diffusion takes place along with a reversible trapping phenomenon such as adsorption.

The analytical solution is then:

$$\frac{T - T_1}{T_0 - T_1} = 1 - \frac{2}{a} \sum_{n=1}^{\infty} \frac{e^{- D_e \alpha_n^2 t} J_0(r \alpha_n)}{\alpha_n J_1(a \alpha_n)} \qquad (1)$$

where $J_0(x)$ and $J_1(x)$ are Bessel functions of the first kind of zeroth and first order, and α_n's are roots of $J_0(a \alpha_n) = 0$.

This approach implies the assumption of negligible variations of D_e over our working temperature range. Therefore, we made tests with various T_0 and T_1 in the 23 ÷ 60 °C interval, always finding D_e values between $4.2\ 10^{-3}$ and $4.6\ 10^{-3}$ cm^2/s.

In the case of Figure 5, T_0 was set at 23 °C and T_1 at 60 °C. The best fit of the experimental data resulted from a choice of $D_e = 4.6\ 10^{-3}$ cm^2/s.

The thermal conductivity k was then calculated as $5.8\ 10^{-4}$ cal/cm s °C, from $D_e = k/C\rho$, and based on a heat capacity C = 0.24 cal/g °C and a bulk density $\rho = 0.525$ g/cm^3.

Table 3. Summary of the diffusivity measurements and the conductivity calculations.

T_0 (°C)	T_1 (°C)	Relative Humidity	D_e (cm^2/s)	k (cal/cm.s.°C)
23	35.5	0	$4.6\ 10^{-3}$	$5.8\ 10^{-4}$
35.5	46	0	$4.2\ 10^{-3}$	$5.3\ 10^{-4}$
46	35	0	$4.2\ 10^{-3}$	$5.3\ 10^{-4}$
35	23	0	$4.6\ 10^{-3}$	$5.8\ 10^{-4}$
23	60	0	$4.6\ 10^{-3}$	$5.8\ 10^{-4}$
60	23	0	$4.6\ 10^{-3}$	$5.8\ 10^{-4}$
23	60	5	$4.0\ 10^{-3}$	$5.0\ 10^{-4}$
60	23	5	$4.0\ 10^{-3}$	$5.0\ 10^{-4}$
23	60	10	$3.6\ 10^{-3}$	$4.5\ 10^{-4}$
60	23	10	$3.3\ 10^{-3}$	$4.1\ 10^{-4}$

Further tests were performed employing charcoal first dried at 110 °C and then humidified with amounts of water corresponding to 5 and 10 per cent in weight. Again, we found that our simple diffusive model effectively describes the experimental results. This might imply that the heat capacity per unit volume may be still considered constant. In this case, k could be calculated from the previously employed $C\rho$ value.

The complete series of our tests is summarised in Table 3. Our values of the coefficient k for dry charcoal are markedly higher than those reported in literature.[10,11,12,13] The latter were derived under stationary conditions, though, whereas we worked with temperature transients.

Therefore, the next step of our research programme shall involve measurements with a constant temperature gradient through the charcoal bed. For this purpose we devised the apparatus shown in Figure 6, which allows for the realisation of assigned temperature steps (ΔT) between inner and outer walls of a cylindrical shell loaded with charcoal.

The thermal conductivity may be inferred from the power required by the central heater in order to maintain a certain ΔT through the charcoal bed. An extensive series of tests is currently under way with both dry and wet charcoal.

IV. Conclusions.

The experiments carried out so far demonstrate the validity of the testing facilities designed and realised at DCMN—Pisa.

Our preliminary results confirm the conservative nature of the assumptions underlying the ENEA—DISP estimates of the highest OGTS temperature reached after a severe accident.

Following the entire programme of tests, all necessary data will be available to assess the applicability of venting for noble-gas removal during severe accident sequences.

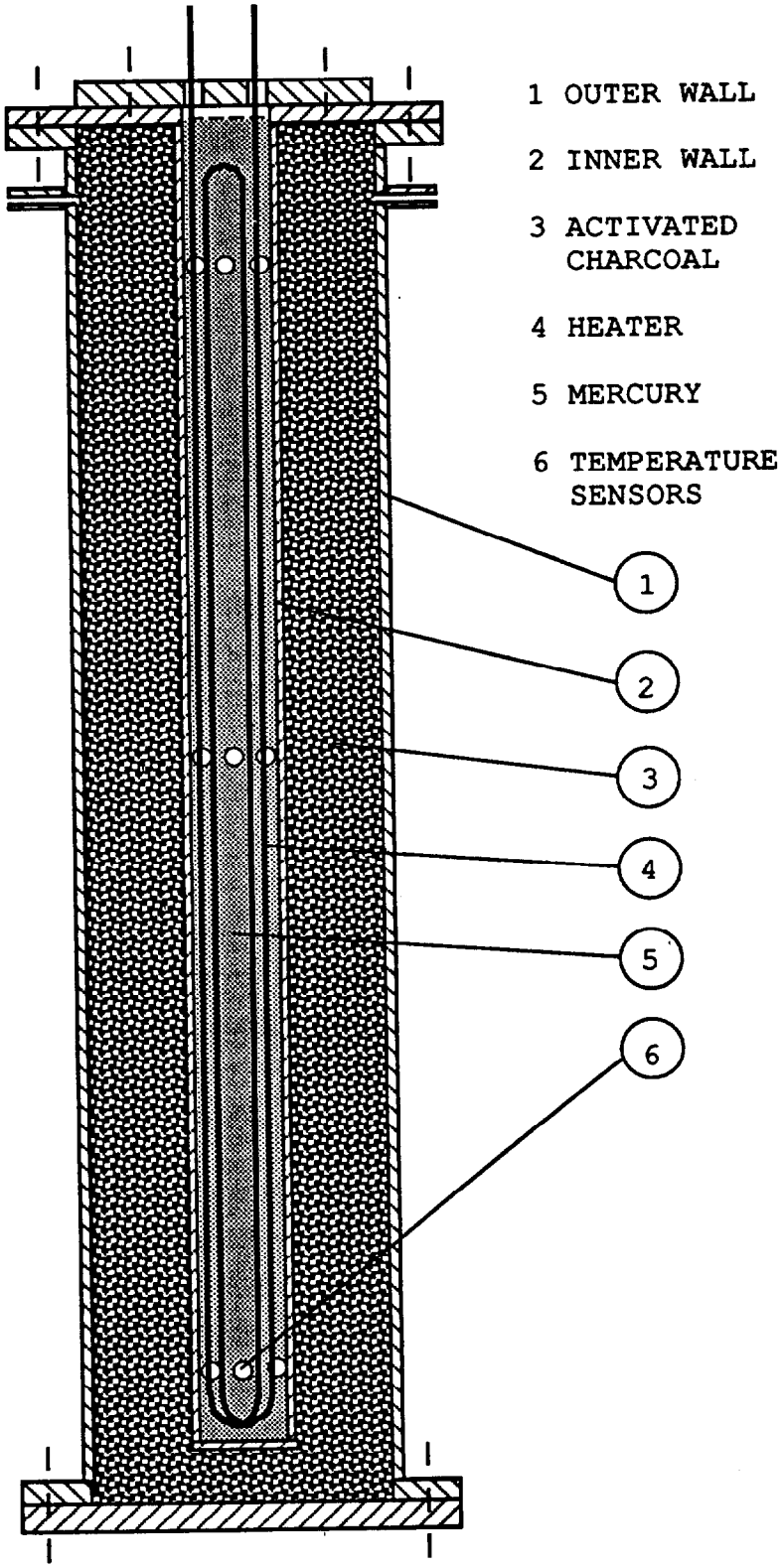

Figure 6. Thermal conductivity measurement apparatus.

References

1 International Nuclear Safety Advisory Group; "Basic safety principles for nuclear power plants;" Report INSAG-3; Safety Series n. 75.

2 Caropreso G., Leonardi A., Perna W., Sgalambro G.; "Theoretical and experimental investigation on the adaptability of charcoal beds to containment filter venting in Italian nuclear power plants;" Proc. 20th DOE/NRC Nuclear Air Cleaning Conference; Boston: Aug. 22-25, 1988.

3 Sgalambro G., Arru L., Cricchi G., Mustacchi C.; "Containment venting through the Off-Gas System: a way of upgrading the accident manageability of the plant;" OECD Specialist Meeting on Severe Accident Management Programme Development; Rome: Sept 23-25, 1991.

4 Sgalambro G.; "Anticipated source term production for different alternatives of containment venting in BWR's;" IAEA TCM on Experience with Containment Venting; Stockholm: Sept. 10-13, 1991.

5 Arru L., Sgalambro G.; "Containment venting alternatives in Italian BWR's: a preliminary approach;" IAEA-SM-296/52-P.

6 Anzano L., Arru L., Sgalambro G.; "Outlines of a possible strategy for containment venting;" OECD Specialist Meeting on Filtered Containment Venting; CSNI Report 148.

7 Castellani F., Curzio G., Gentili A.; "The Caorso Off-Gas System: acceptance test of noble gas delay charcoal beds;" Proc. NUCLEX 78; Basel: 1978.

8 Curzio G., Gentili A.; "The effect of heat produced by radioactive decay on the adsorption characteristics of charcoal beds;" Proc. Noble Gases Symp.; Las Vegas: 1973.

9 Castellani F., Curzio G., Gentili A., Leudet A., Miquel P.; "A comparative study of management strategies for Krypton 85;" Methods of Krypton 85 Management; Harwood Academy Publications; Brussels, 1983.

10 Henrion P.N.; "Stockage dans des cylindres pressurisés du Krypton adsorbé sur du charbon actif;" Report EUR 6419; 1979.

11 Curzio G., Mori A., Vaglini S.; "Profilo di temperatura all'interno di bombole per il confinamento del Kripton 85 caricate con materiale granulare poroso;" Atti 43° Congresso ATI; Ancona: Sept. 20-23, 1988.

12 Chemical Engineers' Handbook; Perry J.H., Editor; McGraw-Hill: New York, NY; 1963.

13 Handbook of Chemistry and Physics; Weast R.C., Editor; CRC Press: Cleveland, OH; 1976.

DISCUSSION

WILHELM: What will be duration of the wet airflow in the dynamic adsorption coefficient measurements? Just the duration of the experiment.

CASTELLANI: The duration is a few hours. In all our past experiments, we have waited a few hours until equilibrium conditions are reached with constant air flow rate. The same procedure shall be adopted for wet air flow experiments.

WILHELM: You measure the dynamic coefficient independent of time but the shock pool will warm up first and then it will pick up water and change very much the dynamic coefficient.

DESIGN OF A PREFILTER TO IMPROVE RADIATION PROTECTION AND FILTERING EFFICIENCY OF THE CONTAINMENT VENTING SYSTEM

by Maurice V. Kaercher,
Electricite de France
Lyon, France

Abstract

The sand bed filters installed on all French pressurised water reactors (PWR) were intended to retain the source term of radioactivity, inside the containment, 24 hours after the beginning of core meltdown but because of its size, the sand filter is outside the containment and therefore after operation, the source term which may be inside the sand filter could provide very high radiation levels on the site.
To cope with this a prefilter was designed that was to be located inside the containment and would retain the source term there. This paper describes the main results of the R&D programs implemented in 1991 and 1992 to develop the prefilter. It covers the following items :

- introduction,
- short presentation of the venting system,
- description of laboratory tests performed in various conditions of temperature and pressure with :
  - . hydroscopic aerosols (CsOH),
  - . non-hydroscopic aerosols (TiO_2, SiO_2, SZn),
  - . a mixture of both,
- assumptions on quantities and sizes of aerosols in two main accident scenarios (core melting and core concrete interaction),
- main results on filtering efficiency, pressure drop, capacity of retention and choice of accurate metallic media,
- basic design requirements for the prefilter,
- conclusion.

1. Introduction

After a short description of the current French venting system which was presented at the 21st conference in San Diego (title : Design and full-scale test of a sand bed filter), this paper points out the improvement of the venting system by a compact prefilter installed inside the reactor building.
The tests presented in this paper were performed in collaboration with :

- Institut de Protection et de Sûreté Nucléaire (IPSN) of the Atomic Energy Commission (AEC),
- AEC Laboratories in Saclay,
- PALL INDUSTRIES SA in Paris,
- PALL Laboratories in Portsmouth (GB).

2.Short presentation of the current venting system

2.1. Description of decompression filtration system (see figure 1)

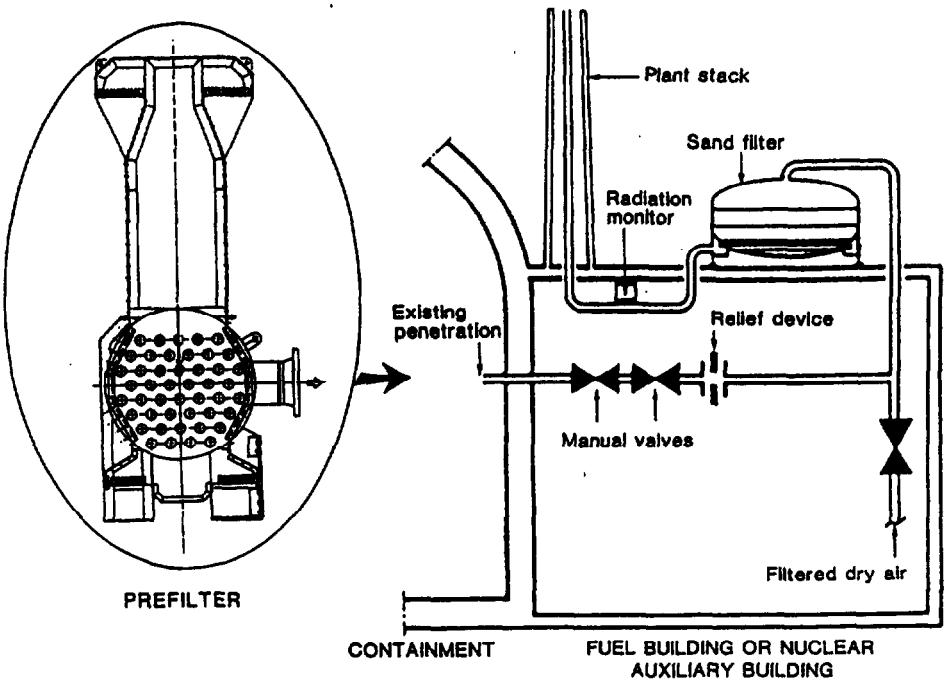

Figure 1 : General Diagram

The decompression-filtration system consists primarily of :

- the new prefilter
- a containment penetration with double insulation comprising two valves in series located outside the containment, and as close to it as possible,
- an orifice plate reducing pressure to atmospheric,
- a sand bed filter,
- a device for measuring radiation released,
- an independent evacuation duct located inside the normal effluent stack of the plant.

2.2. Description of the sand bed filter (see figure 2)

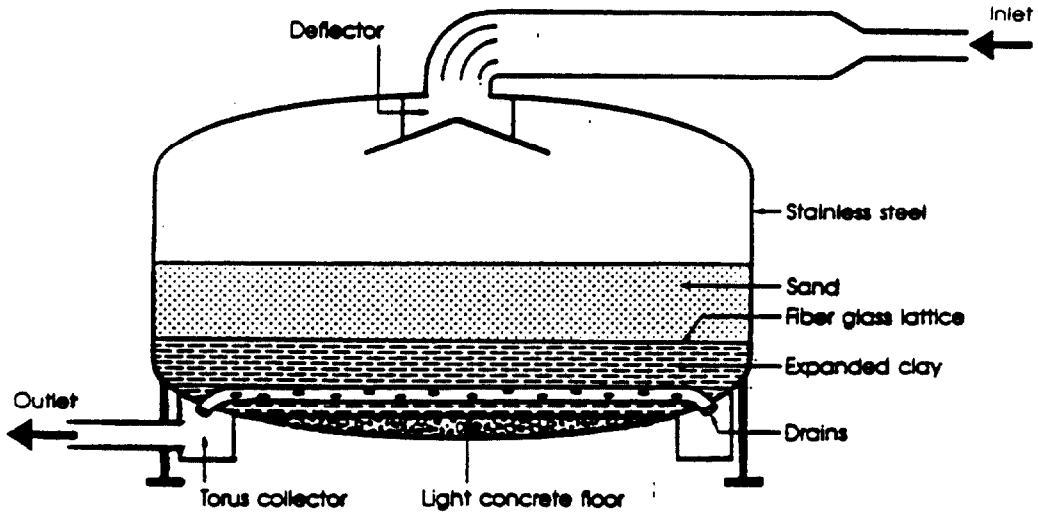

Figure 2 : Sand bed filter section

The sand filter is a stainless steel vessel with diameter 7.32 m, height 4 m, empty weight 12 t and operational weight 92 t.

The sand bed support comprises an expanded clay layer with a basket system for gas recuperation and a cellular concrete floor in the filter bottom.

The filters are fully thermally isolated.

For all sites except Fessenheim, this filtration system is installed on the roof of the nuclear island building, PWR 900 MWE series is fitted with a system common to two plants.

2.3. Operating condition

From the principle viewpoint, it seems worthwhile recalling first of all that safety depends on containment. This fundamental principle should not be brought into question by the existence of a venting device permitting a controlled opening to be made in this containment. In consequence it would be preferable to postpone as long as possible, and if possible to avoid putting this device into operation, by taking into account its mechanical resistance properties.

This being specified, the decision to put the system into operation then out of service is the responsability of the Power Station Director in conjunction with the local and national level of the authorities who are in charge of crisis management. The system is put into operation by opening the containment isolating valves (after closing the incoming conditioning air). The internal containment pressure is then about 5 bars.

The specific start-up criteria of the system are specified in the Severe Accident Intervention Guide prepared by Electricité de France after discussions with the Safety Authorities.

2.4. Qualification tests

Thermal-hydraulic, filtration, thermic and salting-out tests were performed to qualify the decompression filtration system. These tests were carried out in 1990 on a full scale filter on the FUCHIA loop in Cadarache.

2.4.1. Description of qualification tests

An Air-stream mixture (35% air, 65% steam at a temperature of 140°C) was blown through the sand filter for 50 h.

During the first 25 h, caesium aerosols were generated by means of plasma torches with an AMMD of 1 μm at a flowrate of 513 g. Iodine was introduced in molecular form at a flowrate of 70 g/h.

During the following 25 h neither aerosols nor iodine were generated.

2.4.2. Results

The decontamination factor (DF) on caesium and iodine was evaluated by :

- measuring caesium and iodine concentration above and below the sand filter,
- measuring caesium aerosols AMMD and concentration with impactors (ANDERSEN 2000), above and below the sand filter.
- three-dimensional cartography in the sand by means of core samples.

The main results were :

- The AMMD of caesium aerosols measured above the sand filter was close 1 μm (standard deviation about 2.3),
- the diagram (see figure 3) gives the DF for caesium hydroxyde measured on the sand filter as a function of time,
- for iodine, an average DF of 10,
- a very low salting out was noticed during the period without aerosols generation.

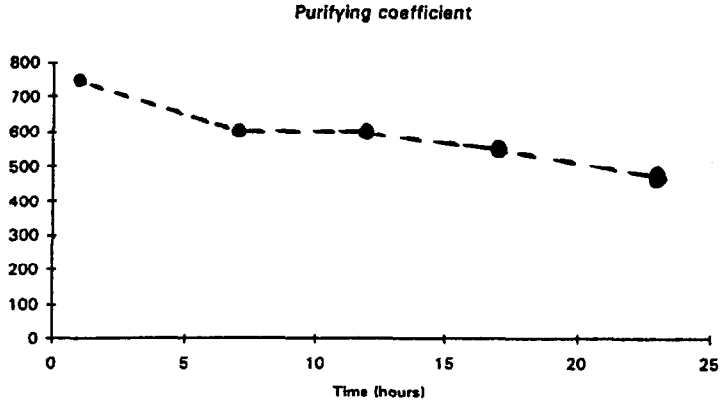

Figure 3 : decontamination factor for caesium hydroxyde

2.5. Radiation protection

The surveys undertaken showed that, as regards on-site and off-site protection, biological shieldings were necessary for direct and indirect dose rate values (skyshine) induced by the limit values corresponding to the radioactivity trapped in the filter for the most pessimistic hypothesis with an extreme source term.

Designing sky shine protection was not easy because of the high costs and the limited mass of a structure acceptable from a seismic point of view.
So studies were led to find new solutions to cope with irradiation problems. These protections would be unnecessary if we could stop 90% of the radioactivity inside the reactor building by a coarse filter called a prefilter.

3. Preliminary tests of metallic media with cesium aerosols

EDF designed a prefilter that was small enough to be installed inside the reactor building and had a DF of more than 90 %, making shyshine protection unnecessary.

Our first reasearches led us to test metallic medias called FH 150 produced by PALL. These medias were tested with the same aerosols (CsOH) as those used for the qualification of the sand bed filter. The results are the following :

- in dry air, we observed a small pressure drop (see figure 5) and a high DF (see figure 4),
- in air mixed with steam we observed, at the beginning of the test a very small pressure drop ; and then a very strong increase in pressure drop which led to the flow through the media stopping (see figure 5). This was attributed to the hydroscopic character of CsOH aerosols.

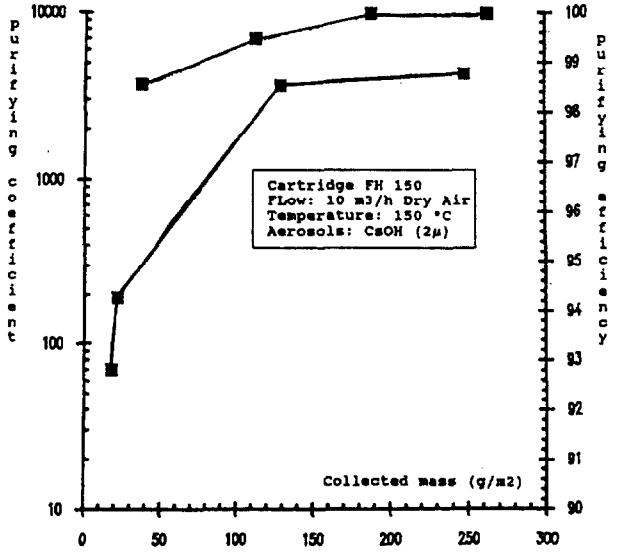

Figure 4 : Decontamination factor (CSOH)

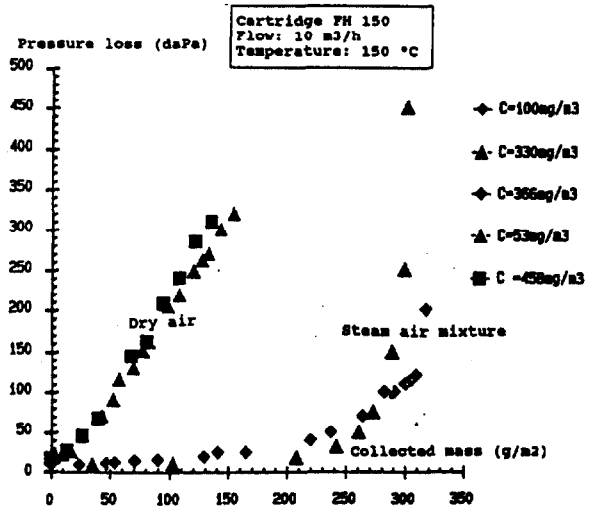

Figure 5 : Pressure drop (CsOH)

4. Tests of metallic medias with insoluble aerosols (TiO_2)

Tests performed with insoluble aerosol (Ti O2) in air mixed with steam did not show any strong increase in pressure drop (see figures 6).

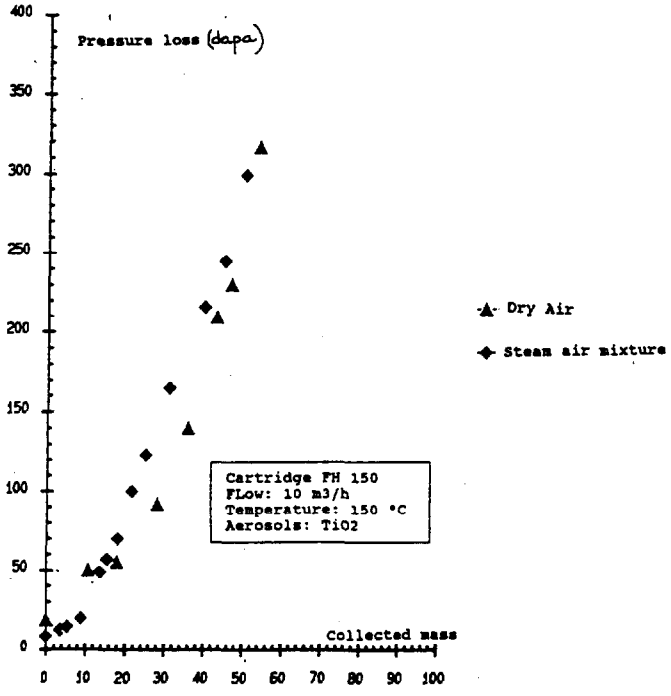

Figure 6 : Pressure drop (TiO_2)

These different behaviors of metallic filtering medias led us to further our knowledge of the nature, the quantity and the radiological activity of aerosols.

5. Investigations of assumptions concerning aerosols

Two groups were considered to investigate assumption concerning aerosol :

- In-vessel release
  In this case, only the volatile aerosols produced by core melting were considered. In filtration tests, these aerosols were modelled by CsOH aerosols which are the most severe for the prefilter.

- Ex-vessel release
  In this case there would be, mixed aerosols in the reactor building, some coming from the core melting, others, non radioactive, coming from concrete degradation. We also stress the fact that the continuous production of non-radioactive concrete aerosols would make radioactivity inside the reactor building decrease by agglomeration and redeposition.
  This phenomena was modelled by the code AEROSOLS B2 (ESCADRE system designed by AEC-IPSN) and it was shown that after a 7.5 h of venting system operation, the proportion of radiactive aerosols and the radioactivity inside the reactor building would be divided by a factor of 10. So 7.5 h would be the minimum time of operation required for the prefilter : after this it could be bypassed.

During operation of the prefilter a mass flow of 5 kg of aerosols per hour was blown through it. This corresponded to a total mass of 37.5 kg. Only 1.5 kg of these aerosols were radiactive : so the proportion of CsOH aerosols in the mixture to be filtered was about 5 %.
It was verified that the total 37.5 kg mass of aerosols would cover all the flows of concrete aerosols production. Filtration tests showed that this aerosol mixture had no hygroscopic behaviour.

6. Main results of filtration tests

The filtration tests were performed on a PALL filtering cartridge (FH200 + PFM40) with a mixture of air, steam and the following aerosols :

- soluble aerosols : CsOH,
- insoluble aerosols,
- mixture of soluble and insoluble aerosols.

Insoluble aerosols were produced by commercial powders of the corresponding size (AMMD = 2μ).

6.1. Filtration tests with CsOH aerosols

These tests were performed in AEC Laboratories in Saclay (schematic diagram of the loop. figure 7). The main results are given in figure 8. We observed a better efficiency of the compound cartridge FH 200 + PFM40 which was plugged at 500 g/m ^{2} of CsOH.

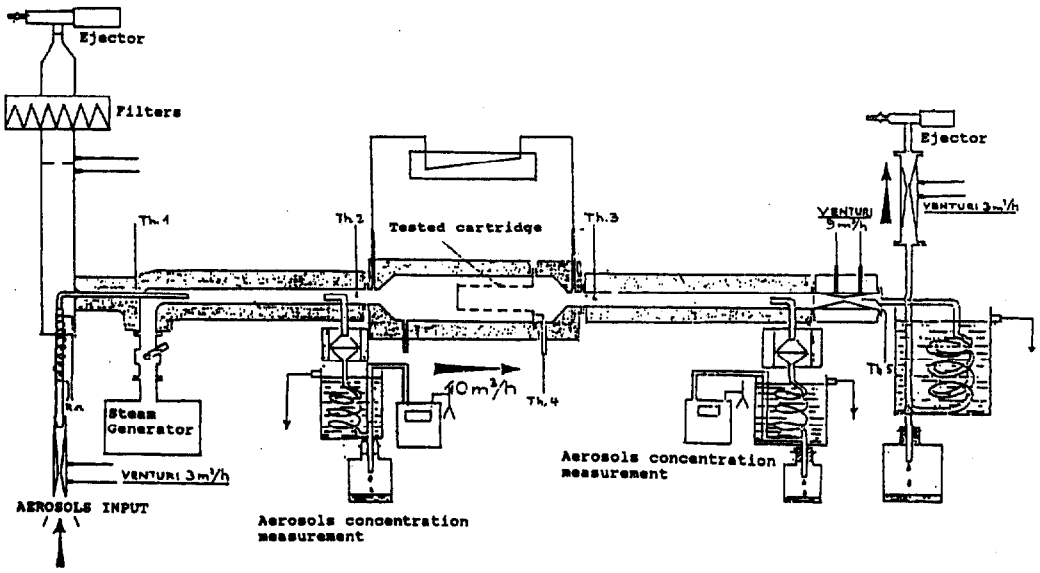

Figure 7 : schematic diagram for AEC test loop

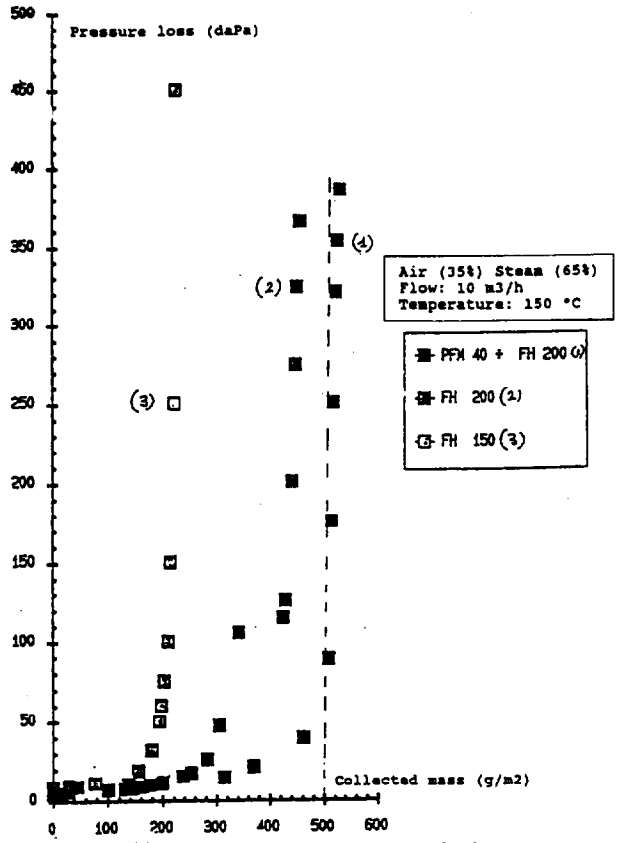

Figure 8 . Pressure drop (CsOH)

6.2. Filtration tests with insoluble aerosols

These tests were performed in PALL Laboratories in Porsmouth (GB) with SiO_2 and TiO_2 aerosols. The main results are given in figure 9.

The results showed

- a moderate increase of pressure drop,
- a positive contribution due to the fall of aerosol coating,
- a filtering efficiency of higher than 90 %.

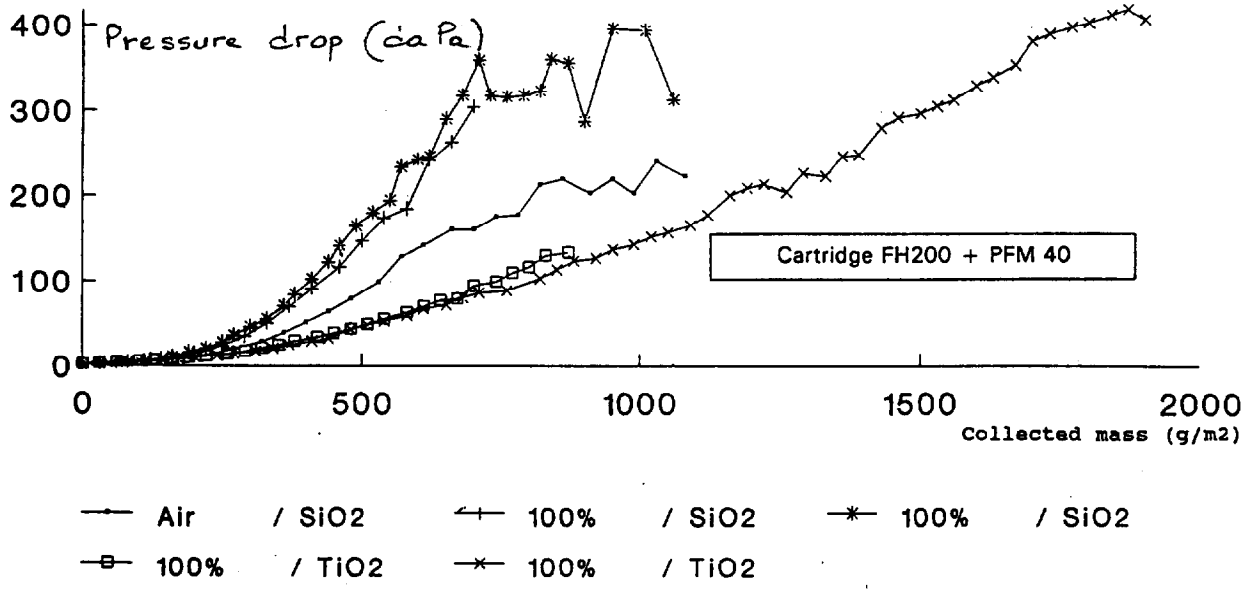

Figure 9 : Pressure drop (FH200 + PFM40)

6.3. Filtration tests with mixture of soluble and insoluble aerosols

These tests performed in AEC Laboratories in Saclay. The mixtures used were :

- pure zinc sulfur (as a reference point),
- zinc sulfur + 5 per cent of CsOH,
- zinc sulfur + 65 per cent of CsOH,
- zinc sulfur + 90 per cent of CsOH.

The main results are given in figure 10. We observed :

- the same behaviour for the mixture with 5 % of CsOH as for pure zinc sulfur.
- a hydroscopic behaviour for the mixture with 90 % of CsOH.

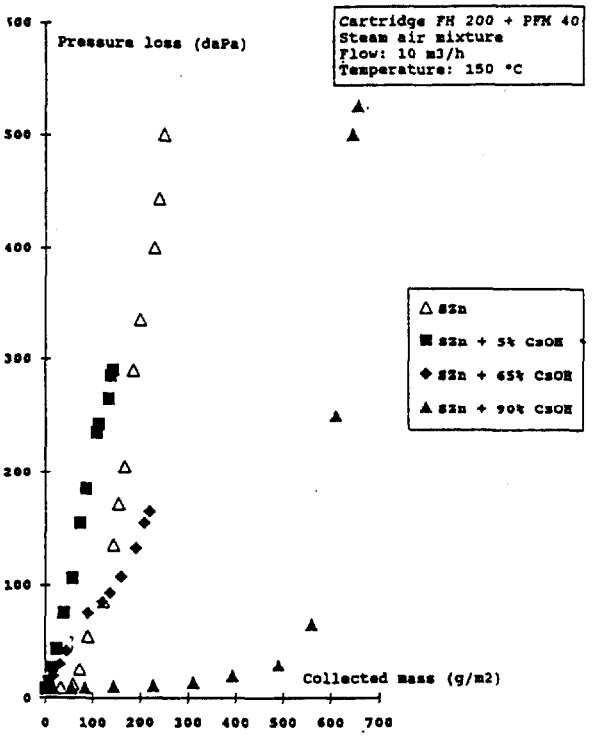

Figure 10 : Pressure drop (FH200 + PFM40)

Therefore a small proportion of CsOH did not alter the normal behaviour of the cartridge.

7. Design and efficiency of the prefilter

The prefilter was made using the PALL filtering cartridge FH 200 + PFM 40 with a surface of 33 m^2.

Thanks to the results of laboratory tests, the filtration surface can catch 37.5 kg of aerosols with a pressure drop less than 500 mbar.
To avoid filter clogging, a check valve (opening pressure 1 bar) bypasses the prefilter.
Moreover, concerning in-vessel release, the prefilter is able to catch 5 kg of CsOH with a small pressure drop.

8. Conclusions

The first prefilter was being installed at Golfech 2 in October 1992 and all the French PWR reactors will be equiped with prefilters between September 1992 and end of 1994.

This prefilter will be tested in full scale on the FUCHIA loop to confirm its efficiency. This test will also put into relief the contribution of the prefilter to the increasing of the purifying coefficient of the venting system.

DISCUSSION

KOVACH: In the early part of the paper, you mentioned that you are dealing with an insoluble aerosol. There is no difference between a dry stream and a wet stream. However, when you showed the data for silicon dioxide there was a fairly significant difference in the pressure drop buildup between the wet and dry streams. Do you think this is unique for SiO_2 or would it occur with other insoluble aerosols, also?

KAERCHER: Your question is, is there any difference in the pressure drop when we use silicon oxide between air flow and air plus inflow, is that correct?

KOVACH: Yes.

KAERCHER: We didn't observe many difference in case of TiO_2 aerosols.

WILHELM: What is the medium of the filter? Is it metal, fiber, or a mixture of both?

KAERCHER: The medium of the prefilter is made with sinter-consolidated steel fibers which provide high load capacity and low pressure drop.

DILLMANN: Do you have a lot of problems with the venting system throughput?. That is one point I am interested in. In our calculations, we see concrete-melt interactions for a long time in the aerosol production range. You have an aerosol production rate that decreases as concrete and melt interact. This, I can't believe.

KAERCHER: The flowrate of core concrete aerosols is connected to the scenario. A nearly constant production (instead of a strong decrease) will boost agglomeration and redeposition of fission product aerosols inside the reactor building and consequently improve the prefilter efficiency.

EXPERIMENTAL STUDY ON AEROSOL REMOVAL EFFECT BY POOL SCRUBBING

Itaru Kaneko, Masanori Fukasawa
NUCLEAR ENGINEERING LAB. TOSHIBA CORPORATION
4-1 UKISHIMA-CHO, KAWASAKI-KU KAWASAKI,210,JAPAN

Makoto Naito
NUCLEAR REACTOR DESIGN DIVISION, TOSHIBA CORPORATION
8 SHINSUGITA-CHO, ISOGO-KU YOKOHAMA,235,JAPAN

Kouichi Miyata
NUCLEAR POWER PLANT PLANNING DIVISION, TOKYO ELECTRIC POWER COMPANY
1-3, UCHISAIWAI-CHO, 1-CHOME, CHIYODA-KU, TOKYO, 100, JAPAN

Masaki Matsumoto
NUCLEAR POWER PLANT ENGINEERING DEPARTMENT, HITACHI Ltd.
1-1, SAIWAICHO 3-CHOME, HITACHI-SHI, IBARAKI-KEN, 317 JAPAN

ABSTRACT

During BWR severe accidents, radioactive aerosols released from a degraded core are expected to be removed in a suppression pool as a result of "scrubbing effect".

In order to understand the scrubbing effect, the authors carried out a scrubbing experiment with a scrubbing pool, which is a cylindrical pressure vessel, 1 meter in diameter and 5 meters high.

The aerosol removal efficiencies were systematically measured, varying eight parameters selected from a mechanistic scrubbing model. Bubble behavior in the pool water was also observed during the tests.

By comparison of mechanistic scrubbing models and test results, the authors developed a simplified model for aerosol removal effects by pool scrubbing. The simplified model predicts decontamination factors by scrubbing effect as a function of five parameters.

Calculated decontamination factors by the simplified model are consistent with measured DF within a deviation of the measurements.

I. INTRODUCTION

During a severe nuclear power plant accident, fission product aerosols will be generated from the degraded core and released into the reactor containment vessel. At BWR plants, aerosols are expected to be discharged into and removed in a suppression pool when drywell pressure increases or containment venting is initiated. This removal effect is considered a potential safety feature of BWR plants.

The authors carried out a scrubbing experiment and measured decontamination factors (DF) of pool scrubbing. Bubbles' sizes and rising up velocities were also observed. Test results, which also include DF obtained since the previous report[1], indicated that particle diameter, scrubbing depth and carrier gas steam fraction are dominant parameters for scrubbing effect. It was also confirmed that bubble diameters represented a certain distribution.

Based on the results, an expression of a simplified model for aerosol removal

effects was developed as a function of the selected parameters, referring to aerosol removal mechanisms of a prototype SPARC code. By comparison of measured DF and the simplified model, proportional factors in the simplified model expression were derived. To confirm an availability of the simplified model, calculated DF were compared with measured DF.

II. TEST DESCRIPTION

A. TEST CONDITIONS

Table 1 shows test parameters and their ranges. Standard value was selected for each parameter. The tests were carried out while varying only one parameter to clarify the influence by a specific parameter.

The aerosol material selected for the standard condition was polystyrene LATEX particles with mono-dispersed diameter and nearly unit density. Dispersed cesium iodide (CsI) particles were also used as representative of fission product aerosols.

Table 1 Test conditions

Parameter	Standard value	Range
Nozzle dia. (cm)	15	1,5,10,15
Scrubbing depth (meters)	2.7	0 - 3.8
Water temperature (°C)	80	20 - 110
Gas temperature (°C)	150	20 - 300
Steam fraction (vol.%)	50	0 - 80
Gas velocity (cm/s)	47	28 - 15000
Gas pressure (kg/cm^2g)	2.0	0.4 - 5.0
Particle dia. (micron)	0.2,0.3, 0.5,1.1	0.1 - 2.0
Particle material	LATEX	LATEX 0.5 - 1.9* CsI

*) Aerodynamic Mass Median Diameter (AMMD). Geometric standard deviation was 1.5 - 2.3.

B. TEST APPARATUS

Figure 1 shows scrubbing pool details. The scrubbing pool is a cylindrical pressure vessel, 1 meter in diameter and 5 meters high. It has five pairs of windows, 20 cm in diameter. A video camera is attached to the outside of each window to observe bubble behavior.

The LATEX particles were measured for optical particle diameter and number concentration by a laser scattering aerosol spectrometer. Cesium iodide particles were measured for aerodynamic mass median diameter (AMMD) and mass concentration by conventional

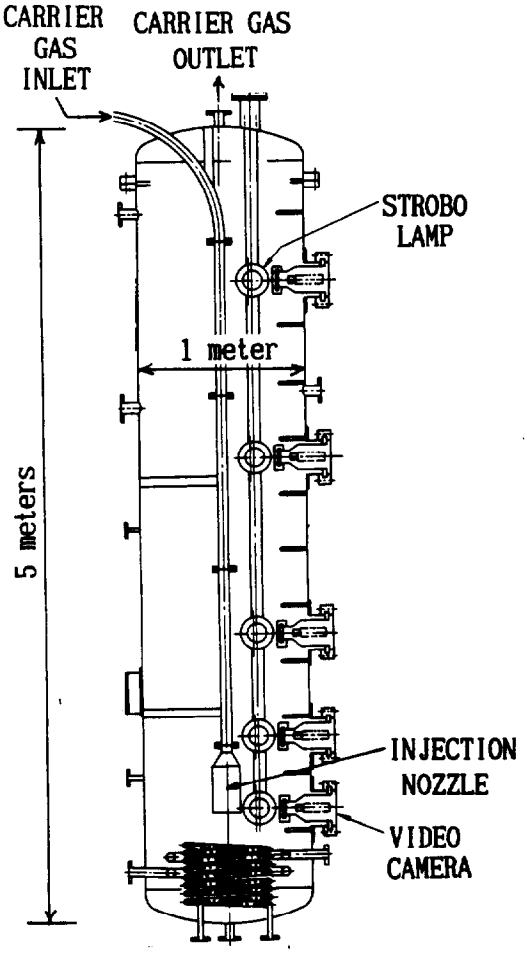

Figure 1 Scrubbing pool details.

Andersen impactors and absolute filters, respectively.

Three types of injection nozzle were used: downward vertical vent pipes (5, 10 and 15 cm in diameter), a slice of typical BWR quenchers with 22 exit holes (1 cm in diameter), a single upward orifice (1 cm in diameter).

Test procedure details were shown in the previous report[1].

C. TEST RESULT

Based on the test results, it was confirmed that DF mainly depended on particle diameter, scrubbing depth and carrier gas steam fraction.

It was also confirmed that bubbles generated by pool scrubbing formed elliptical spheres, which were flattened in the vertical direction (refer to Figure 2). A distribution of their equivalent diameters always represents a certain log-normal distribution without dependence on thermal hydraulic conditions (refer to Figure 3). Since velocity depends on bubble diameter, the bubble rise velocity also represents a certain value.

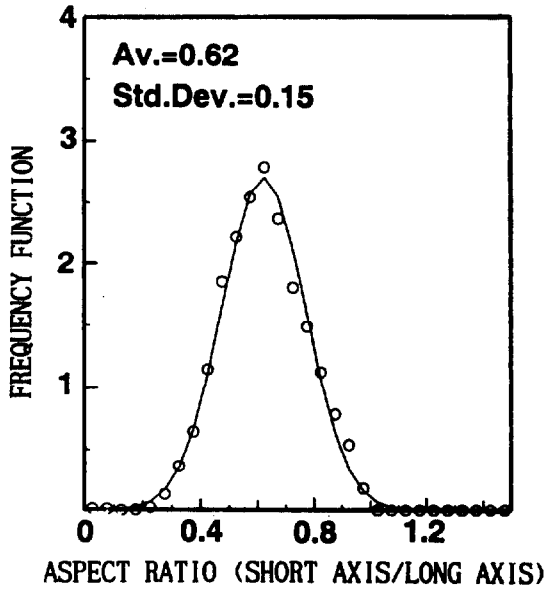

Figure 2 Bubble aspect ratio distribution.

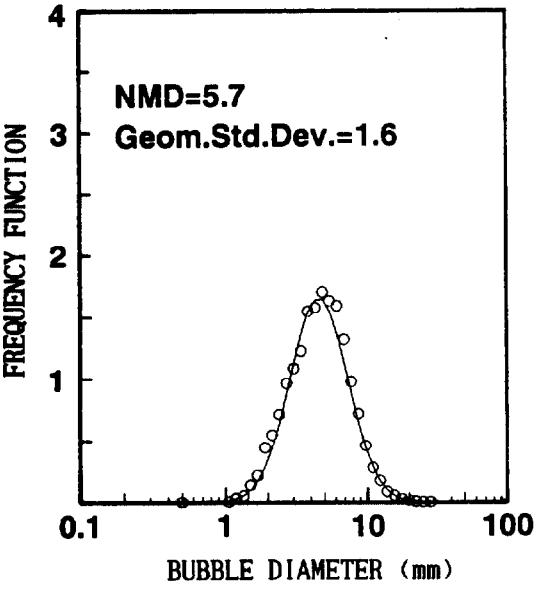

Figure 3 Bubble diameter distribution

III. MECHANISTIC SCRUBBING MODEL

A. SCRUBBING PHENOMENA

Carrier gas with aerosols, which has been injected into pool water, forms many small bubbles. If carrier gas contains steam, condensation of steam will occur around the injection point. Aerosols in the condensed steam are trapped in the pool water. An aerosol removal effect by this process is called an initial steam condensation effect.

Residual aerosols remaining in the bubbles will be transported toward the bubble surfaces during the bubble rising period, by driving forces of gravitational settling, inertial deposition, diffusional deposition and steam condensation (refer to Figure 4). The aerosols that arrive at the surface are expected to be retained in the pool water.

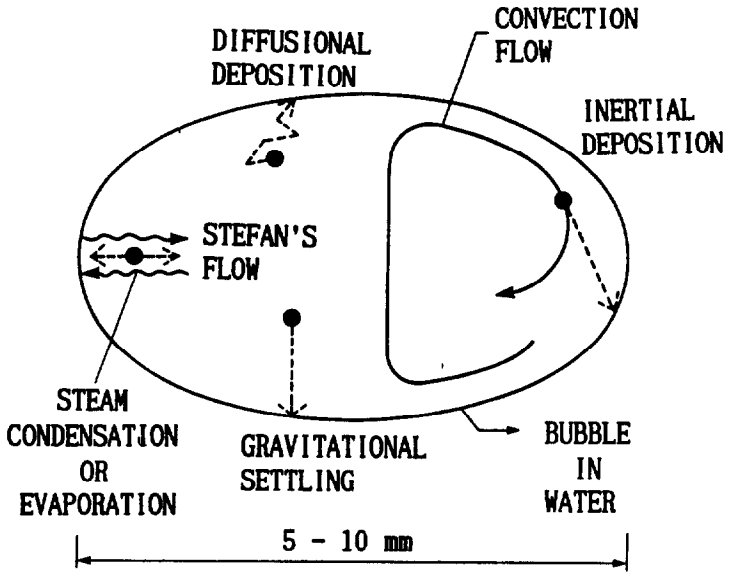

Figure 4 Aerosol removal mechanisms

B. AEROSOL DEPOSITION VELOCITY

Table 2 shows aerosol deposition velocities accounted for by the prototype SPARC code[2]. Both gravitational settling velocity, Vs, and inertial deposition velocity, Vc, increase in proportion to the square of particle diameter. Diffusional deposition velocity, Vd, mainly increases in proportion to particle diffusivity, which decreases in proportion to particle diameter. Deposition velocity by steam condensation or evaporation, Vv, depends on differences of thermal hydraulic conditions between the bubble and the pool water.

Table 2 Aerosol deposition velocity of the prototype SPARC code

Gravitational settling velocity	: $Vs = \frac{Pp \cdot Dp^2 \cdot Cm \cdot g}{18u}$
Inertial deposition velocity	: $Vc = \frac{Vb^2 \cdot Pp \cdot Dp^2 \cdot Cm}{4u \cdot Db} \cdot \sin^2\theta$
Diffusional deposition velocity	: $Vd = 2\,\frac{D \cdot Vb}{h \cdot Db}$
Deposition velocity by steam condensation or evaporation	: $Vv = \frac{Wv}{\{Mw(Pt+Pw)\}/(R \cdot To)}$

Pp : particle density Dp : particle diameter Cm : Cunningham correlation factor g : acceleration due to gravity u : gas viscosity Vb : bubble rising velocity Db : bubble diameter θ : angle measured from vertical pole	Wv : average vapor flux into a bubble Mw : average molecular weight at the surface Pt : total pressure at pool surface Pw : water vapor pressure To : interface temperature R : gas constant D : particle diffusivity

C. SCRUBBING MODEL

Using the above aerosol deposition velocities, DF for pool scrubbing is given as

$$DF = DFs \cdot DFi \cdot \exp\{(Vs+Vc+Vd-Vv) \cdot \frac{Hs}{Vb} \cdot \frac{S_B}{V_B}\} \quad (1)$$

where, Hs is scrubbing depth and Vb is bubble rising velocity, S_B is bubble surface and V_B is bubble volume. DF by the initial steam condensation effect, DFs, is defined as

$$DFs = \frac{fi}{fo} \quad (2)$$

where, fi is inlet carrier gas flow rate and fo is outlet carrier gas flow rate after thermal equilibrium has been attained around the injection point. fo depends on pressure at the injection point and pool water temperature.

DFi is DF by an inertial impaction between injected aerosols and pool water surface at the injection point. DFi is expected to increase in proportion to $\exp(Dp^2)$ on the analogy of the inertial deposition velocity, where Dp is particle diameter. It also depends on gas velocity in the injection nozzle, but it does not depend on scrubbing depth.

IV. SIMPLIFIED MODEL

Based on the test results, which were obtained for the LATEX particles with the vertical vent pipes and the simulative quencher, a simplified model for aerosol removal effect by pool scrubbing was developed.

A. EXPRESSION OF THE SIMPLIFIED MODEL

Based on the test results, Equation(1) can be reduced to a simplified expression as a function of particle diameter, scrubbing depth and carrier gas steam fraction. Bubble diameter and its rising velocity were assumed to be constant. Then, the simplified model expression is given as

$$DF = DFs \cdot \exp(A \cdot Dp^2) \cdot \exp\{(B \cdot Dp^2 - C \cdot Vv) \cdot Hs\} \quad (3)$$

where, A, B and C are proportional factors.

It has been generally predicted by scrubbing models that diffusional deposition would occur at particle diameter of about 0.3 micro meter or below. However, DF did not increase with decrease in particle diameter under test conditions of particle diameter from 0.1 to 1.1 micro meter. This means that removal effect by diffusional deposition did not occur at these conditions. Therefore, diffusional deposition velocity has been eliminated from Equation (3).

Deposition velocity by steam condensation during bubble rising period may not occur because thermal equilibrium was assumed to have been attained at the injection point. In that case, pool water evaporates into the bubble to maintain vapor equilibrium condition during the bubble rising period. Then, deposition velocity by steam evaporation, Vv, always prevents particle depositions in a bubble. Vv should be called an anti-deposition velosity.

B. PARTICLE DIAMETER EFFECT ON THE DF

It is expected that DF strongly depends on particle diameter. Therefore, the authors firstly fixed a profile of particle diameter effect on DF.

Figure 5 shows the correlation between ln(DF) and square of particle diameter under the standard condition. This figure indicates that ln(DF) linearly increases with increase in Dp^2 within particle diameter range from 0.21 to 2.0 micro meters. By the least square method, the following equation was obtained.

$$DF = \exp(2.8+1.5Dp^2) \qquad (4)$$

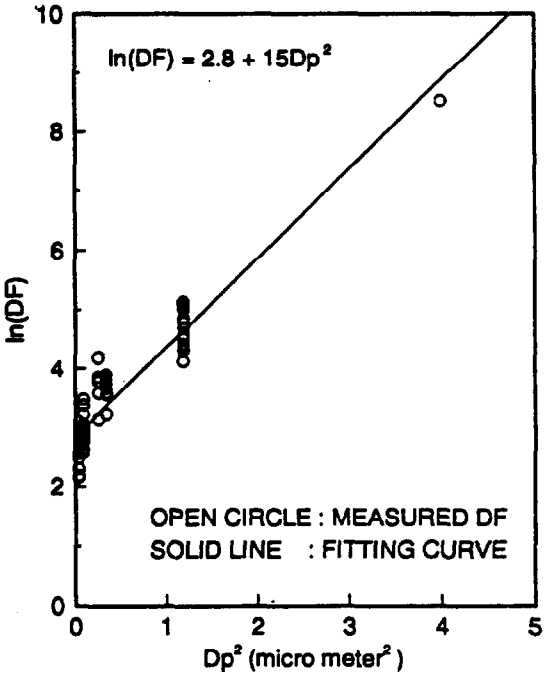

Figure 5 A correlation between ln(DF) and Dp^2 under standard conditions.

C. SCRUBBING DEPTH EFFECT ON THE DF

According to Equation (3), DF exponentially increases with increase in scrubbing depth. The measured DF under the standard condition while varying scrubbing depth also exhibits the same trends. Using proportional factors obtained by the least square method, scrubbing depth effects on DF for each particle diameter are given as[3]

$$DF = 1.56\exp(0.807Hs) \quad (0.21 \text{ micro meter}) \qquad (5)$$
$$DF = 1.54\exp(0.924Hs) \quad (0.31 \text{ micro meter}) \qquad (6)$$
$$DF = 1.59\exp(1.18Hs) \quad (0.57 \text{ micro meter}) \qquad (7)$$
$$DF = 1.92\exp(1.46Hs) \quad (1.1 \text{ micro meter}) \qquad (8)$$

D. DF BY INERTIAL DEPOSITION

DF(0), which is DF at Hs = 0 calculated by the above equations, must be a product of DFs and DFi. DF(0) can be calculated for each particle diameter by Equations (5)-(8). Based on the least square method for DF(0) and Dp^2, the following equation was obtained.

$$DF(0) = 1.5\exp(0.19Dp^2) \qquad (9)$$

The constant coefficient of the above exponent must be DFs and the exponent term itself must be DFi. Then, its index must be the proportional factor "A" in Equation (3).

An effect of carrier gas velocity on DFi was omitted from Equation (9), since it was not observed in the tests with vertical vent pipes and simulative quencher, where velocity ranged from 28 to 970 cm/s.

E. DF BY INITIAL STEAM CONDENSATION

As mentioned earlier, DF by initial steam condensation, DFs, was defined as a

ratio of inlet carrier gas flow rate and outlet carrier gas flow rate. However, this definition is available only when initial steam condensation occurs. Then, the ratio should be defined as another symbol, Rs, given by

$$Rs = \frac{fi}{fo} = \frac{100(1-Wp)}{100-S} \tag{10}$$

where, Wp is steam fraction in a bubble after thermal equilibrium has been attained and S is volumetric carrier gas steam fraction (vol.%).

Wp also can be considered as a ratio of saturated water vapor pressure and total pressure in the bubble. Saturated water vapor pressure, Ps, is given as

$$\log(Ps[mmHg]) = a-b/(c+Tp[°C]) \tag{11}$$

The above equation is well-known as Antoine's equation. Values of the coefficients are as follows.

$$a = 8.10765, \quad b = 1750.286, \quad c = 235.0$$

Antoine's equation can predict Ps within -0.3% or +3.6%, where temperature is from 0 to 190°C. Using Antoine's equation, Wp is written as

$$Wp = \frac{10^{\{a-b/(c+Tp)\}}}{735.559(P+0.099997Hs+1.033227)} \tag{12}$$

where, Tp is pool water temperature, P is pool surface pressure and Hs is scrubbing depth. Then, Rs can be expressed as a function of S, P, Tp and Hs, using Equations (10) and (12).

As mentioned earlier, DFs will be effective when a steam condensation occurs around the injection point, but is ineffective when it does not occur. Therefore, a relationship between DFs and Rs is given as

$$DFs(S,P,Tp,Hs) = \begin{cases} Rs & : \ Rs \geq 1 \\ 1 & : \ Rs < 1 \end{cases} \tag{13}$$

F. SIMPLIFIED MODEL

On the one hand, Equation (4) represents a particle diameter effect on DF at 2.7 meters in scrubbing depth, where DFs and DFi are included. On the other hand, Equation (9) is a product of DFs and DFi. By comparison with Equation (4) and Equation (9), the following correlation was derived.

$$DF = 1.5\exp(0.19Dp^2)\cdot\exp(2.4+1.3Dp^2) \tag{14}$$

Equations (5)-(8) represent scrubbing depth effect on DF at each particle diameter, where the constant coefficients must be a product of DFs and DFi. Comparing with Equation (14) and Equations (5)-(8), it is clear that the second exponent index in the former equation must be equal to the exponent index in the latter equations. Comparing of the two exponent index for each Hs or Dp, the following expression was derived.

$$DF = 1.5\exp(0.19Dp^2)\cdot\exp\{(0.88+0.52Dp^2)\cdot Hs\} \tag{15}$$

An aerosol deposition velocity, which only depends on scrubbing depth, is in-

cluded in the second exponent index on the right side of the above equation. This suggests that an aerosol deposition mechanism, which is neither gravitational deposition nor inertial deposition, exists. Further consideration is required, since there is only limited information on this mechanism.

The constant coefficient of equation (15) was considered as DFs. Then, the simplified model is given as

$$DF = DFs(S,P,Tp,Hs)\cdot\exp(0.19Dp^2)\cdot\exp\{(0.88+0.52Dp^2)\cdot Hs\} \quad (16)$$

Anti-deposition velosity, Vv, has been omitted from the above second exponent index, since it could not confirmed that DF significantly decreased with an increase in pool water temperature, including boiling conditions. However, temperature effect on DF remains in DFs as it is predicred by Equations (10) and (12).

V. COMPARISON OF CALCULATED AND MEASURED DF

The simplified model can predict DF by five parameters. They are particle diameter, scrubbing depth, carrier gas steam fraction, pool water temperature and pool surface pressure. Comparisons of calculated DF by the simplified model and measured DF for the LATEX particles with the vertical vent pipes and the simulative quencher are given below.

Figure 6 to Figure 8 show comparisons of measured DF and calculated DF for particle diameter effect, scrubbing depth effect and carrier gas steam fraction effect on DF, respectively. Results show that calculated DF is in good agreement with measured DF in every case.

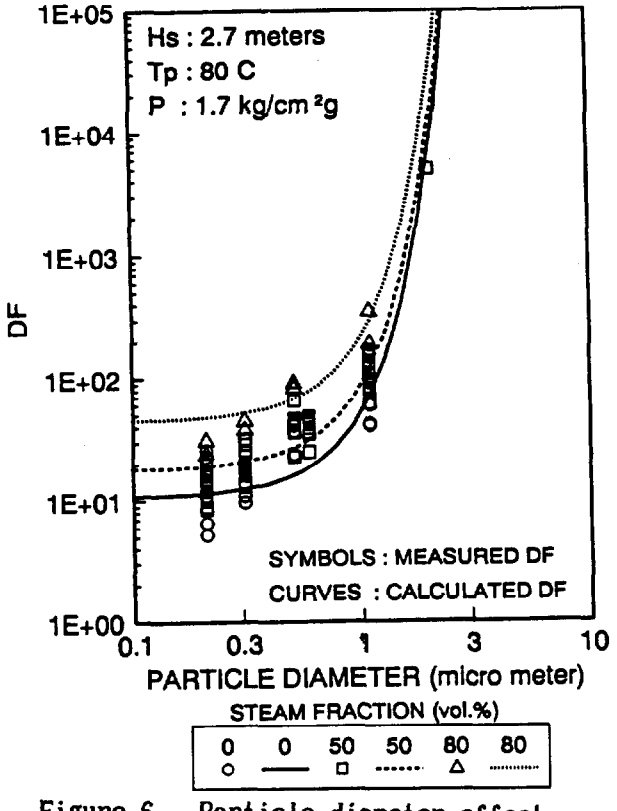

Figure 6 Particle diameter effect on DF.

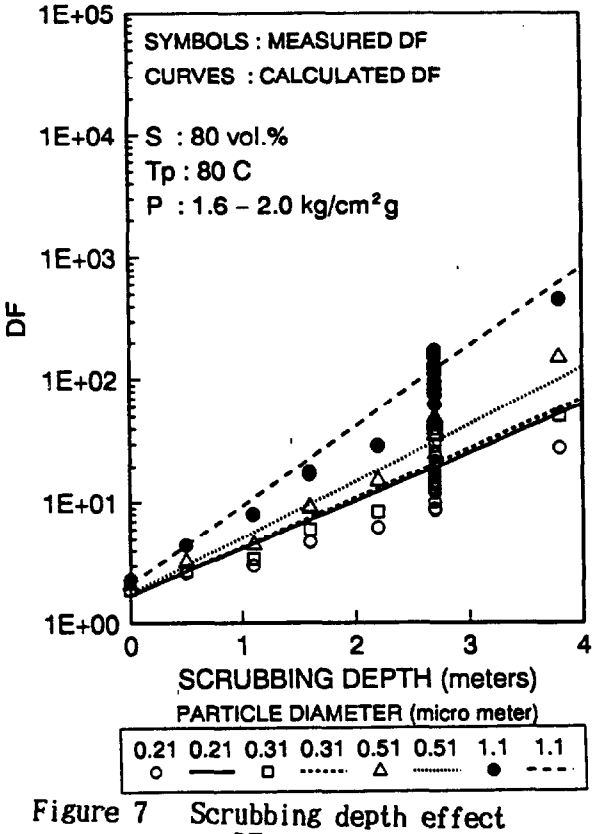

Figure 7 Scrubbing depth effect on DF.

Figure 9 shows a comparison of measured DF and calculated DF for pool water temperature effect on DF at pool surface pressure of 2.0 kg/cm^{2}g. As the figures indicate, measured DF are hovering around calculated DF.

The comparison for pool surface pressure effects on DF is shown in Figure 10. Pool surface pressure range is so narrow that there is only a little data to make comparisons. Based on the limited information, the simplified model tends to predict smaller DF than measured DF.

Figure 11 shows the correlation between calculated DF and measured DF under all test conditions. As this figure indicates, most of the measured DF are within -50% or +100% of calculated DF. The average ratio of calculated DFs and measured DFs is 1.0 and its standard deviation is 0.5. Considering the fact that the deviation of measured DF at the standard test condition was within factor two (+100% to -50%), it can be said with a reasonable degree of certainty that calculated DF are in very good agreement with measured DF.

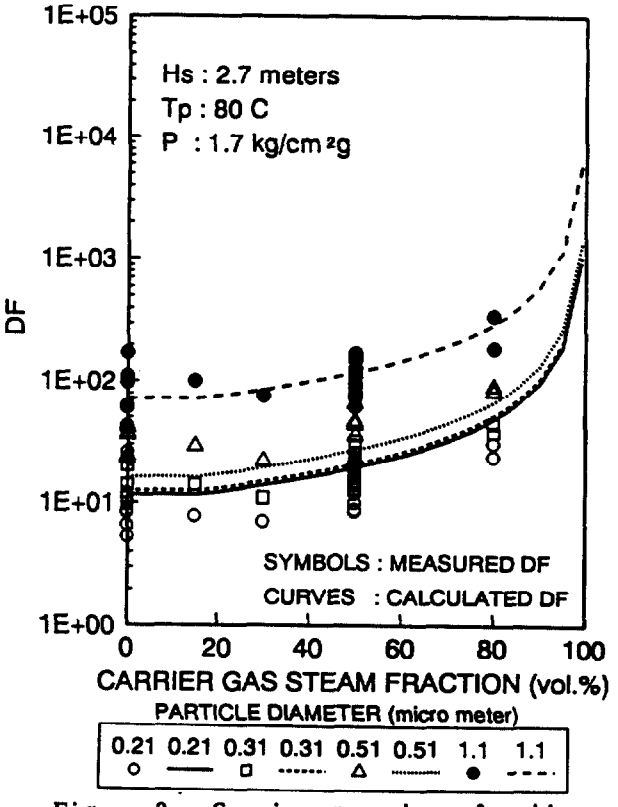

Figure 8 Carrier gas steam fraction effect on DF.

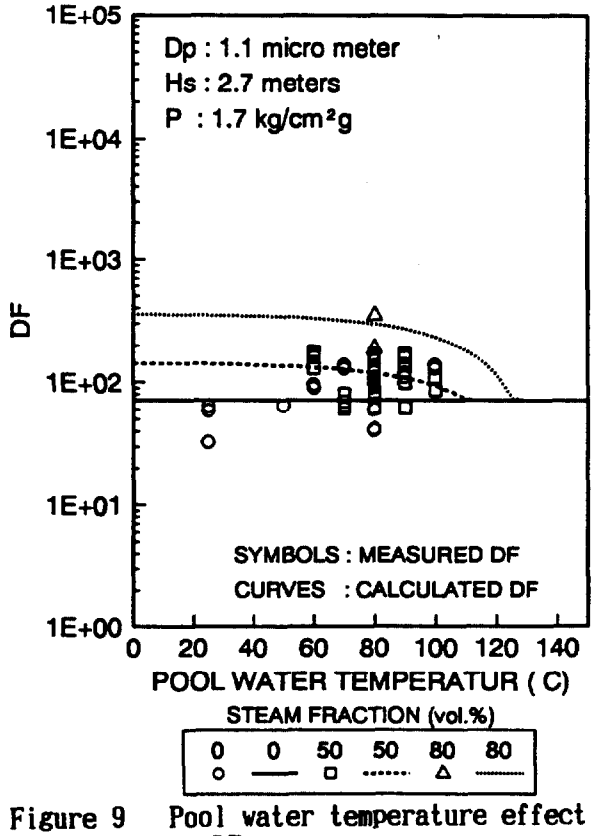

Figure 9 Pool water temperature effect on DF.

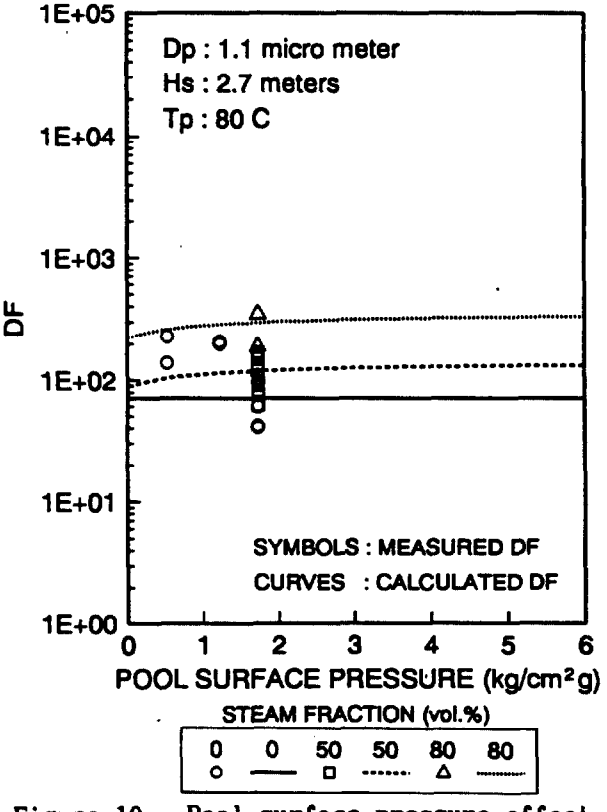

Figure 10 Pool surface pressure effect on DF.

VI. DISCUSSION

As mentioned above, the simplified model is applicable to pool scrubbing under a wide range of conditions. However, a large uncertainty remains in test conditions where carrier gas steam fraction exceeds 80 vol.%.

Figure 12 shows scrubbing depth effect on DF for subcooled and boiled pool water, comparing with DF calculated by the prototype SPARC code[1]. The SPARC code predicts that DF for boiled pool water is smaller than that for subcooled pool, since anti-deposition velocity by steam evaporation at boiling condition is calculated to be greater than that at a subcool condition.

On the other hand, the marked decrease in DF under boiling conditions was not observed during tests, where carrier gas steam fraction was under 80 vol.%. Based on it, the authors did not include the effect of steam evaporation in the simplified model.

If carrier gas contains over a few volumetric percent of non-condensable gas, heat transfer coefficient across the bubble surface becomes very small. In this case, deposition velocity by steam evaporation would maintain a small value, even if pool water were boiled. For the reason, decreases in DF at boiling conditions were not observed, during tests with under 80 vol.% of carrier gas steam fraction.

Several discussions in the above few paragraphs are summarized as follows. DF at boiling conditions, including over 80 vol.% of the steam fraction, will be decided by a combination of the following two factors. The first factor is that DF increases with increase in carrier gas steam fraction. The second is that DF decreases with increase in deposition velocity by steam evaporation.

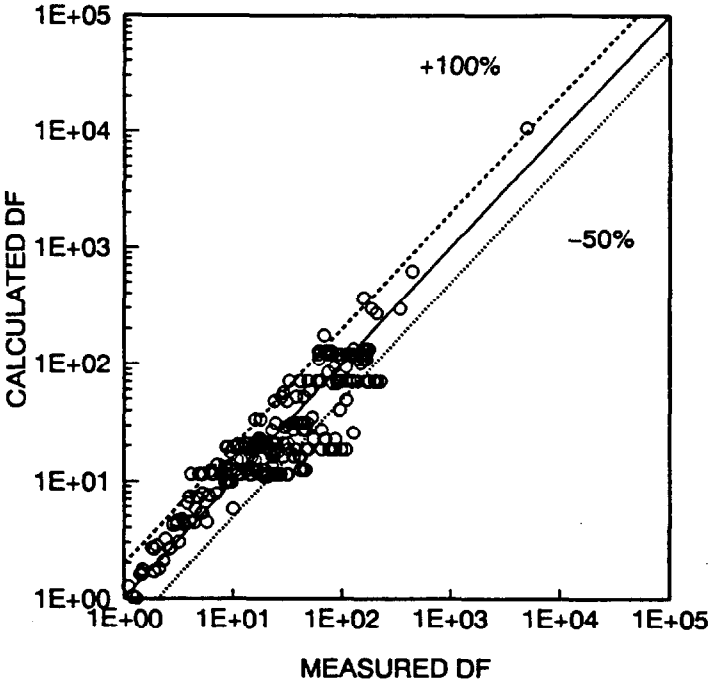

Figure 11 A correlation between calculated DF and measured DF under all test conditions.

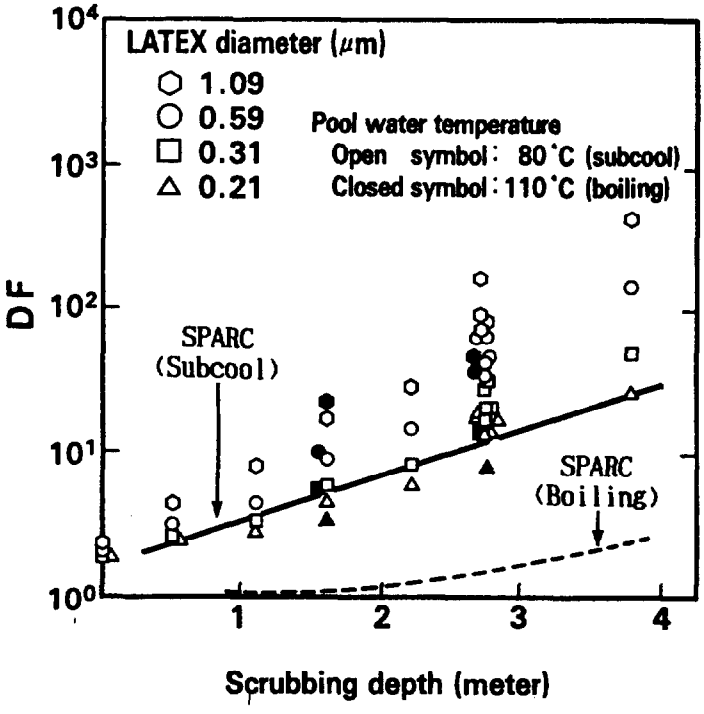

Figure 12 Scrubbing depth and pool water effect on DF compared with prototype SPARC calculation for 1 micro meter LATEX.

VII. CONCLUSION

During this study, aerosol removal efficiencies by pool scrubbing, which were defined as decontamination factors, were systematically measured, varying the eight parameters. The results show that DF mainly depends on three parameters: scrubbing depth, particle diameter and carrier gas steam fraction. Based on prototype SPARC models and measured DF for the three parameters, the simplified model was developed. This simplified model can predict DF within the deviation of the measurements under these test conditions.

This simplified model also can calculate total DF for complicated dispersed aerosols, since it can predict each particle diameter effect on DF.

VIII. ACKNOWLEDGEMENT

This scrubbing experiment was made possible largely through grants from a joint study group organized by Tokyo Electric Power Co. Inc., Tohoku Electric Power Co. Inc., Chubu Electric Power Co. Inc., Hokuriku Electric Power Co. Inc., Chugoku Electric Power Co. Inc., Japan Atomic Power Co. Inc., Toshiba Corporation, and Hitachi Ltd.

IX. REFERENCES

(1) J.Hakii, I.Kaneko et al., "EXPERIMENTAL STUDY ON AEROSOL REMOVAL EFFICIENCY FOR POOL SCRUBBING UNDER HIGH TEMPERATURE STEAM ATMOSPHERE", Proceedings of 21st DOE/NRC Nuclear Air Cleaning Conference, San Diego, 13-16th August, 1990

(2) 'Technical bases and user's manual for the prototype of a Suppression Pool Aerosol Removal Code (SPARC)', NUREG/CR-3317, PNL-4742, May 1985.

(3) J.Hakii, I.Kaneko et al., "EXPERIMENTAL STUDY ON AEROSOL REMOVAL EFFECT BY POOL SCRUBBING", Proceedings of the Second Workshop ON LWR Severe Accident Research at JAERI, Tokyo, 25-27th November, 1991.

DISCUSSION

GREENE: If aerosol is not uniformly distributed throughout the steam-gas bubble, will the condensation DF be overpredicted by your model?

KANEKO: Yes, the model assumes aerosol is uniformly mixed in the bubble and DF will be proportional to the amount removed by condensation.

"THE PHEBUS FP INTEGRAL SOURCE TERM EXPERIMENTAL PROJECT, WITH EMPHASIS ON IODINE SELECTIVE FILTERING"

by
R. ZEYEN *
J.G. WILHELM **
M. LUCAS ***

PHEBUS FP PROJECT
at CEN Cadarache [1)]

* Commission of the European Communities (CEC)
Joint Research Centre, JRC-ISPRA
seconded to CEN Cadarache
** Kernforschungszentrum Karlsruhe (KfK)
Laboratorium für Aerosolphysik und Filtertechnik (LAF II)
*** Commissariat à l'Energie Atomique (CEA)
Institut de Protection et de Sûreté Nucléaire (IPSN)
Département de Recherches en Sûreté (DRS)

ABSTRACT

The PHEBUS FP (Fission Product) Project is concerned with LWR severe fuel damage and fission product source term experimentation.

Highly irradiated fuel pins are run in accidental conditions until significant UO_2 melting occurs. Structural material and fission product aerosols and vapours are swept into a scaled-down primary circuit. A circuit leak is simulated and a reactor containment provided for long term FP behaviour study. The fraction and nature of real radioactive fission product mixtures that reach the containment, and their behaviour in the containment are critical to accident source term estimates and relevant to future filter system designs.

Considerable work is performed to measure the behaviour of the different airborne fission products including the identification of the iodine species. Special interest will be devoted to the possibility of the existence of airborne compounds for which the off-gas filter has not been designed today. Iodine chemistry is studied and monitored in the containment using on-line measurements and filters as well as off-line sampling techniques.

The selective retention of airborne iodine at elevated temperature and high pressure was preliminarily tested (at KfK Karlsruhe) with different sorbents to prove the operational capabilities of iodine species samplers, used as an important means for the analysis of the containment atmosphere.

PHEBUS FP is a CEC-JRC and CEA-IPSN co-sponsored project operating in the existing Cadarache based PHEBUS experimental reactor, with the direct participation of Canada, Japan, Korea and the United States.

1)CEA, CEN Cadarache, bât 245
F 13108 St. Paul-lez-Durance
tel: 33.42254638 fax: 33.42257078

1. INTRODUCTION

Hypothetical severe accidents in a pressurised water reactor (PWR) may lead to the release of fission products to the environment. The amount of radioactivity released as a fraction of the initial core inventory is referred to as "Source Term", the major objective to be studied in the PHEBUS Fission Product programme. The physical and chemical forms in which the various FPs are present within the reactor coolant circuit (RCS) and in the containment building, in the course of an accident sequence, determines the amount and composition of gas mixtures which could be released, and the subsequent biological consequences, should the containment building be breached.

The PHEBUS FP experiments, which will be performed at the CEA's laboratories in Cadarache in France starting in spring 1993, will yield precious data, required for the development and validation of computer models for the prediction of the release rates from the fuel pins and subsequent behaviour in the RCS and containment vessel.

Instrumentation has been provided all along the simulated primary circuit and particularly in and around the containment vessel, in order to follow, through on-line and post-test analysis, the fission product history over about one week of experimentation. The first test FPT-0 will be run with lightly irradiated fresh fuel, and used to test-out the facility. The five subsequent tests, one per year, will use high burn-up PWR fuel followed by an experimental circuit and conditions associated to particular reactor accident sequences.

The behaviour of fission product iodine deserves special attention due to its potential radiological impact and to the complexity of the iodine chemistry. Iodine escapes from the fuel under accidental conditions, driven by temperature, insignificantly as elemental I_2, but mainly in the form of CsI vapour or aerosols. In low pressure conditions only part of the CsI will deposit in the primary circuit, the remaining part will reach the containment and will deposit onto the sump surface. Readily soluble in water it then dissociates and hydrolyses into non-volatile I^- depending on concentration, temperature, pH etc. Iodates can then be formed in the sump through decomposition of HOI. The important value in reactor safety studies is the partitioning coefficient i.e. aqueous over gaseous iodine concentration, responsible for eventual release from a broken containment vessel. This coefficient is affected by radiolysis, pH and mass transfer in the sump, but also by the formation of organic iodine compounds by reaction of I_2 with organic contaminants or in contact with paint, volatile methyl iodide CH_3I being the most common organic species.

2. THE PHEBUS FP EXPERIMENT

The PHEBUS FP installation is a 1/5000 replica of a 900 MWe PWR reactor, comprising the reactor core using high burn-up fuel in a 20 rod array, the simulated circuit with a test matrix specific reactor component (steam generator, pressuriser, relief tank, etc.) and a containment vessel with sump (see Fig. 1). The existing PHEBUS reactor is used for the fuel irradiation and degradation process, already successfully performed in the LOCA and SFD tests. A large stainless steel container (caisson), in the new building adjacent to PHEBUS will contain the simulated circuit, downstream of the fuel bundle, as main safety barrier. More physical circuit details are given in Ref [1], [2] and summarized hereafter.

3.1. In-pile test section containing the fuel bundle (Fig. 2):

Fig. 2 gives a cross section of the test section at the level of the fuel. 20 PWR fuel rods, irradiated up to 32 GWd/t in the BR3 (Belgium) reactor, are assembled by 2 AFA zircaloy grids around one central steel clad Ag,In,Cd control rod, insulated by a variable density zirconia shroud, held inside the pressure tube.

The bottom coolant inlet is closed prior to the experimental transient by a hydraulic "foot valve". During this transient a small controlled steam flow, later replaced by uncondensable gases, carries the fission products and structural material aerosols up through the tubular section, with a large temperature gradient, into the horizontal part of the primary circuit.

3.2. Primary circuit (Fig. 3):

Due to geometric reactor constraints, the primary circuit has to start with a 5 m long horizontal line, followed by the measurement zone «C», the steam generator U-tube (or other experimental components) and the measurement zone «G», shortly prior to the containment inlet (Fig. 3 shows the circuit inside the safety steel "caisson"). In the first scoping test FPT-0 the circuit temperature is trace heated to 700°C, with a transition zone down to 150°C in the steam generator.

The circuit tubing will be fully replaced after each test, with the experimental component, steam generator, replaced by another component or, by a minimum-retention line into the containment.

3.3. Containment (Fig. 4):

The reactor containment is simulated by a 10 m^3 vessel with a 0.1 m^3 sump having reduced free surface, for representativity reasons. Three cylindrical condensers are designed to keep the containment walls dry, condensing out the surplus steam from the bundle, producing interactions of their painted surfaces with the containment gas phase. Its condensates are recovered, flow monitored and sampled for post-test chemical analysis. Three independent organic coolant loops control temperatures of the condensers, the containment walls and the sump.

The following effects can be simulated and/or observed during the experiments (not exhaustive list):

- aerosol behaviour and settling,
- iodine chemistry checking the combined influence of the inventory, sump pH, gas and sump temperatures, radiolysis, mass transfer and surface adsorption,
- interaction with paint,
- containment spray,
- depressurisation.

The containment is designed for mild incidental hydrogen deflagration; its inner surfaces have to be decontaminated after each experiment.

3.4. Effluent system:

The containment content will pass through a condenser followed by an aerosol and iodine filter system for the purpose of gas cleaning and total mass balance calculation. The ultimate destination of the gaseous effluents is a 100 m^3 "atmosphere" tank, initially filled with nitrogen and whose gas volume is used for recirculating/diluting the hydrogen containing mixture from the containment. The atmosphere tank will later be equipped with a palladium plate catalyst designed by GRS Köln for automatic H_2 depletion before a final release to the stack. Containment depressurisation can become an experimental feature, if enough containment sampling instrumentation is available at the end of the aerosol and chemistry phase.

3. INSTRUMENTATION

The PHEBUS FP instrumentation plan is illustrated here but has been described in more details in Ref [3], [4] and [5].

3.1. ON-LINE INSTRUMENTATION and SEQUENTIAL SAMPLING

3.1.1. Test-Section Instrumentation:

Relevant items of a long list of *in-pile instrumentation* are highlighted here:

- High temperature thermocouples, W/Re wires, Re sheathed and Ir coated will be mainly used in the centreline of un-irradiated scoping-test fuel rods. In later experiments two fresh fuel rods will be situated at the periphery of the bundle, otherwise made up of highly irradiated fuel pins (pre-irradiated up to 36 GWd/t in BR3).
- ultrasonic thermometers, in two bundle corner positions, both having seven axial measurement zones over the mid-core area. These rather sophisticated devices, fabricated by the European Community Institute TUI at Karlsruhe, are supposed to measure up to fuel melting when W/Re thermocouples have stopped operating properly. The advantage of measuring axial profiles in one device is notable.
- the bundle temperature control for the experiment conduct, if all temperature sensors fail, is handled by shroud outer surface "K" type thermocouples, using a pre-transient correlation procedure.
- neutron flux measurements will be performed in the driver core, but also axially along and close to the test bundle in order to survey fuel and Ag,In,Cd control rod material relocation.
- in follow-up tests a sequential coupon device will be installed in a gradient zone on top of the fuel for vapour deposit sampling at high temperature (1200 to 700°C).

3.1.2. Primary Circuit Instrumentation:

Fig. 5 shows a sketch of the circuit instrumentation as located on and around the primary circuit; again some relevant items can be mentioned:

- flow rates of steam and hydrogen coming from the fuel will be gauged by several thin thermocouples, correlating small temperature variations propagating along the flow lines.

- the oxygen potential is measured at point «C», to get an understanding of the fuel oxidising/reducing conditions.
- several γ spectrometers using high purity Ge detectors are located at relevant positions along the circuit line, most important of which is the first one at point «C», the closest to the accidented fuel bundle, thus the first insight into the γ emitting source term. At this point two spectrometers are dedicated to the on-line discrimination of moving versus deposited FPs in the circuit line. This is a difficult task considering the "moving" tubing (thermal expansion) linked to heavy shielding and collimator equipment. Other γ spectrometers will survey gas and deposits in the steam generator's cold leg and prior to the containment inlet.
- INEL Idaho Falls provide us with a redesigned version of their PBF aerosol light extinction photometer, a valuable on-line device for both semi-quantitative information on special release events and experimental guidance for sampling.
- sequential gas capsules and filters together with impactors should give information of the gas species and aerosol nature, density and granulometry at various times. Samplers prior to the steam generator have to operate at 700°C, those after the SG at 150°C. The timing of these samplers can be adjusted during the experiment evolution according to the release phenomena.
- one thermal gradient tube (TGT) for the study of condensation patterns, between 700°C and 150°C, separating FP species like CsI and CsOH. Only one TGT will be used at point «C» because recovery for PTA and interpretation might be hazardous. Its temperature control with transient gas through-flow is a difficult task.

3.1.3. Containment Instrumentation:

The containment instrumentation is illustrated on Fig. 6. Important on-line measurements are:

- wall and gas temperatures, pressure and sump level.
- moisture, H_2, and O_2 sensors in the gas phase, selective electrodes for I^- ions and pH in the sump. All these sensors are doubled for redundancy.
- «on-line» chemical separation of I^- versus IO_3^- ions, their ratio is co-responsible for volatile iodine formation, is envisaged for later tests.
- the condensate flow is measured and led out of the containment for analysis.
- three γ spectrometers continuously detect the activity of certain isotopes in the containment gas phase, on the condensers' painted surfaces and in the sump.

Sequential or off-line devices on the containment are:

- a sequential deposition coupon device, designed to recover 8 metal coupons exposed at 8 different time windows.
- sequential aerosol impactors of a modified ANDERSEN MK II type, foreseen for the first scoping test; real on-line classifying will be performed on a diffusion type ball bed stack in follow-up tests.
- a long series of filters and capsules to yield more data on aerosols (to be compared to impactors) and on gas and liquid composition for long lived isotopes.

- airborne iodine species monitoring is a specially treated item in PHEBUS FP: eight selective filters are installed, operating sequentially during a predetermined time sequence, for the study of time-dependent iodine behaviour. Retained iodine concentrations will be quantitatively determined post-test through sensitive γ measurements within one week. One quasi on-line selective filter equipped with a γ spectrometer diode will follow the species evolution over several periods of the long term chemistry phase of the experiment. More details of the filters and their qualification tests are given in the following separate paragraph 3.1.4.
- one painted coupon is maintained in the sump liquid for interaction, it will be recovered post-test for a γ scan and off-line surface analysis.

3.1.4 R & D on Airborne Iodine Speciation Samplers:

Monitoring different iodine species and concentrations in a post-accident containment is crucial for the PHEBUS FP experimentation. In the same way the filtering of all iodine species during power reactor containment venting is vital for accident management and health protection by air cleaning.

Several experimental programmes have made use of iodine selective filters, however not in the particular PWR containment severe accident conditions using real source term species. Taking into account these requirements and knowing that condensation has to be avoided, the iodine filter operating conditions have been defined as following:

160°C, 0.1 to 0.3 MPa, H_2 concentration up to 9%, high steam content and relative humidity

The LAF II of the Kernforschungszentrum Karlsruhe has offered their iodine test facilities to carry out an extensive test programme addressing the two main objectives:

① selection of appropriate adsorber materials for elemental and molecular iodine,
② testing of the filter assembly under real conditions: gas composition, temperature and pressure.

① *Material pre-test series*

Candidate adsorber materials for molecular iodine in steam containing gas mixtures were:
1) DSM 11: a porous silicic acid structure, KI impregnated,
2) silver coated copper "Knit-Mesh",
3) silver coated stainless steel 2 μm fibre fleece (see Ref. [6]).

Organic iodine can be retained by ID 625, a silver coated binary doped molecular sieve. This material also retains I_2: it has to be located downstream of molecular iodine sorbents. This zeolite has previously been extensively tested and reported upon in Ref. [7], only its operation in 160°C steam had to be checked here.

Both molecular iodine $^{131}I_2$ and methyl iodide $CH_3{}^{131}I$ have been produced and separately blown in a steam/air mixture through the hot test bed: in order to avoid condensation the sorbent temperature has to exceed the containment dew point temperature by a significant margin, 10 - 20°C: temperatures between 130°C and 180°C have been tested.

TAIFUN tests were run at 25 cm/s flow velocity over variable times (several minutes) and concentrations ranging from 0.1 to 36 mg/m^3. Nitrogen flushing was necessary for pre-test conditioning and post-test activity removal. After dismantling the retained activity on the different filters was determined by high sensitivity shielded γ spectrometers. Automatic PC driven data retrieval added to the test's quality control.

Results of the material pre-test series can be summarised as follows:

1. At 180°C all materials tested reacted with or decomposed methyl iodide. Iodine species separation cannot be guarantied at this temperature level with the materials used.
2. Knit-mesh filters show the highest removal of $^{131}I_2$ in combination with the smallest retention of CH_3I-^{131}I (Table 1 and 2 for a 140°C test). Iodine already adsorbed on DSM 11 tends to desorb contemporarily and displace the removed activity to downstream filter elements.

Table: 1

Material	Residence Time	I_2 Removed per Element
Knit-mesh 1	0.04 s	96.63 %
Knit-mesh 2	0.04 s	3.34 %
Knit-mesh 1+2	0.08 s	99.97 %

Table: 2

Material	Residence Time	CH_3I Removed per Element
Knit-mesh 1	0.04 s	0.29 %
Knit-mesh 2	0.04 s	0.11 %
Knit-mesh 1+2	0.08 s	0.40 %

3. ID 625 achieves very convenient removal efficiencies at 160°C (Table 3). A residence time of 0.3 s, i.e. three filter elements, is sufficient for a convenient removal efficiency.

Table: 3

Material	Residence Time	CH_3I Removed per Element
ID 625 1	0.1 s	98.730 %
ID 625 2	0.1 s	1.067 %
ID 625 3	0.1 s	0.025 %
ID 625 4	0.1 s	0.002 %
ID 625 1-4	0.4 s	99.82 %

⑪ *TAIFUN integral test series*

The filter pack as shown in Fig. 7 is made up of a tubular housing, ID 25 mm, containing the following components in three successive stages:

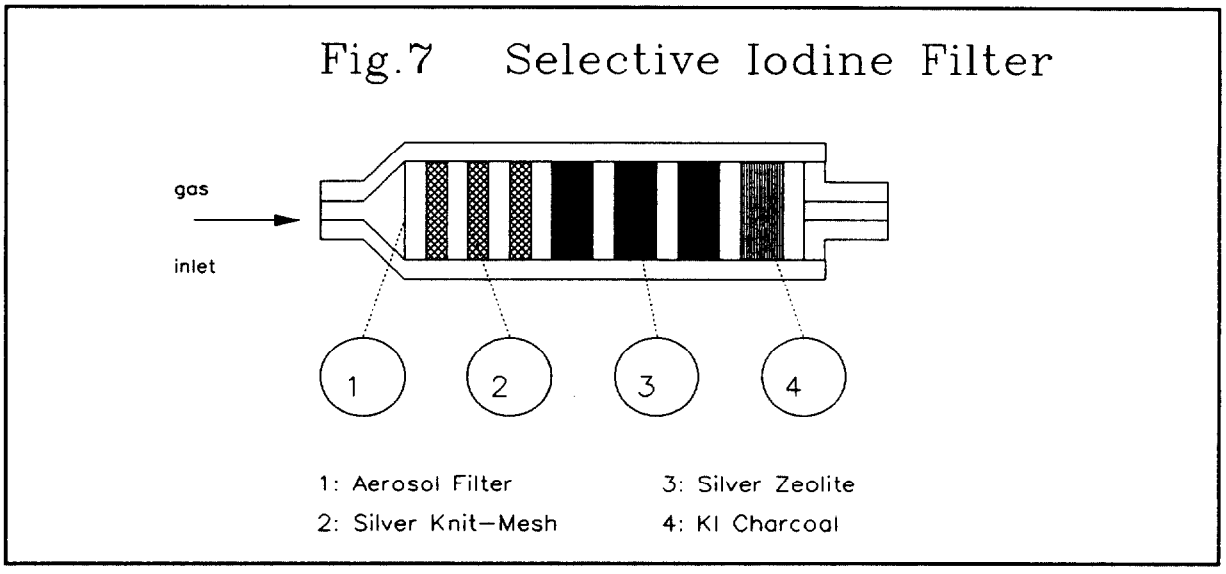

1. An aerosol filter, metallic PORAL or Quartz paper, depending on its minimum chemical reactions with fission products; this item is not further discussed here,
2. Silver knit-mesh for molecular iodine, three 12 mm deep compressed elements[1)],
3. Heavy metal doped silver zeolite for organic iodine, three or four 25 mm deep granular beds. The zeolite granulometry ranges from 1.5 to 2.25 mm[1)].

The CH_3I stage can contain three or four units, i.e. the last filter element could also be replaced by a potassium iodide impregnated charcoal bed (S.S. 207B) according to the needs.

The KfK TAIFUN facility has been previously described in Ref. [8].

The test conditions of a series of eight tests are listed in Table 4; the linear gas velocity (face velocity) was kept constant at ≈ 25 cm/s. The percentage of iodine species removed by the different filter elements have been added in Table 4 for both I_2 and CH_3I tests and varying gas composition.

1) Silver type samplers must be stored carefully to prevent poisoning of the surface.

Table: 4 TAIFUN Integral Test Series: Test Conditions and Results

Test N°	Iodine Species	Material	Residence Time per Element [s]	Gas composition	Temp./ Pressure [°C/MPa]	Iodine Removed Knit-Mesh [%]	Species per Element Zeolite [%]
F1	CH_3I	3 KM [1)] 4 Z	0.05 0.1	air	160/0.1	0.04 0.03 0.06	99.25 0.58 0.02 0.00
F2	CH_3I	3 KM 4 Z	0.05 0.1	air	160/0.1	0.05 0.06 0.06	82.84 16.93 0.06 0.00
F3	CH_3I	7 Z	0.1	86 - 95% N_2 4 - 5% O_2 10% H_2O	160/0.3		85.75 6.60 4.26 3.28 0.10 0.01 0.00
F4	I_2	3 KM 4 Z	0.05 0.1	86 - 95% N_2 4 - 5% O_2 10% H_2O	160/0.3	99.41 0.49 0.01	0.09 0.00 0.00 0.00
F5	CH_3I	3 KM 4 Z	0.05 0.1	76 - 86% N_2 9 -10% H_2 4 - 5% O_2 10% H_2O	160/0.3	0.05 0.04 0.03	62.99 13.67 11.71
F6	I_2	3 KM 4 Z 1 A C	0.05 0.1 0.1	60% N_2 30% H_2O 7% H_2 3% O_2	160/0.3	87.69 4.41 0.68	4.00 1.70 0.56 0.96
F7	CH_3I	3 KM 4 Z 4 A C	0.05 0.1 0.1	60% N_2 30% H_2O 7% H_2 3% O_2	160/0.3	0.03 0.01 0.01	89.24 8.06 0.80 0.61
F8	I_2	3 KM 4 Z 4 A C	0.05 0.1 0.1	60% N_2 30% H_2O 7% H_2 3% O_2	160/0.3	72.50 0.91 0.15	16.44 4.76 2.52 1.04

1)KM: Knit-Mesh Z: Zeolite A C: Active Charcoal

Some relevant results are shortly discussed here:

* No significant pressure effect can be noticed comparing for example data from test F1, F3 and F7 with CH_3I. The F4 test on the other hand shows very high molecular iodine removal efficiencies when silver Knit-Mesh is used; 0.3 MPa pressure is applied.

* Hydrogen has the uncomfortable effect of allowing penetration of I_2 to CH_3I adsorbers: note the flattening of the 2 H_2 curves in Fig. 8.

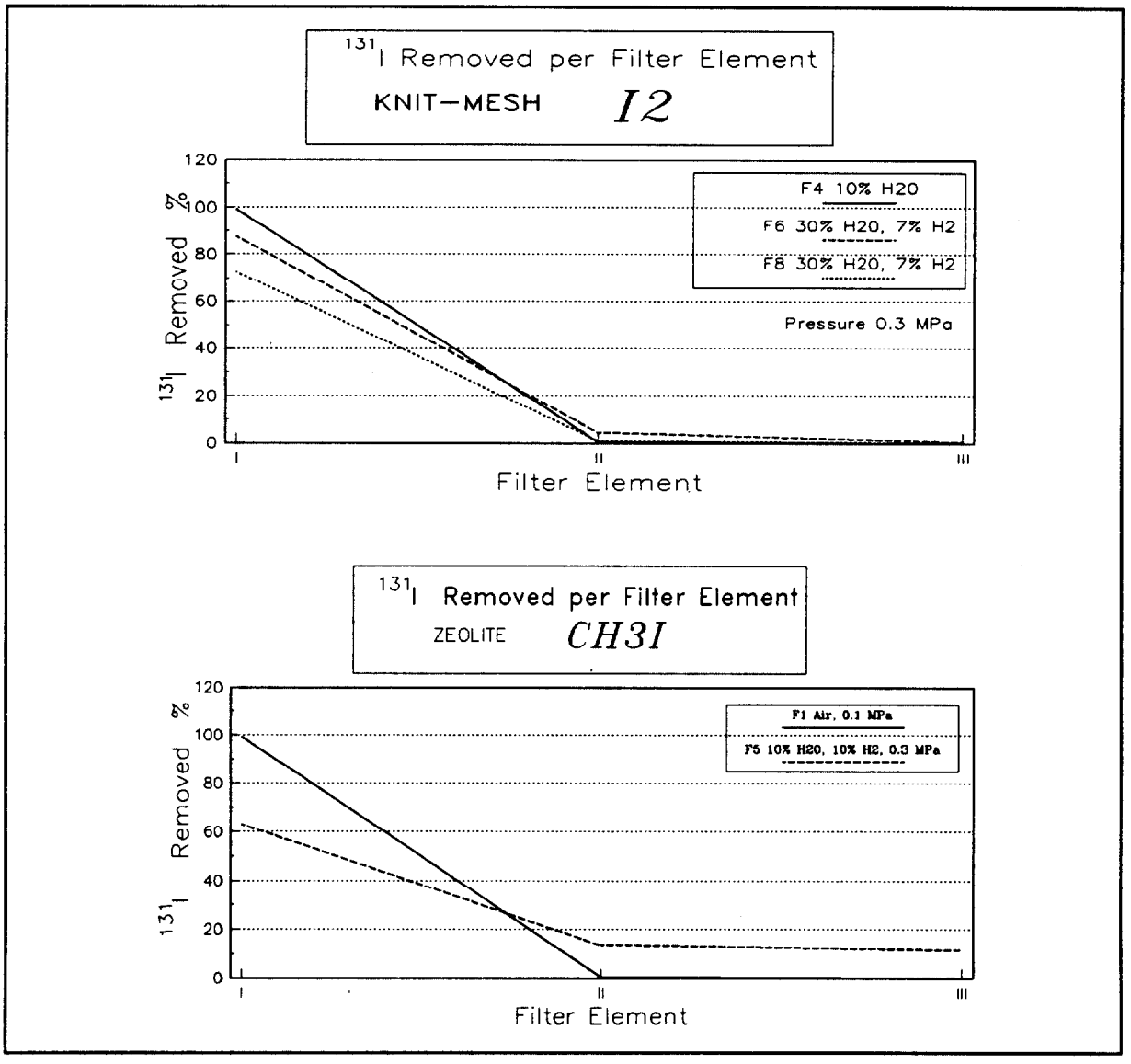

Fig. 8 Hydrogen Effect on Removed Iodine using CH_3I and I_2

One possible explanation of this effect could be the build-up of hydrogen iodide in the silver knit-mesh filters, with subsequent trapping of this ^{131}I activity in successive zeolite stages. For a clearer indication of the presence of HI in the gas it seems reasonable to add an active charcoal stage as a final filter system. Tests 6, 7 and 8 show no burning effect of charcoal at 160°C, which

where previously observed using charcoal from recently delivered batches. Adding more zeolite (or charcoal) elements and with the help of supplementary calibration it might reasonably be possible to detect other iodine species than those for which our selective filter system had been originally foreseen. There is definitely need for further investigations if HI or other iodine species have to be quantified.

* No hydrogen catalytic effects of zeolite with respect to H_2/O_2 reactions were observed; it has to be said that element temperatures have not been measured in each filter stage in order to focus on this effect.

The selective filter system as described previously will be further submitted to a qualification exercise in real PHEBUS FP geometries, reduced gas velocities (gas saving in the scaled-down experiment) and minimum iodine concentrations in a new tracer test facility, actually in its licensing stage at CEA Cadarache.

On-line Selective Iodine Filter

The same adsorber materials will also be used in a newly designed **"on-line iodine selective sampler"** where each filter stage is scanned alternately by a γ spectrometer. The integrated aerosol concentration and the molecular and organic iodine contents can thus be followed over several hours of operation, during various separate time periods. The problem of background noise from the high inlet aerosol filter activity, compared to the last iodine stages has yet to be tackled by sophisticated collimation and counting techniques.

3.2 POST-TEST ANALYSIS (PTA)

PTA is a most important item in PHEBUS FP instrumentation, not at least because of the shortcomings of on-line instrumentation.

The first major operation is the samplers' (around 25) recovery and transfer to the "CECILE" hot cell, below the main "caisson". After a first gross γ scan the samplers are dismantled and the sensitive components fine γ scanned again, before packaging and transport to different specialised laboratories. Iodine samplers have a general priority due to the ^{131}I isotope's short half-life. Their different adsorber stages will be γ scanned on an automatic turn-table device, taking care of the very different activity levels of the different filter stages (range: 10^4)

The post-test analysis programme is a complex series of flow sheets from recovery to a series of analysis techniques ranging from scanning electron microscopy coupled to energy dispersive spectroscopy (SEM/EDS) and particle recognition equipment (PRC) up to many types of chemical techniques for compound and species recognition and concentration determination. Neutron activation analysis (NAA) is a widely used accurate method for isotopic/elemental analysis of non-γ emitters, fissile particles and decayed iodine. More details on the PTA working plan can be found in Ref. [9].

4. FUEL BUNDLE POST-IRRADIATION EXAMINATIONS (PIE)

Shortly after the irradiation experiment the test section will be un-coupled from the circuit and stored in a vertical examination and control station (PEC). This PEC houses a radial and axial γ scan and radiography facility with possibilities of computer tomography.

In a second phase, several months later, the test section will be transported in a specific shielded flask to a hot lab where horizontal and vertical cuts will be performed. These small sections will then be dispatched to outside laboratories for further detailed elemental analysis and FP inventory measurements.

The upper tubular plenum of the test section has a special interest: the surfaces of this part have been located in a severe thermal gradient during the release phase and interesting deposits will have accumulated thereupon. This is why these tubular sections will be cut into small sections and treated, according to a PTA flow sheet, for detailed deposit analysis.

5. CONCLUSIONS

PHEBUS FP is presently the largest experimental programme in the area of severe accident studies. It benefits of the interest of the international safety community and will contribute significantly to the quantification of source term and environmental impact of nuclear power plants. The first test is to be run in spring 1993.

Airborne iodine selective filters have been developed and tested under severe but real accident conditions. The materials adopted for the filtering of molecular and organic iodine species behave well enough for the sequential determination of their relative concentration. Deviations from the pre-established efficiency curves might give indications on the presence of iodine species for which the filters had not been primarily designed.

The selective iodine filter design could be improved by increasing the number of elements to the organic iodine filter stage or by adding active charoal filters at the outlet of the device.

6. ACKNOWLEDGEMENT

The authors are grateful to H.E. Sims (AEA Harwell) and E.C. Beahm & R.A. Lorenz (ORNL) for their critical review of this paper. The valuable contribution of MM. H.-G. Dillman and H. Lehning and co-workers at KfK for the successful execution of the test programme is gratefully acknowledged.

7. REFERENCES

[1] P. von der Hardt, A. Tattegrain: "The PHEBUS Fission Product Project", paper presented at the Fall Meeting of the European Materials Research Society, Strasbourg, November 4-8, 1991.

[2] H. Scheurer, R. Zeyen: "PHEBUS FP Facility Description", report EUR 13803/EN.

[3] B. Clément, Ch. Ktorza, H. Scheurer, R. Zeyen: - "The Integral Source Term Experiment PHEBUS FP, with Special Emphasis on In-pile and Circuit Instrumentation". CEC/CEA International Conference on Irradiation Technology, Saclay, 20 - 22th May, 1992.

[4] P. von der Hardt, G. Lhiaubet: "PHEBUS FP Instrumentation", paper at the first PHEBUS FP Seminar, Cadarache June 5-7, 1991.

[5] R. Zeyen, B. Clément: "Instrumentation for Integral Severe Accident Simulating Experiments" - OECD/CSNI Specialist Meeting on Instrumentation to Manage Severe Accidents, Köln, 16 - 17th March, 1992.

[6] H.-G. Dillmann, J.G. Wilhelm, "Investigation into the design of a filter system for PWR containment venting" - 21st DOE/NRC Nuclear Air Cleaning Conference.

[7] H.-G. Dillman, H. Passler, J.G. Wilhelm: "Filtered Venting for German Power Reactors" - Nuclear Technology, Vol.92, October 1990.

[8] J.G. Wilhelm et al.: "Testing of Iodine-Filter Systems under Normal and Post-Accident Conditions" - Proc. Air Cleaning Conf. Oak Ridge, Tennesse, August 28 - 31, 1972, CONF-720823, p. 434.

[9] A. Tani, P. von der Hardt, C.G. Benson: "A Working Plan for Post-Test Analyses of Samples in PHEBUS FP", JAN '92, EUR report to be published.

8. ABBREVIATION GLOSSARY

CEA	Commissariat à l'Energie Atomique
CEC	Commission of the European Communities
LAF	Laboratorium für Aerosolphysik und Filtertechnik
INEL	Idaho National Engineering Laboratory
IPSN	Institut de Protection et de Sûreté Nucleaire
FP	Fission Product
FPT x	Fission Product Test N° x
GRS	Gesellschaft für Reaktorsicherheit
KfK	Kernforschungszentrum Karlsruhe
SG	Steam Generator
PIE	Post-Irradiation Examination
PTA	Post-Test Analysis
SFD	Severe Fuel Damage
TUI	Transuranium Institute (CEC)

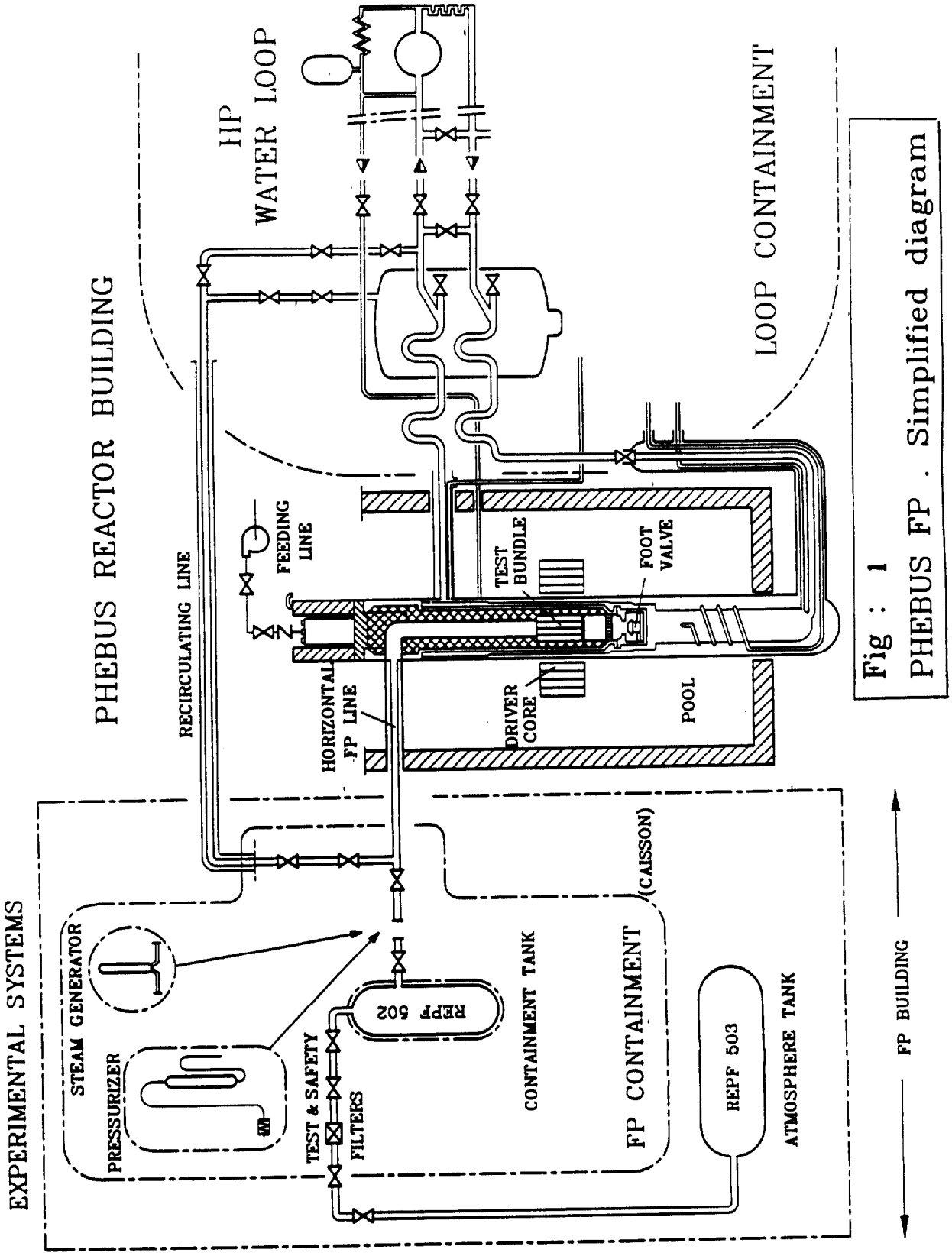

Fig : 1
PHEBUS FP . Simplified diagram

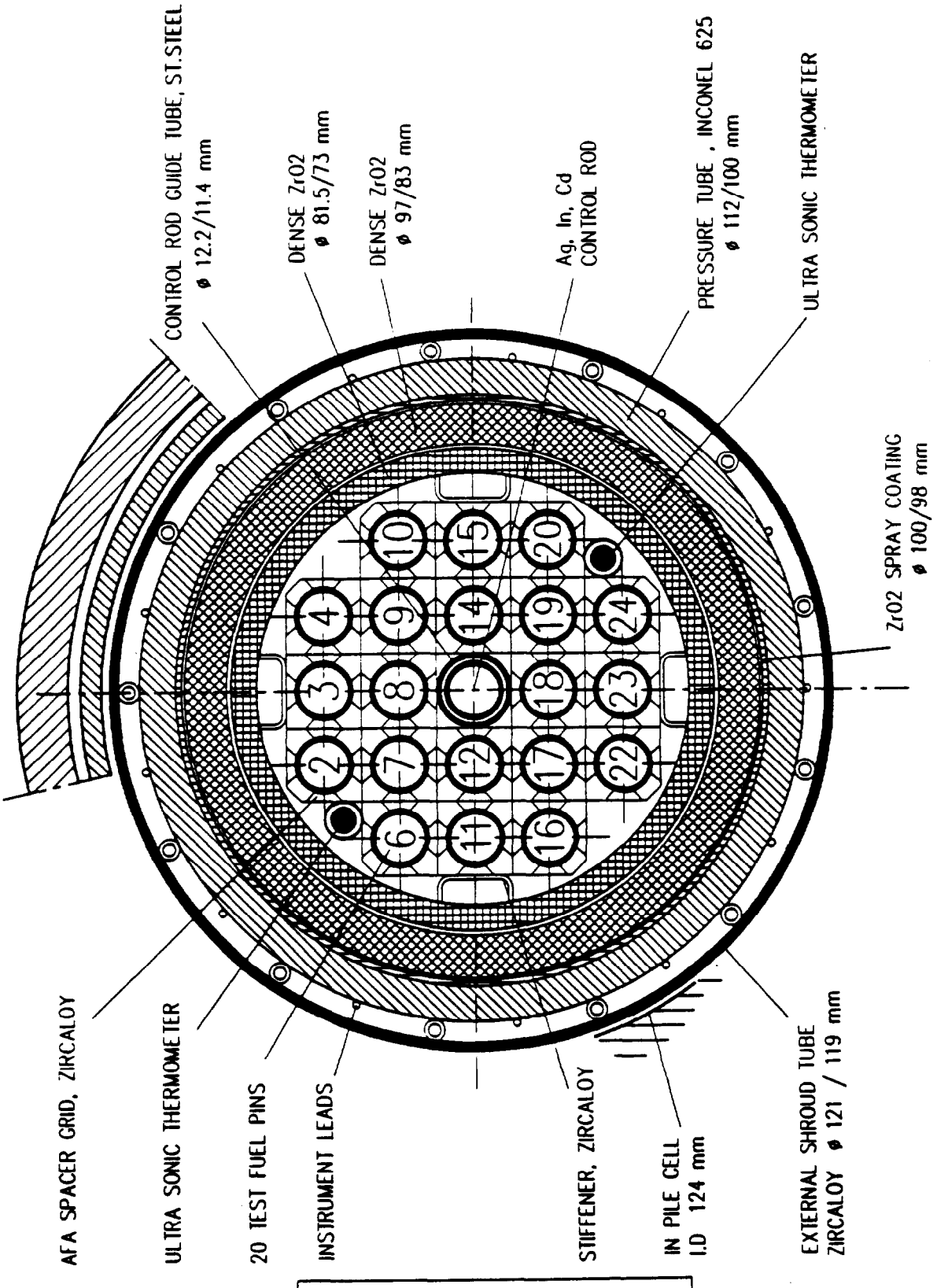

FPTO In-Pile Test Section
horizontal section Fig.2

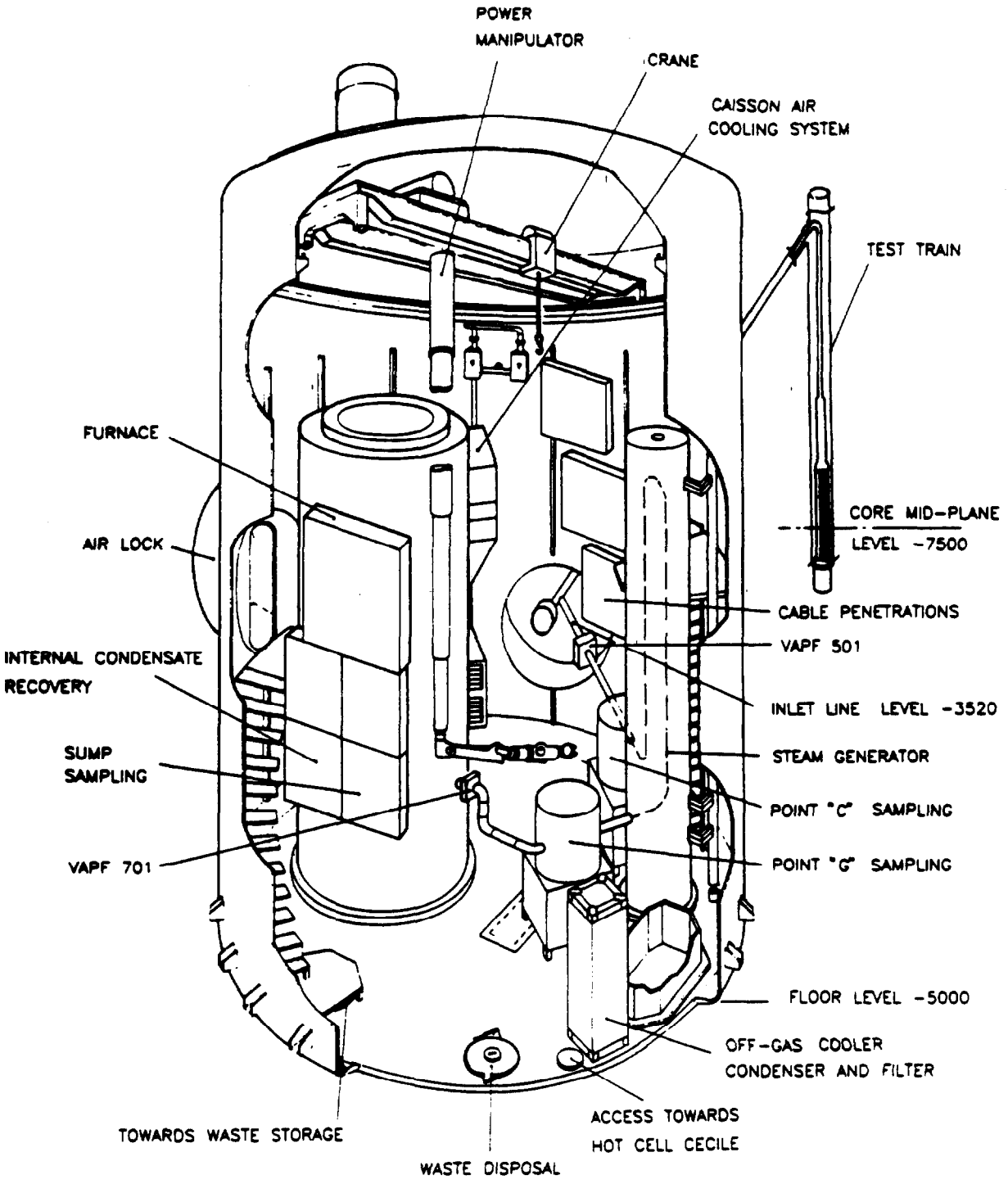

ISOMETRIC VIEW OF THE PP CAISSON

Fig : 3

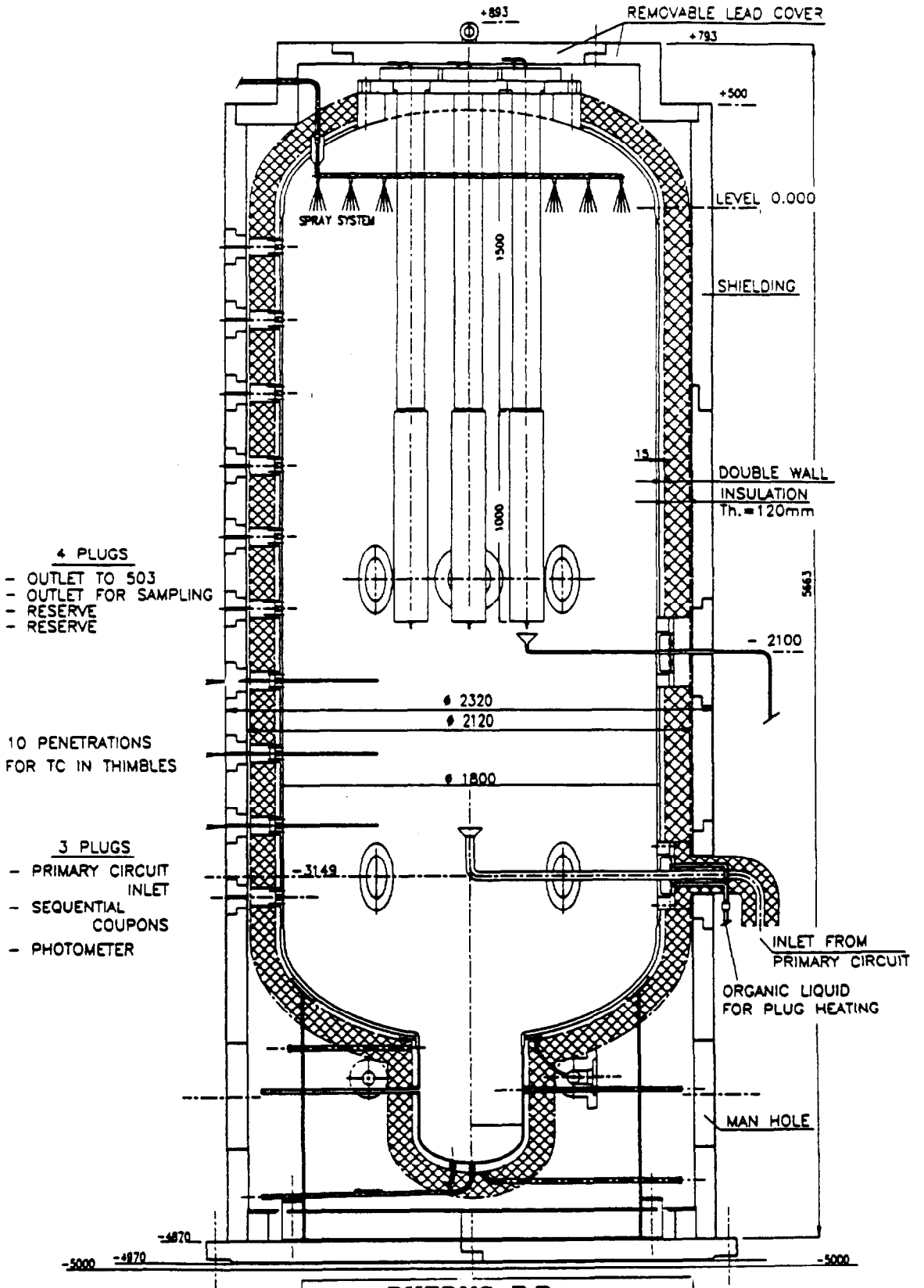

PHEBUS F.P.
REPF 502 VESSEL

Fig.4

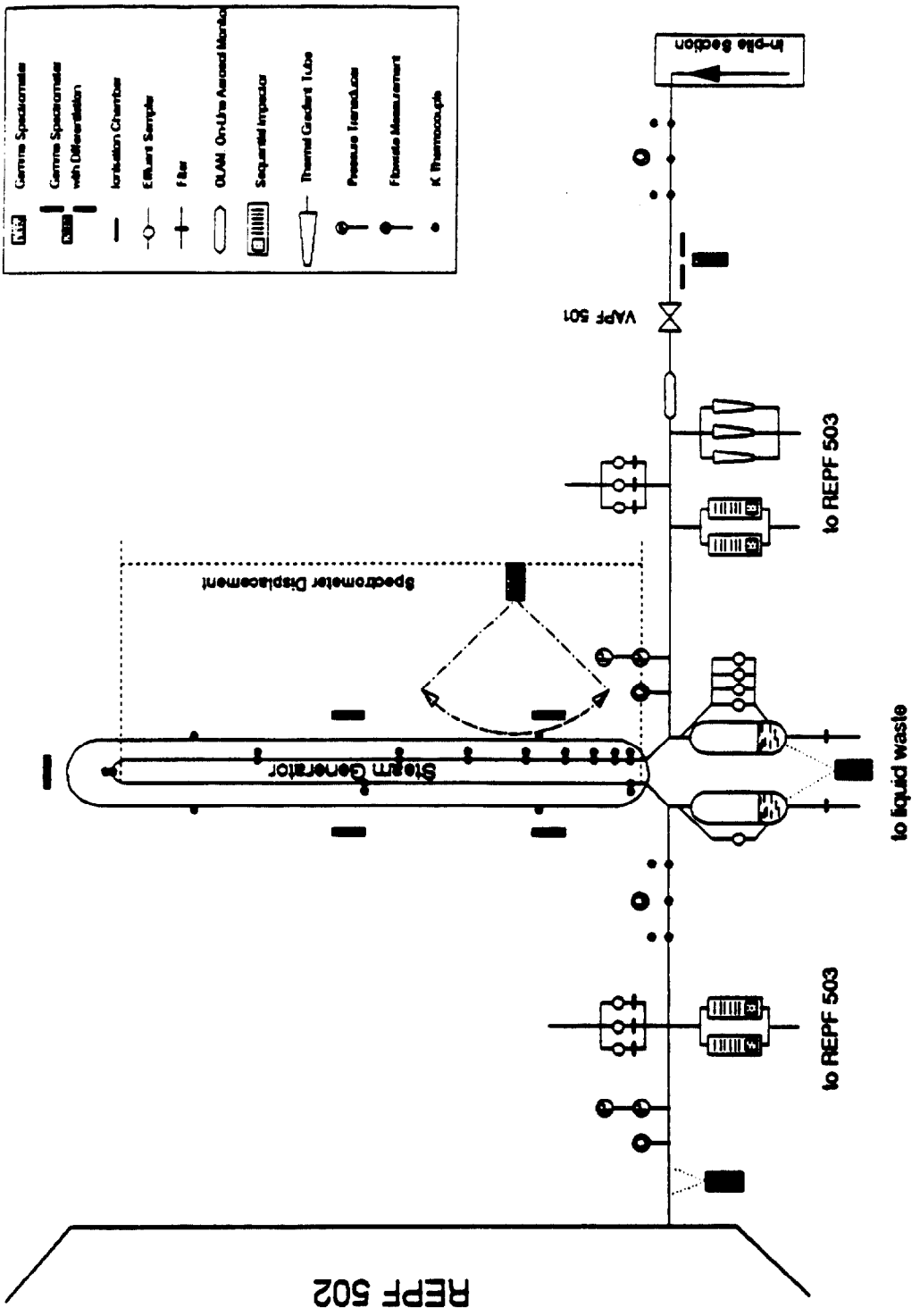

INSTRUMENTATION PLAN FOR THE FPTO TEST
PRIMARY CIRCUIT

Fig : 5

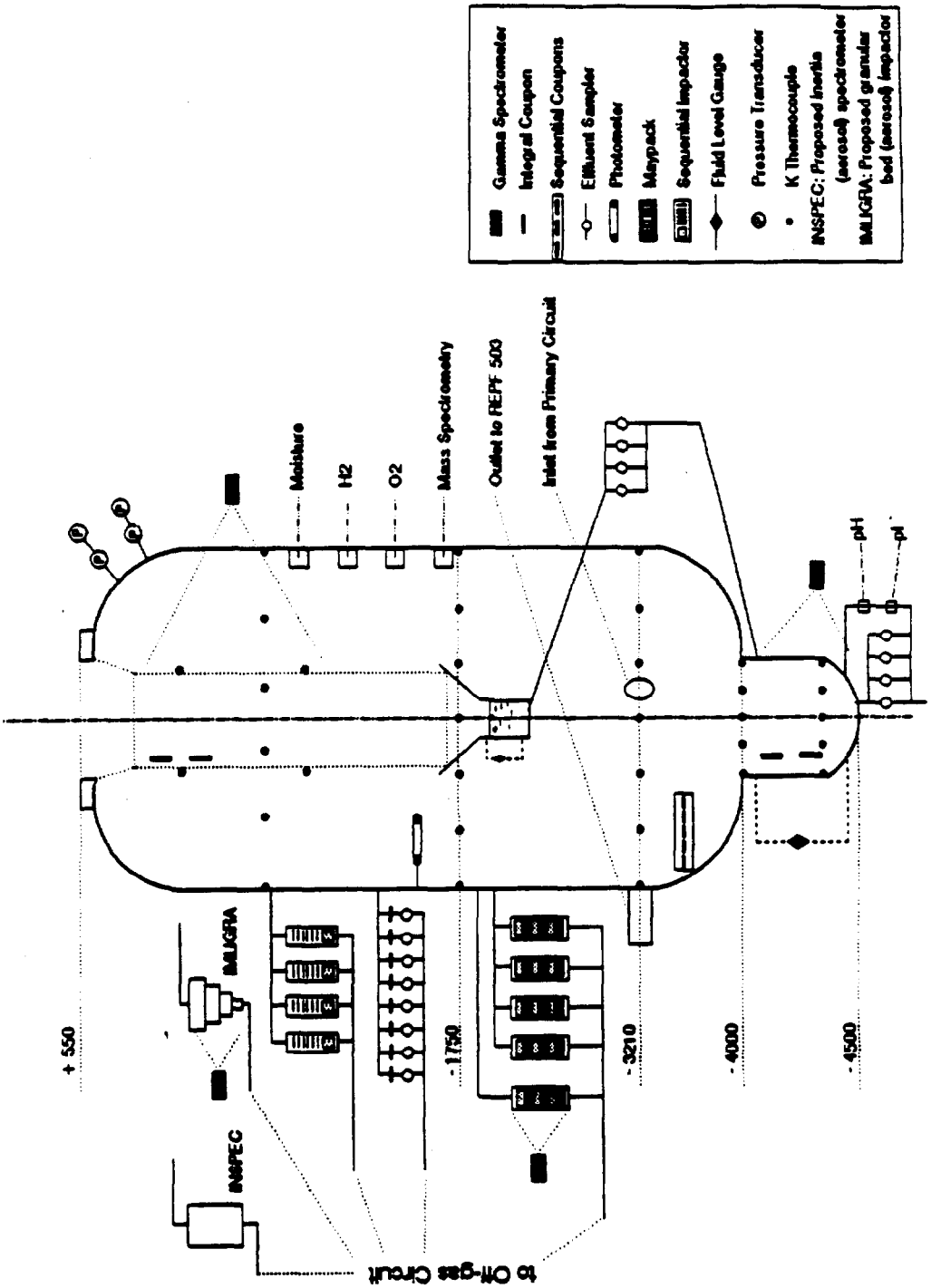

INSTRUMENTATION PLAN FOR THE FPTO TEST CONTAINMENT VESSEL

Fig : 6

CLOSING COMMENTS OF SESSION CO-CHAIRMAN WILHELM

I would only like to comment on the need of iodine filters in case of a severe accident. With respect to the severe accident source term under discussion, and the need of iodine filters to mitigate the environmental burden, I am very surprised that there are doubts whether iodine filters are still needed.

I suppose the underlying idea may be the extremely small amount of iodine released to the containment atmosphere in the Three Mile Island accident. In that case, the blowdown practically functioned as an iodine trap. This cannot be expected in the sequence of events of other severe accidents. Moreover, a large part of the iodine will react in the containment atmosphere with organic compounds to become organic iodine compounds, because high concentrations of organics will be present as a result of burning and vaporizing. Those compounds and their radicals produced by irradiation are available for a reaction with iodine. Organic iodine will not be trapped at a high degree in the water. It should be recalled that the high iodine activity which arrived from Chernobyl had not been expected in Germany, but has caused large losses of fresh vegetables by contamination and of money paid for compensation; and this, at a distance of more than 1,000 miles.

CLOSING COMMENTS OF SESSION CO-CHAIRMAN MILLER

It is very well stated that some of the diversity that we see may not be optimized. It would be nice if we all got together and figured out what is the best way to attack this backend and then do it.

NRC FORM 335 (2-89) NRCM 1102, 3201, 3202

U.S. NUCLEAR REGULATORY COMMISSION

BIBLIOGRAPHIC DATA SHEET

(See instructions on the reverse)

1. REPORT NUMBER (Assigned by NRC. Add Vol., Supp., Rev., and Addendum Numbers, if any.)
NUREG/CP-0130
CONF-9020823
Vol. 1

2. TITLE AND SUBTITLE
Proceedings of the 22nd DOE/NRC Nuclear Air Cleaning Conference

Sessions 1 - 8

Held in Denver, Colorado
August 24-27,1992

3. DATE REPORT PUBLISHED
MONTH: July
YEAR: 1993

4. FIN OR GRANT NUMBER

5. AUTHOR(S)
M. W. First

6. TYPE OF REPORT

7. PERIOD COVERED *(Inclusive Dates)*

8. PERFORMING ORGANIZATION – NAME AND ADDRESS *(If NRC, provide Division, Office or Region, U.S. Nuclear Regulatory Commission, and mailing address; if contractor, provide name and mailing address.)*
Harvard School of Public Health
The Harvard Air Cleaning Laboratory
665 Huntington Avenue
Boston, MA 02115

9. SPONSORING ORGANIZATION – NAME AND ADDRESS *(If NRC, type "Same as above"; if contractor, provide NRC Division, Office or Region, U.S. Nuclear Regulatory Commission, and mailing address.)*
Office of Nuclear Safety
U.S. Department of Energy
Washington, DC 20585

Office of Nuclear Regulatory Research
U.S. Nuclear Regulatory Commission
Washington, DC 20555

International Society of Nuclear Air Treatment Technologies, Inc.
P.O. Box 29246
Columbus, OH 43229

Harvard School of Public Health
The Harvard Air Cleaning Laboratory
665 Huntington Avenue
Boston, MA 02115

10. SUPPLEMENTARY NOTES

11. ABSTRACT *(200 words or less)*
This document contains the papers and the associated discussions of the 22nd DOE/NRC Nuclear Air Cleaning Conference. Major topics are: (1) advanced reactors, (2) reprocessing, (3) filter testing, (4) waste management, (5) instruments and sampling, (6) reactor accidents, (7) filters and filter performance, (8) adsorber testing and performance, (9) carbon testing, and (10) ventilation systems.

12. KEY WORDS/DESCRIPTORS *(List words or phrases that will assist researchers in locating the report.)*
Nuclear Air Cleaning Conference,

13. AVAILABILITY STATEMENT
unlimited

14. SECURITY CLASSIFICATION
(This Page)
unclassified
(This Report)
unclassified

15. NUMBER OF PAGES

16. PRICE

NRC FORM 335 (2-89)